NTNU – Trondheim
Norwegian University of
Science and Technology

Methods of Reliability Analysis for Marine Structures

David Larsson

Marine Technology
Submission date: June 2015
Supervisor: Bernt Johan Leira, IMT

Norwegian University of Science and Technology
Department of Marine Technology

NTNU
Norwegian University of Science and Technology
Department of Marine Technology

MASTER THESIS, SPRING 2015
for
Master Student David Larsson

METHODS OF RELIABILITY ANALYSIS FOR MARINE STRUCTURES

Metoder for beregning av marine konstruksjoners pålitelighet

Methods for analysis of structural reliability have been successfully applied in the area of marine structures in a number of cases. Such methods can broadly be classified into three different levels. The type of input data, methods of calculation and resulting reliability measure will accordingly also be different for each level. Generally, the different levels are designated as:

- Level I : Partial coefficient methods
- Level II : Safety index methods
- Level III : Probability of failure methods

The complexity of computation methods increases significantly from one level to the next.

The candidate shall address the following topics :

1. Differences and relationships between the different levels of methods are briefly described.

2. Examples of application of reliability methods found in the literature are to be reviewed. In particular, the following topics can be addressed:

    - Direct application of reliability methods for design purposes and for development of improved design-formats

    - Inspection-planning

    - Requalification and assessment of residual lifetime

The required data basis for application of structural reliability methods is also to be commented upon.

3. Techniques which are available for the purpose of increased computational efficiency of structural reliability analysis are to be addressed. Particular focus is on application of response surface formulations in combination with Monte Carlo simulation methods.

4. A particular calculation example is agreed upon with the supervisor in order to illustrate the sequential steps which are required by response surface/Monte Carlo procedures. The candidate

may apply an existing computer program, or develop a dedicated program based e.g. on Abaqus/MATLAB (or MAPLE).

The work scope may prove to be larger than initially anticipated. Subject to approval from the supervisor, topics may be deleted from the list above or reduced in extent.

In the thesis the candidate shall present his personal contribution to the resolution of problems within the scope of the thesis work.

Theories and conclusions should be based on mathematical derivations and/or logic reasoning identifying the various steps in the deduction.

The candidate should utilise the existing possibilities for obtaining relevant literature.

The thesis should be organised in a rational manner to give a clear exposition of results, assessments, and conclusions. The text should be brief and to the point, with a clear language. Telegraphic language should be avoided.

The thesis shall contain the following elements: A text defining the scope, preface, list of contents, summary, main body of thesis, conclusions with recommendations for further work, list of symbols and acronyms, references and (optional) appendices. All figures, tables and equations shall be numerated.

The original contribution of the candidate and material taken from other sources shall be clearly defined. Work from other sources shall be properly referenced using an acknowledged referencing system.

Supervisor: Professor Bernt J. Leira

Deadline: June 10th 2015

Trondheim, January 13th, 2015

Bernt J. Leira

Abstract

Analytical solutions of structural reliability problems are often tedious or impossible to obtain. The task is further complicated when the safety margin, i.e. the relation between variables and response, is implicit. Such is the case for many practical problems, where structural response is obtained from finite element models and/or by semi-analytical equations. This thesis describes a practical approach to solution of such problems by response surface methods, i.e. ways of approximating the analytical safety margin by sampling at discrete points. If each such sample is computationally demanding, it is necessary to limit the number of sampling points without introducing unacceptable lack-of-fit. Theoretically, once the response surface is given, an accurate approximation of failure probability can then be found by the Crude Monte Carlo method. However, with low probabilities of failure and/or high dimensionality, this method becomes computationally unfeasible.

Two response surface methods are tested for a stiffened panel, where the effects of distribution types are investigated by comparing between more realistic models and corresponding gaussian approximations. The evaluations are performed for a stiffened panel based on three different limit states; von-Mises stress in the plate along the midspan, axial capacity and a check according relevant classification guidelines. For von-Mises stress and ultimate capacity limit states, finite element software ABAQUS is used to sample the safety margin. The third is modelled from Det Norske Veritas recommended practice for buckling of stiffened panels, corresponding to a check for plate side at midspan. A purely quadratic response surface as suggested by Bucher and Buorgund [4], along with a hyperplane based on vector projection as suggested by Kim and Na [15] are employed. From the quadratic response surface, probability of failure is evaluated by Crude Monte Carlo, Importance Sampling and a First Order Reliability method (FORM).

The response surface obtained by vector projection yields similar results as the quadratic response surface in combination with simulation methods, but with some deviations. These differences are generally larger for the non-gaussian case than for the gaussian distributions. From the results, it can not be concluded whether the differences are method-specific or caused by underlying calculations, e.g. variable transformations.

Effects of probability distributions are important, and the results with all variables taken from the gaussian distribution is highly conservative compared to using more relevant probability densities.

It is shown how the structural reliability problem can be solved for implicit limit states in a sensible manner. The procedures shown are efficient from a computational perspective, and the results from both approaches are equivalent. A difference between the two methods in terms of applicability is noted. The purely quadratic, "Bucher-Buorgund", response surface samples the safety margin using two iterations with enough sampling points in each to uniquely determine the polynomial description, and simulations are used to find the most accurate probability of failure measure. The Vector Projection approach samples the safety margin by continuously establishing a hyperplane approximation and shifting the sampling points until a convergence criteria is met. The probability of failure is evaluated simultaneously by FORM, which is highly efficient compared to Monte Carlo. This leads to an unknown, potentially fairly large, number of safety margin samples but swift probability of failure calculations. If the results are considered equivalent, it can then be recommended to use the Bucher-Buorgund approach for problems where the safety margin samples are computationally demanding but the failure probabilities are moderate, whereas the Vector Projection approach is feasible for any probability of failure when the safety margin sampling is fast.

The results in terms of failure probabilities are not thought of as directly applicable to design but are deemed valid in the sence of highlighting some important considerations and show the essence of solving similar problems. A valid starting point for further analysis and design purposes would be to extend the model with respect to boundary conditions, imperfections and an increased number of basic variables along with correlation effects.

Sammandrag

En analytisk lösning av pålitlighetsproblemet för konstruktioner är ofta svår eller omöjlig att finna. Om säkerhetsmarginalen, d.v.s. relationen mellan de ingående variablerna och dess inverkan på respons, är okänd eller implicit blir utmaningen än större. I många praktiska problem är fallet just sådant, då man bara känner till relationen mellan variabel och respons genom exempelvis en FE-modell. Det här examensarbetet visar två olika tillvägagångssätt för lösning av dylika problem genom användning av responsyte-metoder, vilket innebär en tillnärmning av den analytiska säkerhetsmarginalen. Det finns ett antal sådana metoder, där alla går ut på att minimera antalet regressionspunkter som används men ändå bibehålla tillräckligt god representation av den analytiska säkerhetsmarginalen i det mest intressanta området. Anledningen till att det är intressant att minimera antalet provtagningspunkter är att dessa medför en beräkning som ofta är krävande, som i fall av omfattande FE-modeller.

Två responsyte-metoder är testade genom ett exempel som representeras av tre olika definitioner av svikt. I beräkningarna ingår dessutom en jämförelse av fördelningstyper, genom att använda både de sannolikhetsfördelningar som anses mest praktiskt relevanta, och normalfördelningen med motsvarande förväntning och standardavvik. Anledningen till detta är att det är avsevärt enklare att genomföra beräkningarna när alla variabler kommer från normalfördelningen, därför är det intressant att se vilken skillnad denna förenkling medför. Exemplet består av en förstyvad panel, vilket är en vanlig beståndsdel i marina konstruktioner. De tre gränstillstånden är definierade som flytspänning i plåten, överskridelse av axiell kapacitet samt kontroll enligt rekommendationer för buckling av dylika strukturer från Det Norske Veritas, motsvarande kontroll i panelens mitt. Den ena responsytemetoden är en rent kvadratisk tillnärmning enligt Bucher och Buorgund [4] med två iterationer. Den andra föreslås av Kim och Na och baserar sig på en linjär tillnärmning som itereras fram tills ett konvergenskriterium är nått. Med den förstnämnda beräknas sannolikheten för svikt med hjälp av FORM, direkt Monte Carlo och Importance Sampling.

Resultaten visar att bägge metoder ger motsvarande resultat, men med vissa skillnader som är större för de mer realistiska sannolikhetsfördelningarna än för normalfördelade variabler. Det kan således inte fastslås om det finns signifikanta resultatmässiga skillnader mellan metoderna eller om skillnaderna beror på de underliggande beräkningarna, kanske framförallt transformationer och simuleringarnas omfattning.

För den kvadratiska responsytan gav direkt Monte Carlo och Importance Sampling nära identiska resultat medan FORM som regel avviker en del. Om man antar att simuleringsmetoderna ger det svar som ligger närmast det analytiska, kan man i så fall fastslå att denna metod i regel ger en god representation av säkerhetsmarginalen i det mest intressanta området men att responsytans designpunkt avviker från den faktiska. Sannolikhetesfördelningens form visade sig vara av stor vikt, då normalfördelade variabler gav stora skillnader åt det konservativa hållet jämfört med de mer realistiska fördelningsfunktionerna.

En praktisk iakttagelse är att Bucher och Buorgunds responsyta itereras två gånger, varifrån sannolikheten för svikt med fördel simuleras fram. Kim och Na's förslag baseras på en linjär tillnärmning, där sviktsannolikheten räknas ut med FORM. Denna process upprepas tills ett konvergenskriterium är uppnått. Alltså ger den ena metoden ett bestämt antal testpunkter varifrån responsytan skapas. Den andra metoden ger ett okänt antal testpunkter men en snabb beräkning av sviktsannolikhet. Därav är Kim och Na's metod lämplig när proverna för säkerhetsmarginalen innebär snabba beräkningar, och är oberoende av nivån för sviktsannolikhet. Bucher och Buorgunds metod är snarare att föredra när varje provtagning är mer omfattande, eftersom man vet hur många punkter som skall testas och därmed kan förutspå omfattningen av analysen. Om man däremot misstänker låg sviktsannolikhet och har många variabler, blir de påföljande simuleringarna krävande.

Resultaten i sig är inte direkt applicerbara för dimensionering på grund av ett antal förenklingar som bör undersökas närmare. En lämplig utgångspunkt för vidare arbete är att expandera modellen med fler variabler för tvarsnittsdimensioner och materialegenskaper, tillsammans med korrelationseffekter av dessa samt för laster. En annan effekt som bör ses närmare på är inspänningarna, då dessa visar stort utslag på panelens kapacitet. Vidare undersökning av formfel samt dess inverkan är också relevant.

Preface

This thesis is written at the Department of Marine Technology, Norwegian University of Science and Technology, and submitted as partial fulfillment of the grade Master of Science in Marine Technology.

All parts of this report, including text, figures and appendices are created by the author unless stated otherwise.

The patient help and support from the supervisor, Professor Bernt Johan Leira, is gratefully acknowledged.

David Larsson
10 June 2015

Nomenclature

Abbreviations

CDF	cumulative distribution function
CMC	crude monte carlo (direct sampling)
FORM	first order reliability methods
FSA	formal safety assessment
IMO	international maritime organization
IS	importance sampling
LSF	limit state function
PDF	probability density function
POD	probability of detection

Symbols

β	safety index
E	elastic modulus
ϵ_u	ultimate strain
f	sample spread factor
g	safety margin
γ_m	model uncertainty factor
$\bar{\lambda}$	reduced slenderness
μ	mean or dimensionless imperfection coefficient
p_f	probability of failure
$p_{f,CMC}$	probability of failure, crude Monte Carlo
$p_{f,HL}$	probability of failure from Hasofer-Lind safety index
$p_{f,IS}$	probability of failure, Importance Sampling
p_{lat}	lateral pressure load
s_{ax}	axial stress
s_E	Euler buckling stress
s_f	yield strength
s_u	ultimate strength
σ	standard deviation
t_p	plate thickness

Contents

List of Figures

List of Tables

Chapter 1

Introduction

1.1. Scope of Work

This thesis aims to present the fundamental theory of Structural Reliability, with emphasis on marine and offshore structures. The calculations are focused on response surface methodology, which is highly relevant from a practical perspective due to the possibility of implementing different models, including Finite Element models and classification requirements. Two different response surface methods are tested and compared using a relevant example. In particular, the following questions will be addressed:

- Which detailed steps are required to solve the reliability problem given a mechanical model?
- Will the tested response surface methods yield different results?
- Are there differences between the tested response surface methods in terms of applicability to different problems?
- If the gaussian distribution is employed as an approximation for all variables, will this have a significant impact on the results?

Effects of sampling procedure, differences between reliability methods and the effect of probability distributions are also investigated. The limit states are chosen so that the implications of different probability of failure levels can be seen.

1.2. Background

This section aims to describe the context of which structural reliability plays an important part, and to address its relevance for the design of ships and offshore structures.

1.2.1. Rules-Based vs Risk-Based design

The common design procedure of ships and offshore structures today can be attributed the *Rules-Based Design*, meaning that the ship is designed with functional requirement and cost effectiveness as the overall goals while staying within the regulatory framework. Thus, the safety perspective is captured by the underlying rules, and so forms a design constraint.

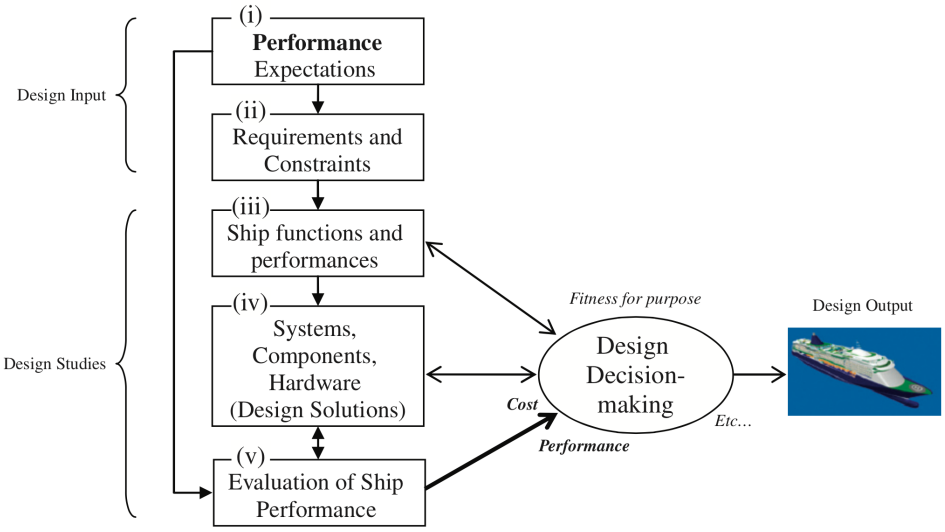

Figure 1.1: High level explanation of Rules-Based Design, as shown by Vassalos in [26]

Risk is generally acknowledged as the product:

$$(\text{Probability of an event}) \times (\text{Consequences of the event})$$

In the wider sense, risk can be defined on any activity that leads to a potential loss of human life, property, revenue or cause of environmental damage.

So-called *Risk Based Design* aims to shift the safety perspective from a constraint to a design objective [26]. Thus, risk can be considered as part of the design process rather than a limiting factor. The purpose of such a shift is meant as an incentive to reduce risk and promote innovation, by prescribing acceptable risk levels instead of design parameters or technology as in a rule-based approach. Obviously, detailed design regulations exist to minimize risk and are still highly applicable to standard designs. However, if risk can be minimized using other solutions there would be more room for innovation.

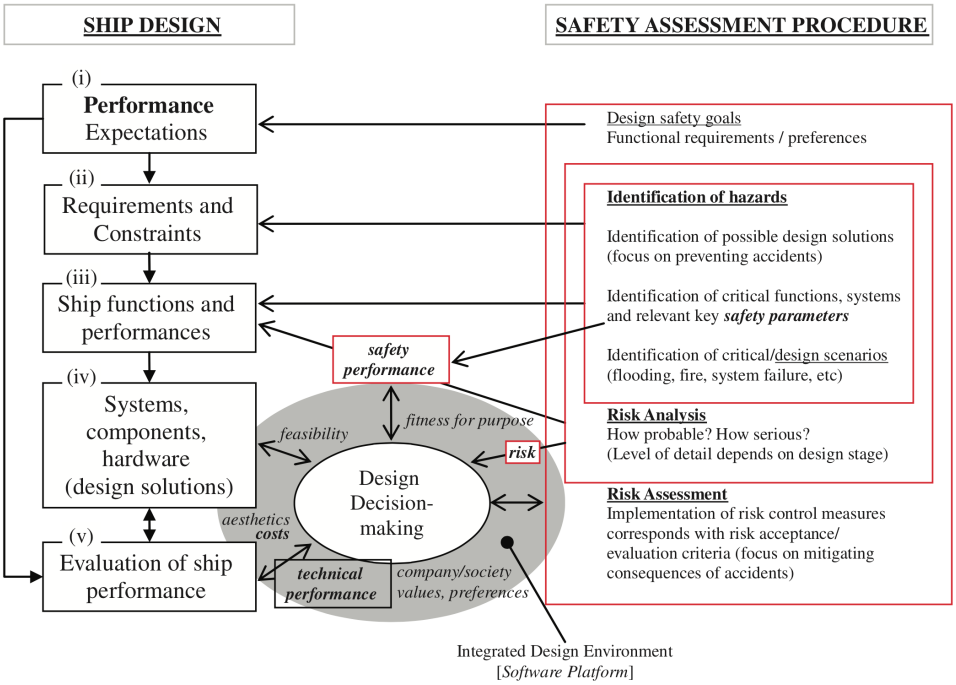

Figure 1.2: High level explanation of Risk-Based Design, as shown by Vassalos in [26]

1.2.2. Formal Safety Assessment-FSA

In 1988, disaster struck the Piper oilfield in the North Sea. The Piper Alpha production production platform exploded, causing the death of 167 persons including 2 crewmen from the rescue vessel Sandhaven.

While risk assessments where mandatory in the norwegian offshore industry since 1986 [26], the chain of events leading up to the Piper Alpha disaster is considered as one of the drivers for the implementation of risk assessments in the UK and the rest of the world [23]. A specific procedure that is widely applied today is the *Formal Safety Assessment*, FSA, meant as a tool in the rule-making process (initially for the IMO regulations) by establishing a link between risk, safety and cost. The process can be roughly divided into five steps of the following order [26]:

- Identification of hazards
- Assessment of the risks arising from these hazards
- Identification of risk-control options
- Cost/benefit assessment of such measures
- Recommendations for decision making

A Formal Safety Assessment, as may be noted from the above description, is a complex and substantial procedure that requires large effort. Thus, an FSA is more of a high-level tool suitable for regulatory changes rather than specific projects.

1.2.3. Goal-Based Standards

In 2002, the Bahamas and Greece suggested that IMO should be more involved in setting the construction standards for marine vessels. Following the discussion of Risk-Based Design, IMO [24] issued the *Goal-Based Standards* main principles as:

- "Broad, over-arching safety, environmental and/or security standards that ships are required to meet during their lifecycle"
- "The required level to be achieved by the requirements applied by class societies and other recognized organizations, administrations and IMO"
- "Clear, demonstrable, verifiable, long standing, implementable and achievable, irrespective of ship design and technology"
- "Specific enough not to be open to differing interpretations"

The detailed objectives of the Goal-Based standards are ready to be applied under SOLAS to the design of oil tankers and bulk carriers over 150m in length with building contracts signed after the end of June 2016. The IMO Assembly of November 2011 decided in their strategic plan for 2012-2017, to plan for a new GBS concerning oil tankers and bulk carriers, as well as for other types of ships [24].

The Goal Based Standards will thus act as the framework for new guidelines and regulations, where Formal Safety Assessments and Structural Reliability Analysis will supply the supporting arguments for their establishment.

Chapter 2

Structural Reliability Theory

2.1. Level I - Partial factors

A common way to evaluate structural safety is the *Limit State Design*. The general meaning is that the loads on the structure are found from a chosen limit state, forming the basis for strength or operability calculations. If the load on a structural member is denoted S and the corresponding resistance to such a load is R, then a safety factor F is found from:

$$F = \frac{S}{R} \tag{2.1}$$

Clearly, $F \leq 1$ implies that the load is larger than resistance, and thus failure for the considered limit state. Such a general analysis, however, is insufficient by mainly two reasons. First, it would be difficult to say what the sufficient factor should be. Furthermore, the structural rules should be applicable to a range of structures within a defined interval of designs. An overall factor as above would show little consideration to the details that differ two designs contained in the same requirement. Also, the weighing of safety measure between different components would probably be unbalanced.

To overcome these issues, the concept of *Partial Factors* are introduced. Here, each key component of the structure has its own requirement, so that the assembly of components fulfill the total structural safety demand. If the yield strength of steel is taken as an example, a partial factor $\gamma_{s,f}$ would be defined by:

$$s_{f,des} = \frac{s_{f,sp}}{\gamma_{s_f}} \tag{2.2}$$

Where $s_{f,des}$ is the value used for design and $s_{f,sp}$ the specified value. By this, the partial factor (if larger than one) lowers the design strength of the material thus making the strength calculations more conservative. The reason for introducing such a factor would be to compensate for the stochastic nature of the actual yield strength i.e setting it lower than it "probably" is so that deterministic calculations can be withheld. If the actual yield stress belongs to a gaussian distribution with $\mu_{s_f} = 235$ MPa and $\sigma_{s_f} = 15$ MPa, its probability density is in accordance with the curve of figure 2.1.

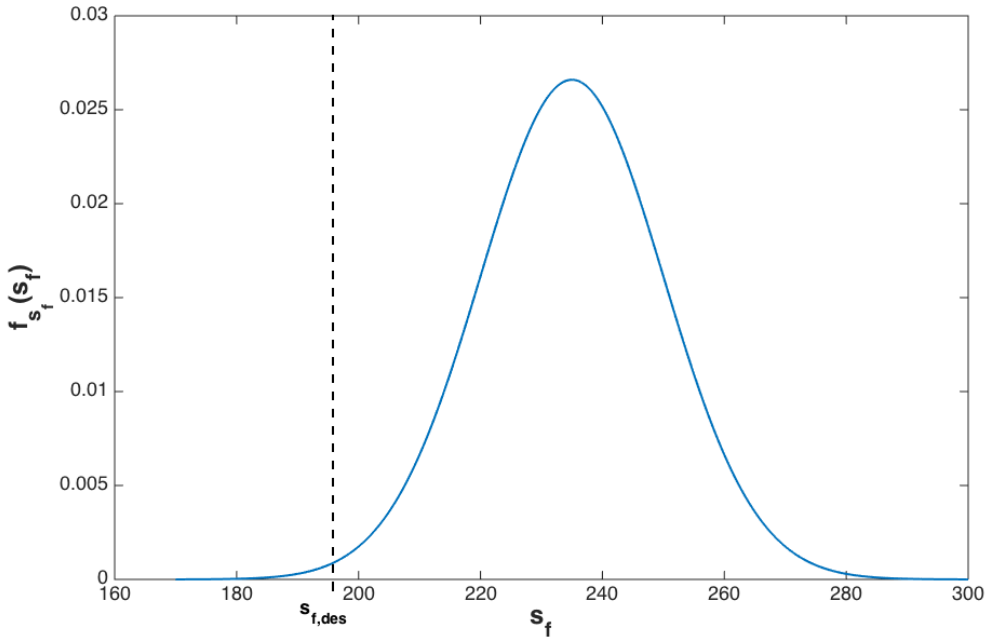

Figure 2.1: Probability density for a gaussian yield stress

If the specified value is taken at the mean, a partial factor of 1.2 correspond to a design yield stress as indicated in figure 2.1. For a load variable, the relation of eq. 2.1 would be inversed in order to be conservative. The requirement for the i^{th} structural member when subject to k load variables would then be:

$$\frac{R_{sp,i}}{\gamma_i} \leq \sum_{j=1}^{k} \theta_j S_{sp,j} \tag{2.3}$$

Where θ_j denotes the partial safety factor for the corresponding load. An alternative approach would be to use safety factors smaller than unity for resistance variables and larger than unity for loads. The design value would then be the specified value multiplied by its partial factor for both load and resistance.

It can be noted that due to the continous distribution of most stochastic variables, as in the case of yield strength, there will be a slight probability that the actual value is below the design value, no matter how large the partial factor. On the other hand, this probability might be so low that it is negligable. Such high factors would bring additional costs e.g. in material use, fuel consumption, fabrication cost etc.

An important consequence of the method of partial factors is the *lack of invariance*, implying that these factors have different physical meaning depending on the formulation used when defining the load and resistance [17]. An example is the above discussion on whether to divide by a safety factor larger than one or multiply by a factor smaller than one for resistance scaling. Caution is thus required so that definitions used in design correspond to those of the rules from which the factors are taken.

Apart from mentioned restrictions, the method of partial factors provides an efficient basis for the designer in the sense that the factors are easily applied to the calculations. Due to the straight-forward implementation, verification procedures are easily performed.

2.2. Level II - Safety index Methods

The basis for all Level II-approaches is the notion of a *limit state function*, "LSF". Recall that a safety factor could be written as in equation 2.1. Now, instead of considering the relation between resistance, R, and load, S, as a factor, a safety *margin* is defined as:

$$g(R,S) = R - S \tag{2.4}$$

When load is greater than resistance, the structure is prone to failure. Thus, failure is expected for $g < 0$. The limit state function is defined as the limit between failure and safe domains, i.e. $g = 0$. A measure of the probability of failure is now introduced as the *safety index*. Consider the limit state, and that resistance and load consist of one or more random variables. The limit state function can hence be graphically interpreted as a line, curve or surface, depending on the number of dimensions (variables) included and the formulation of the limit. This surface (or curve/line) splits the total domain into a safe region and a failure region.

If the safety margin consists of two independent standard gaussian variables, z_1 and z_2, the limit state becomes a curve. This curve along with probability density of the variables $f_{Z_1,Z_2}(z_1, z_2)$ is shown in figure 2.2.

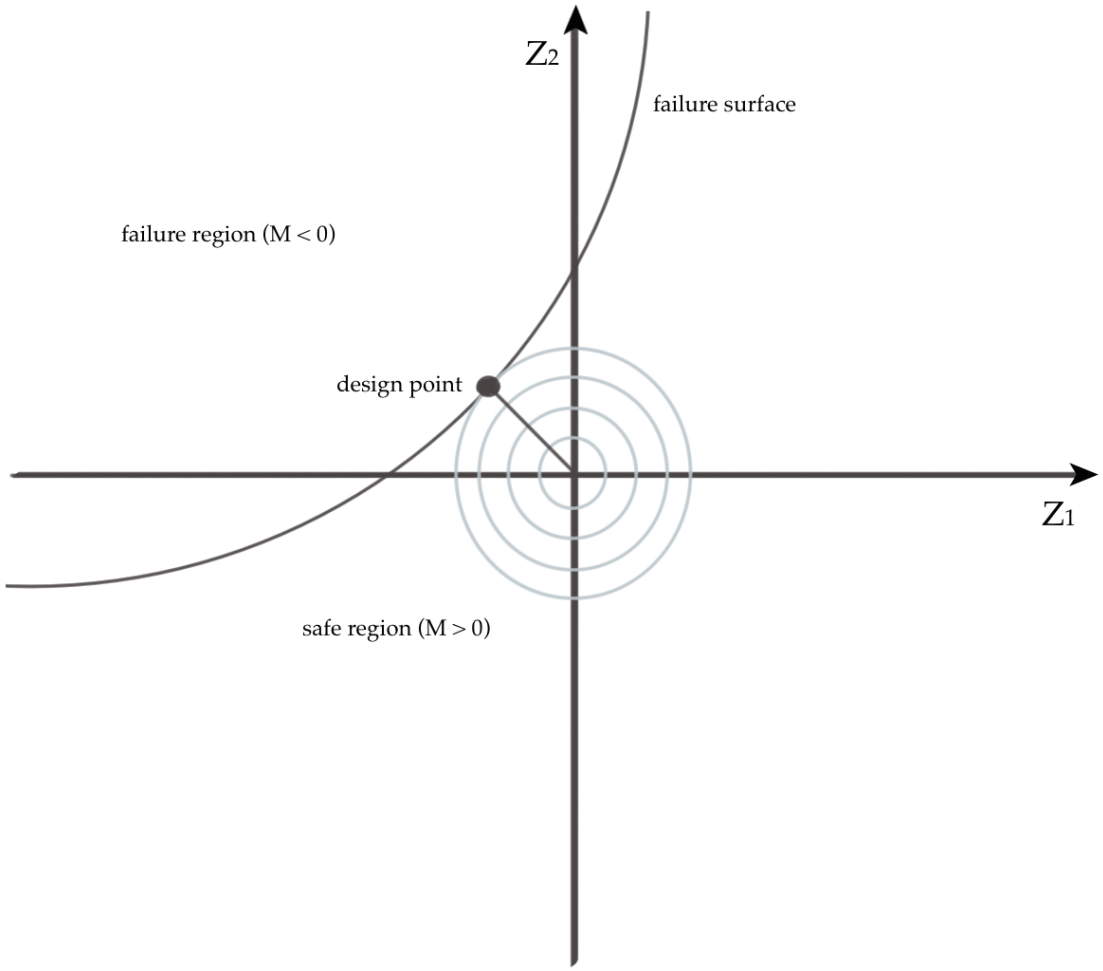

Figure 2.2: Graphical interpretation of the design point and the corresponding safety index. Circles represents contours of the joint standard Gaussian probability density.

2.2.1. Cornell Safety Index

Consider a safety margin as of equation 2.4. Assume that load effect and resistance are two independent normal random variables, R and S. They are thus characterized by their mean values μ_R and μ_S with variances σ_R^2 and σ_S^2. Hence, the safety margin will also be a normal random variable with $\mu_g = \mu_R - \mu_S$ and variance $\sigma_g^2 = \sigma_R^2 + \sigma_S^2$.

As any normally distributed random variable, g can be transformed into the standard normal distribution, giving it zero mean and standard deviation equal to one. If the transformed variable is g', the transformation is given by:

$$g' = \frac{g - \mu_g}{\sigma_g} \tag{2.5}$$

The probability of failure in terms of the safety margin can be written as $p_f = P[g \leq 0]$. Inserting $g = 0$ into equation 2.11 gives:

$$g'(0) = \frac{-\mu_g}{\sigma_g} \tag{2.6}$$

Failure probability can then be written as:

$$p_f = P\left[g'(0) \leq 0\right] = \Phi\left(\frac{-\mu_g}{\sigma_g}\right) \tag{2.7}$$

Where Φ is the cumulative distribution for a standard gaussian variable. The Cornell Safety Index, $\beta_C =$, was suggested in 1969 as:

$$\beta_C = \frac{\mu_g}{\sigma_g} \tag{2.8}$$

Combining this safety index with the probability of failure as expressed by equation 2.11 gives the relation:

$$P_f = \Phi(-\beta_C) = 1 - \Phi(\beta_C) \tag{2.9}$$

It can be shown that this relation holds for normal random load and resistance variables when the safety margin is linear. It can also be used as an approximation when the limit state function is non-linear by Taylor-expansion about a point on the failure surface and including only the 1^{st} order terms. The drawback of using the Cornell Safety index in these cases is that the safety index depends highly on the choice of linearization point and the choice of failure function [29]. The consequence becomes that different safety indices will be attained for the same structure when using different but equivalent safety margin definitions.

2.2.2. Hasofer-Lind Safety Index

In the previous section, the safety margin was denoted $g = R - S$. To generalize, it is now written as $g(x_1,\ x_2,\ \ldots\ x_n)$ where the variables x_i are normally distributed and independent. The failure limit is defined as $g = 0$. As mentioned previously, a failure surface can be described by many different, but equivalent, safety margins. How can the design point and the safety index be accurately approximated so that the results are equal for all equivalent limit state functions? Hasofer and Lind proposed a geometrical interpretation, stating that the design point and the corresponding safety index is approximated directly from the point on the failure surface closest to the origin (in standardized coordinates). Mathematically, the design coordinates , $z_i^\star$, at the design point is thus expressed as in equation 2.10.

$$[z_1^\star,\ z_2^\star,\ \ldots\ z_n^\star] = min\left(\sum_{i=1}^{n} z_i^2\right) \tag{2.10}$$

where z_i is the standardization of the i^{th} random variable X_i. Such a standardization is of the form (equivalent to eq. 2.5):

$$z_i = \frac{x_i - \mu_{X_i}}{\sigma_{X_i}} \tag{2.11}$$

The solution of equation 2.10 is now a question of optimization so that the RHS is sufficiently minimized. There are many different procedures for such problems. Thoft-Christensen & Baker [29] suggest the following algorithm:

$$\alpha_i = \frac{-\frac{dg}{dz_i}(\beta\bar{\boldsymbol{\alpha}})}{\sqrt{\sum_{k=1}^{n}\left(\frac{dg}{dz_k}\beta\bar{\boldsymbol{\alpha}}\right)^2}} \quad , \quad i = 1,\ 2,\ \ldots\ n \tag{2.12}$$

where $\bar{\boldsymbol{\alpha}} = [\alpha_1\ \alpha_2\ \ldots\ \alpha_n]$ represents a unit vector in the direction of the approximated design point so that $\bar{\mathbf{z}}^\star = \beta\bar{\boldsymbol{\alpha}}$. The individual components, α_i of this unit vector are commonly abbreviated *sensitivity factors* since they represent the relative importance of the corresponding random variable when considering failure. To be able to solve for all vector components and the safety index, one more equation is needed. Fortunately, the demand that the safety margin is equal to zero on the failure surface is yet to be utilized. By re-writing all the standardized variables on vector form, it can be solved for the safety index β.

$$f(z_1^\star,\ z_2^\star,\ \ldots, z_n^\star) = g(\beta\alpha_1,\ \beta\alpha_2,\ \ldots, \beta\alpha_n) = 0 \tag{2.13}$$

Equations 2.12 and 2.13 are now to be evaluated at a "guessed" design point. A new design point is found, which will be used as input for the next iteration step. With the safety index sufficiently converged, the approximate probability of failure can now be found as in equation 2.9, even for non-linear safety margins.

2.3. Concluding remarks on Level II methods

It should be noted that all preceding subjects of this chapter are approximations based on linear approximation of the failure curve/surface. I.e the theory is based on a Taylor expansion of the full limit state function where only the first-order terms are included in the calculations. Hence they belong to the category "First Order Reliability Methods", or FORM.

Indeed, for a curved surface these approximations might be questionable. Second Order Reliability Methods (SORM) are based on the same concepts, but uses a quadratic approximation which would then follow a curve/curved surface more closely than a tangential line. This method will not be described further in this thesis. However, the Level III-methods in the following chapter can still be applied with sufficient accuracy to such problems.

It has been shown how the design point and the corresponding safety index can be found (or approximated) for most cases of practical relevance. As can be noted, all Level II methods are, in essence, easily computed. However, for complex safety margins and variables of different distributions, the necessary transformations and differentiations might be tedious.

The results are subjected to optimization errors, especially in the case of non-linear safety margins. It must also be considered that the Hasofer-Lind safety index and it's associated computation algorithms does not necessarily give the correct design point, only local minima in the region of the first guessed sampling points. Hence, for failure surfaces with more than one such "local design point", it can be difficult to ensure that the global design point is found.

2.4. Level III - Transformations

2.4.1. Non-normal independent random variables

Until this point, it has been assumed that all random variables used in the safety margin are normally distributed. This is rarely the case in reality. Environmental loads, material properties and other governing circumstances can belong to a wide range of probability distributions.

However, as long as the distribution of all participating variables are known (or can be approximated in a sensible way), the Hasofer-Lind safety index can still be applied if some steps are added to the process, as described by Rackwitz and Fiessler [27]. First, the original distribution must be mapped onto the normal space. Let x_i be a random variable belonging to any non-normal distribution. x_i is now thought of as normally distributed about the *design point* and will maintain it's original value exactly at the design point. As any normal random variable, X_i can also be standardized:

$$z_i' = \frac{z_i - \mu_i'}{\sigma_i'} \tag{2.14}$$

The unknowns here, to be treated later, are the mean (μ_i') and variance (σ_i') of this approximate normal distribution . If F_{X_i} is the true distribution of the original variable, the approximation becomes:

$$F_{X_i}(x_i) \approx \Phi(z_i') = \Phi(\frac{x_i - \mu_i'}{\sigma_i'}) \tag{2.15}$$

By the inverse of eq. 2.15, the approximation of x_i as a standard gaussian variable is given by eq. 2.16.

$$z' \approx \Phi^{-1}\left[F_{X_i}(x_i)\right] \tag{2.16}$$

Differentiation of both sides of eq. 2.15 yields:

$$\frac{d}{dx_i}\left(F_{X_i}(x_i)\right) = \frac{d}{dx_i}\left(\Phi\left(\frac{x_i - \mu_i'}{\sigma_i'}\right)\right) \rightarrow f_{x_i}(x_i) = \frac{1}{\sigma_i'}\phi\left(\frac{x_i - \mu_i'}{\sigma_i'}\right) \tag{2.17}$$

The right hand term of the above equation along with 2.15 gives two useful relations containing the unknown approximative values for mean and variance. The solutions become:

$$\sigma_{X_i}' = \frac{\phi\left(\Phi^{-1}\left(F_{X_i}(x_i)\right)\right)}{f_{X_i}(x_i)} \tag{2.18}$$

$$\mu_{X_i}' = x_i - \Phi^{-1}\left(F_{X_i}(x_i)\right)\sigma_{X_i}' \tag{2.19}$$

With the exception that μ' and σ' must be updated for each iteration step, the procedure described by equations 2.12 and 2.13 can now be applied.

2.4.2. Correlated variables

It has been shown how the safety index can be found for independent variables belonging to any distribution. In a practical sense, correlation can easily be motivated as a common fact among both load and resistance variables.

How can the same be achieved when such correlation between the variables exists? Indeed, to be able to use the Hasofer-Lind Safety index, even the correlated random variables must be transformed to the space of standardized, independent normal random variables. There are two main ways to achieve this [13]:

- **Rosenblatt transformation**-When the full scope of joint probability distributions are explicitly known.
- **Nataf transformation**-When only marginal distributions and correlation matrices are known.

The knowledge of the full joint probability distribution is not very common in practical applications. And, when it is known, it somewhat reduces the benefits of using level II methods on behalf of level III, which are yet to be described. Thus, the focus of this section will be on the transformation method of Nataf. Consider the correlated set of random variables $\mathbf{x} = [x_1\ x_2 \ldots x_n]$, with mutual correlation coefficients ρ_{ij}. These coefficients are then assembled in the $n \times n$-matrix $\boldsymbol{\rho}_X$:

$$\boldsymbol{\rho}_X = \begin{bmatrix} 1 & \rho_{X,12} & . & \rho_{X,1n} \\ \rho_{X,12} & 1 & . & \rho_{X,2n} \\ . & . & . & . \\ \rho_{X,1n} & \rho_{X,2n} & . & 1 \end{bmatrix} \tag{2.20}$$

As discussed in section 2.4.1, these sets of variables are approximated by $\mathbf{z} = [z_1\ z_2 \ldots Z_n]$ in the space of standardized normal random variables. The correlation coefficients of the substituted variables are denoted ρ'_{ij}. The transformation becomes:

$$F_{\mathbf{X}}(\mathbf{x}) = \Phi(\mathbf{z}) \rightarrow \mathbf{z} = \Phi^{-1}\left[F_X(\mathbf{x})\right] \tag{2.21}$$

The approximate joint density function becomes:

$$f_{\mathbf{x}}(\mathbf{x}) = \phi(\mathbf{z}, \boldsymbol{\rho}'_{ij})\,|\mathbf{J}| \tag{2.22}$$

There is now a need for the explicit expression of $\phi(z_i, z_j; \rho'_{ij})$. According to the definition of a standard normal PDF, it is written:

$$\phi_2(z_1, z_2, \rho'_{ij}) = \frac{1}{2\pi\sqrt{1-\rho'^2_{ij}}} exp\left[\frac{z_i^2 - 2\rho'_{ij} z_i z_j + z_j^2}{2\left(1-\rho'^2_{ij}\right)}\right] \tag{2.23}$$

To find the value of ρ'_{ij}, one can consult tabulated semi-empirical formulas developed for this purpose by Liu and Der Khiureghian [14]. Alternatively, the following integral can be solved iteratively.

$$\begin{aligned}\rho_{ij} &= \int_{-\infty}^{\infty}\int_{-\infty}^{\infty}\left(\frac{x_i - m_i}{\sigma_i}\right)\left(\frac{x_j - m_j}{\sigma_j}\right)\phi_2(z_1, z_2, \rho'_{ij})\frac{f_{X_i}(x_i)f_{X_j}(x_j)}{\phi(z_i)\phi(z_j)}dx_i dx_j \\ &= \int_{-\infty}^{\infty}\int_{-\infty}^{\infty}\left(\frac{x_i - m_i}{\sigma_i}\right)\left(\frac{x_j - m_j}{\sigma_j}\right)\phi_2(z_1, z_2, \rho'_{ij})dz_i dz_j\end{aligned} \tag{2.24}$$

To create the final vector of standardized, uncorrelated normal RV's (denoted $\mathbf{Y}$), Liu and Der Khiureghian [14] states the following relation, based on Cholesky decomposition:

$$\mathbf{Y} = \mathbf{\Gamma}_0 \mathbf{D'}^{-1}\left(\mathbf{X} - \mathbf{M'}\right) \tag{2.25}$$

Where $\mathbf{\Gamma}_0$ is the lower triangular of $\boldsymbol{\rho}'$, $\mathbf{M'} = [\mu'_1\ \mu'_2 \ldots \mu'_n]$ and $\mathbf{D'}^{-1} = diag\left[\sigma'_i\right]$ are the vector of equivalent means and the diagonal matrix of equivalent standard deviations. These are solved for using equations 2.18 and 2.19.

2.5. Level III - Probability of failure methods

Until now, different approaches for approximation of the probability of failure has been discussed. What it boils down to, are different ways to work around the full probability of failure problem depending on what information is available and how the safety margin and its participating variables are expressed. In this chapter, approximate solutions to the exact probability problem shall be discussed. The safety margin (eq. 2.4) is described by main components, Load (S) and Resistance, (R). The probability of failure is defined as:

$$p_f = P\left(R - S \leq 0\right) = P\left(R \leq S\right) \tag{2.26}$$

If the load and resistance are two joint, random variables with marginal distributions distributions $f_R(r)$ and $f_S(s)$ and joint distribution $f_{RS}(r,s)$, eq. 2.26 becomes:

$$p_f = \iint_D f_{RS}(r,s)drds \tag{2.27}$$

It has been argued that both load and resistance can be composite functions of one or more random variables. If the safety margin contains n such variables $\mathbf{X} = x_1\ x_2 \ldots x_n$, it is denoted $g(\mathbf{x})$ and the complete problem becomes:

$$p_f = \int \cdots \int_{g(\mathbf{x})\leq 0} f_{\mathbf{X}}\left(\mathbf{x}\right) d\mathbf{x} \tag{2.28}$$

As might be suspected, the solution of such an n-dimensional integral will swiftly become impossible to solve with reasonable effort as n increases. And, since n for a complex structure will often be larger than what the integral can be solved for (analytically or numerically) refuge must be taken to numerical methods.

2.5.1. Monte Carlo Simulation -Direct Sampling

To find the probability of failure, we could use a sample of N structures and count the number of failures η that occur within the sample. The value of η/N would then be an approximation of the probability of failure. As N increases, the approximation will become better and better so that:

$$\frac{\eta}{N} \rightarrow p_f \quad as \quad N \rightarrow \infty \tag{2.29}$$

Of course, such samples are never physically available. However, using Monte Carlo-methods they can be simulated with reasonable accuracy. Melchers [17] proposes an indicator function:

$$I\left[g(\mathbf{x}) \leq 0\right] = \begin{cases} 1 & \text{if } g(\mathbf{x}) \leq 0 \\ 0 & \text{else} \end{cases} \tag{2.30}$$

Knowing the probability distributions of the acting variables, each of them can be simulated. Using a random number generator to attain a vector of uniformly distibuted numbers $\mathbf{r}$ of the same length as $\mathbf{x}$. Denote a sample of the i^{th} variable x_i. $\hat{x}_i$. This estimate can then be found by the inverse probability density of x_i:

$$\hat{x}_i = F_{X_i}^{-1}\left(r_i\right) \tag{2.31}$$

Having established a sample of all random variables, $\hat{\mathbf{x}}$, the safety margin can be evaluated. Consequently, a value of either zero or one for the indicator function is attained. By repeating the process N times, an estimate of p_f is found in analogy to (2.29) :

$$\hat{p_f} \approx \frac{1}{N}\sum_{j=1}^{N} I\left[g(\mathbf{x}) \leq 0\right] \tag{2.32}$$

According to sample statistics, the variance of such a sample of I is given as:

$$Var\left[I\right] = \frac{1}{N-1}\sum_{j=1}^{N}\left[I_j - \frac{1}{N}\left(\sum_{j=1}^{N} I_j\right)\right]^2 \tag{2.33}$$

The variance of the approximated probability of failure is thus:

$$Var\left[\hat{p_f}\right] = \frac{1}{N^2} Var\left[I\right] \tag{2.34}$$

From eq. 2.32 and 2.33, it can be noted that the variance of $\hat{p_f}$ decreases proportional to $\sqrt{N}$ and directly with the variance of I. Melchers [17] refers to Broding et al [3] whom suggests the following first approximate for the $\hat{p_f}$-confidence level C [%]:

$$N > \frac{-ln\left(1-C\right)}{\hat{p_f}} \tag{2.35}$$

Regardless of the accuracy of the above equation, it is obvious that the sample size will be large for accurate simulations. Considering the complexity of the equations associated with each "test", the computational efforts will therefore prove to be unmanageable [20] for complex structures and/or low probability of failures. Another important drawback of the procedure is that the design point is not explicitly found.

2.5.2. Importance Sampling

The indicator function from eq. 2.30 can be used to represent the limits in the integral of equation 2.28 as:

$$p_f = \int \cdots \int_{g(\mathbf{x})\leq 0} f_{\mathbf{X}}(\mathbf{x})\, d\mathbf{x} = \int \cdots \int I\left[g(\mathbf{x}) \leq 0\right] f_{\mathbf{X}}(\mathbf{x})\, d\mathbf{x} \tag{2.36}$$

The consequence becomes that the integration is taken over the whole domain of the variables as opposed to the failure surface, by letting only the combinations of variables leading to failure contribute to the total sum. Now, a vector of numbers from an importance-sampling probability density function, $h_{\mathbf{V}}(\mathbf{v})$, is incorporated to the integrand:

$$p_f = \int \cdots \int I\left[g(\mathbf{x}) \leq 0\right] \frac{f_{\mathbf{X}}(\mathbf{x})}{h_{\mathbf{V}}(\mathbf{v})} h_{\mathbf{V}}(\mathbf{v}) d\mathbf{x} \tag{2.37}$$

According to basic probability theory, the integral in 2.37 is the n-dimensional first moment (expected value) of $I\left[g(\mathbf{v}) \leq 0\right] \frac{f_{\mathbf{X}}(\mathbf{v})}{h_{\mathbf{V}}(\mathbf{v})}$. Thus, the probability of failure can now be approximated as a mean of a sample of this product:

$$p_f \approx \frac{1}{N} \sum_{i=1}^{N} \left\{ I\left[g(\hat{\mathbf{v}}_i) \leq 0\right] \frac{f_{\mathbf{X}}(\hat{\mathbf{v}}_i)}{h_{\mathbf{V}}(\hat{\mathbf{v}}_i)} \right\} \tag{2.38}$$

As for the direst sampling, equation 2.38 can now be evaluated by generating a series of random number vectors, $\hat{\mathbf{v}}_i$, of the uniform distribution and evaluate for the distributions $f_{\mathbf{X}}$ and $h_{\mathbf{V}}$. Since $f_{\mathbf{X}}$ is the distibutions of the random variables, it is known. $h_{\mathbf{V}}$ however, must be chosen. The steps of the procedure are as follows:

- **Locate "shift-point":** This point is found as the point of maximum likelihood of $f_{\mathbf{X}}$ on the failure surface.
- **Define importance sampling function:** According to Melchers [17], an appropriate distribution of $h_{\mathbf{V}}$ is the n-dimensional standard normal probability density function about the "shift-point".
- **Run simulation:** Generate the sequence of random numbers and evaluate eq. 2.38.

If the non-linearity of the limit state is low, with gaussian pdf as sampling function, the generated points will be shared almost equally between failure and safe domain invariant of the failure probability. This is the essential benefit of importance sampling, since it means that very low probabilities of failure can be simulated by small sets. As compared to direct sampling where the extent of the simulation grows fast with decreasing p_f. The method can, if necessary, be made more efficient. What determines the computational efficiency is the degree of proportionality between $f_{\mathbf{X}}$ and $h_{\mathbf{V}}$ in the failure domain [17]. Drawbacks of this method are that the point of maximum likelihood on the failure surface might be tedious to find and require preparatory numerical analysis, if at all identifiable. Also, similar to direct sampling, it does not give an explicit design point.

2.5.3. Directional Simulation

The integral given by eq. 2.28 descibes the reliability problem analytically. $\mathbf{x}$ is as before the vector of variables involved in the limit state function, $g(\mathbf{x}) \leq 0$. These can be transformed into standard gaussian space, $x_i \rightarrow z_i$. It was stated in section 2.2.2 that the design point is located at the point on the LSF that minimizes the problem of equation 2.10. We can write the sum on the RHS of this equation in terms of a new random variable, u:

$$u^2 = z_1^2 + z_2^2 + z_3^2 \ldots z_n^2 \tag{2.39}$$

where n is the length of $\mathbf{x}$, i.e the dimension of the reliability problem. u^2 is now χ^2- distributed with n degrees of freedom [22].

Considering an idealistic case where the LSF in standard space ($g^\star(\mathbf{z}) = 0$) is a hypersphere of radius R, the probability of failure for the problem becomes:

$$p_f = P\left[g^\star(\mathbf{z}) \leq 0\right] = P\left[R^2 - u^2 \leq 0\right] = 1 - \chi^2\left(R^2\right) \tag{2.40}$$

The contribution of failure probability from the j^{th} subdomain, when the failure domain is split in to m contributions then becomes:

$$p_{f,j} = \left[1 - \chi^2\left(R^2\right)\right] / m \tag{2.41}$$

The method of directional simulation describes how the failure probability can be approximated when the LSF is no longer a hypersphere, by utilizing the above subdomains as approximations to the actual failure surface for a set of points, "directions", on $g^\star(\mathbf{z}) = 0$. For each point, the radius to the hypersphere is written R_j. A visualization of the procedure, taken from Nie et. al [22] is shown in figure 2.3.

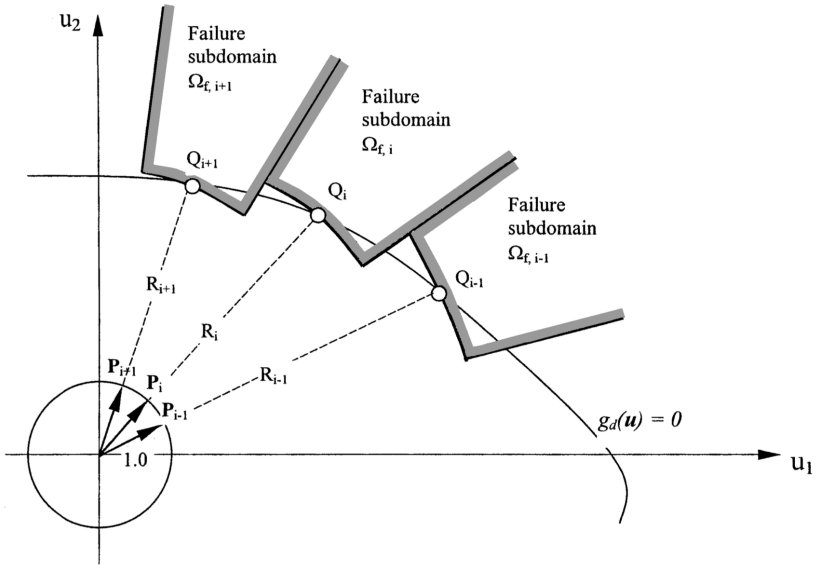

Figure 2.3: 2D-vizualization of Directional Simulation, from Nie et. al [22]

For each of these points, a new subdomain is found as:

$$p_{f,j} = \left[1 - \chi^2\left(R_j^2\right)\right] / m \tag{2.42}$$

Again, m is the number of subdomains/points. The total failure probability now becomes:

$$p_f = \frac{1}{m}\sum_{j=1}^{m}\left[1 - \chi^2\left(R_j^2\right)\right] \tag{2.43}$$

It was discussed that reliability index methods in general can converge to a false design point, since for complex failure surfaces there might be many local minima. The procedure of Directional Simulation, i.e that the failure surface is approximated over a region that can be chosen, eliminates this discrepancy. On the other hand, as for the other level III-methods described here, the design point is not found explicitly.

2.5.4. Particle Swarm Optimization

The Particle Swarm Optimization("PSO") algorithm can be applied to any optimization problem for continous functions. It was developed to model the behaviour of animal flocks or fish schools, where the individual benefit from fellow food search (and information sharing) is weighed against that any food found must be shared with the rest of the group.

The design point is, again, given by the set of coordinates in the standard gaussian space that minimizes eq. 2.10, with the restricition that this point must be on the Limit State surface. It will now be shown how PSO can be used to simulate the search of this point. To begin with, PSO is an algorithm that solves maximization problem, so the optimization mentioned must be rewritten to such a form. There are numerous approaches to achieve this. It will not be discussed in detail here, hence we will assume a transformation so that the problem now consists of maximizing $H(\mathbf{x})$

As before, the reliability problem is of n dimensions. Now a set of T_{pop} individuals will be generated to manouver this n-dimensioned space until they "find" the design point. To perform this, two parameters will be assigned to each individual; *fitness* and *velocity*. Fitness, in this case, ranks the individuals depending on their distance from origo. For two individuals, x_a and x_b, and a fitness function H, this means that x_a is better then x_b when $H(x_a) > H(x_b)$. The velocity is calculated for each of the $j = 1,\ 2,\ 3,\ \ldots\ n$ dimensions, and each of the $i = 1,\ 2,\ 3,\ \ldots\ T_{pop}$ individuals. For the h^{th} iteration step it is calculated from:

$$V_{ij}^{(h+1)} = wV^{(h)} + c_1 r_1 \left(P_{ij}^{(h)} - I_{ij}^{(h)}\right) + c_2 r_2 \left(P_{gj}^{(h)} - I_{ij}^{(h)}\right) \tag{2.44}$$

where r_1 and r_2 are samples from a uniform distribution on the interval (0,1), refreshed at each iteration. c_1, c_2 are deterministic parameters and w is the inertia parameter. Furthermore, I^0 is a matrix of size $\left(n, T_{pop}\right)$. Each row contain uniform random numbers on the interval that defines the search interval for the i^{th} parameter. In words, $I^{(h)}$ is then the matrix that holds the coordinates of each individuals position. $P_{ij}^{(h)}$ is the best position that each individual has taken so far. $P_{gj}^{(h)}$ is the best position any individual has taken.

The LHS of eq. 2.44 is composed of three terms. The first can be thought of as the inertia term. It states how much inertia is carried from the previous step, i.e the ability for the individuals to change direction upon retrieval of new information. Small w means good "maneuverability", large w means a larger contribution from velocity history. By these reasons, small and large w optimizes the algorithm to search for local and global maxima, respectively. A tradeoff is often suggested so that w is in the region between 0.8 and 0.9 [10].

The next term, as described by Elegbede [10], is the "individual experience". It states how the individual has improved it's position throughout the simulation. The last term is the "group experience", where the entire set of individuals are compared to the best result so far.

c_1 and c_2 have a typical optimal value for each problem, but as a reference Elegbede [10] suggest a value below half of the search space domain. Otherwise, the particles tend to leave the search domain regularly.

The term velocity in this case becomes a bit misleading and should rather be seen as the change of position from one step to the next according to:

$$I_{ij}^{(h+1)} = I_{ij}^{(h)} + V_{ij}^{(h+1)} \tag{2.45}$$

The procedure is now repeated until a given convergence criteria is met.

Comparing to the other level III-methods described here, PSO is the only one giving an explicit design point. When compared to FORM, a first-order algorithm, PSO requires no differentiations and should thus be easier to implement. In addition, it recovers the global solution whereas FORM might only give a local (false) design point. For the typical population sizes, ranging from 20 to 100 [10], this method requires small computational efforts due to the small matrix sizes and the fact that only a few random numbers have to be drawn for each iteration. Also, the typical number of iterations required is relatively small.

2.5.5. Optimized Fitting

The method of optimized fitting, suggested by Naess et. al [19], is based upon the introduction of a variable λ that can take any number between zero and one. The safety margin is then rewritten to take account of this parameter as:

$$g(\lambda) = g - \mu_g (1 - \lambda) \quad 0 \leq \lambda \leq 1 \tag{2.46}$$

Thus, the original safety margin is given as $g(1)$. The failure probability is then suggested as:

$$p_f(\lambda) \approx q(\lambda) exp\left\{-a(\lambda - b)^c\right\} \quad \text{as} \quad \lambda \to 1 \tag{2.47}$$

Where q is a function that varies slowly with λ compared to the exponential term. The method of optimized fitting is then based on the assumption that this failure probability has a regularity in λ. This implies that the simulations can be done in a certain interval of lambda, and interpolated towards higher values. Higher values of λ, i.e in the region of 1, gives a low probability of failure. Low failure probabilities requires a larger computational effort to converge as compared to the same system with higher failure probability. Hence, effort will be saved if the simulations can be restricted to the regions of high failure probability. Since $q(\lambda)$ is a slowly-varying function, and the region of interest is when λ approaches unity, it is approximated as a constant that fits well with the tail values of λ. The coefficients $q,\ a,\ b,\ c$ are now found from log-level mean square minimaziation of the following expression:

$$F(q,\ a,\ b,\ c) = \sum_{j=1}^{M} w_j \left[log\left(\hat{p_f}(\lambda_j)\right) - log(q) + a\left(\lambda_j - b\right)^c\right] \tag{2.48}$$

Here, w_j is a weight factor that puts more emphasis on the more "certain" data points, whereas $\lambda_0 \leq \lambda_1 < \ \ldots\ < \lambda_M$ are points where the failure probability is empirically estimated. Writing $y_j = log\left(\hat{p_f}(\lambda_j)\right)$ and $x_j = \left(\lambda_j - b\right)^c$ with b and c as constants, the optimal values of a and q can be found from linear regression as:

$$a^\star(b,c) = -\frac{\sum_{j=1}^{M} w_j \left(x_j - \bar{x}\right)\left(y_j - \bar{y}\right)}{\sum_{j=1}^{M} w_j \left(x_j - \bar{x}\right)} \tag{2.49}$$

and

$$log\left(q^\star(b,c)\right) = \bar{y} + a^\star \bar{x} \tag{2.50}$$

These values can now be used in a Levenberg-Marquardt solution of eq.2.48 [19].

The simulations as such are, as mentioned, done for the points mentioned above, i.e $\lambda_0 \leq \lambda_1 < \ \ldots\ < \lambda_M$ which forms the basis for the fitting. Also, the weight points must be determined. This can be done in different ways and will not be explained in detail here. When these steps are performed, a relation is attained that can be used to find approximate failure probability in the upper tail of λ without actually having to simulate it.

2.6. Response Surface Methods

In many physical problems, an explicit expression for the limit state is not known. Other times, it exists but is not on closed form or has a complexity that makes it inconvenient or impossible to evaluate e.g the partial derivatives required for Hasofer-Lind reliability index computation as described by section 2.2.2.

Commonly, structural behaviour is evaluated through commercial finite element codes. In such cases, the response is not known but can be evaluated at discrete points for combinations of the random variables. From these samples, an expression for the safety margin can be formed by regression or interpolation so that the probability of failure can be evaluated from any of the methods described previously. The approximate polynomial for the structural response in terms of the random variables in such a way is commonly abbreviated *response surface*.

It must often be considered that each of the sampling points require some extent of computational effort, depending on model and solution techniques, which might act highly restrictive on the number of points that can be obtained within reasonable cost. It is often stated in the literature that the safety margin can be described by a second order polynomial due to generally low curvatures, especially in the vicinity of the design point [17], [5]. Even so, the regression of a full second order polynomial requires a large set of samples. For n random variables, the size v of the set of samples required for unique determination of all coefficients becomes $v = 1 + n + n(n+1)/2$.

Any reliability method is highly sensitive to the description of the limit state in the region of the design point, since this is where the density of failure probability is at its largest. Thus, the polynomial should accurately model the safety margin especially in this part of the n-space of random variables. When this location is not known beforehand, and the fact that each sampling point is computationally demanding, it becomes obvious that sampling the safety margin arbitrarily for a full second-order polynomial is highly inefficient. A more suitable approach would be to incorporate some a priori knowledge into the sampling procedure to make it more efficient and minimize the lack of fit from the regression close to the design point. A vast number of such improved response surface methods has been developed, from which a selection will be presented in the following sections.

2.6.1. Bucher-Bourgund Response Surface

The following technique was suggested by Bucher and Bourgund [4]. Here, cross-terms are excluded from the second order polynomial description of the safety margin, decreasing the number of coefficients to be determined substantially. The suggested polynomial thus become:

$$\bar{g}(\mathbf{x}) = a + \sum_{i=1}^{n} b_i x_i + \sum_{i=1}^{n} c_i x_i^2 \tag{2.51}$$

where $\bar{g}$ is an approximation of the safety margin. a, b_i and c_i are coefficients of corresponding variable x_i It follows that a set of $v = 2n + 1$ sampling points are required for determination of all coefficients. The sampling procedure is based on variables expressed as uncorrelated, normally distributed with mean and standard deviation μ_i and σ_i respectively. A spread factor f_i is assigned each variable. A sample is then taken at a central point located at the mean for all random variables, and support points are calculated at $x_i = \bar{x}_i \pm f_i\sigma_i$. The resulting sample size becomes $2n + 1$ which correspond to the required number of samples for unique determination of the polynomial of equation 2.51. Once $\bar{g}$ is established, a first estimate of the design point can be searched e.g by FORM. The actual safety margin,g, is now evaluated at the approximate design point and a linear interpolation is performed to set the new center point:

$$\mathbf{x}_m = \bar{\mathbf{x}} + (\mathbf{x}_D - \bar{\mathbf{x}}) \frac{g(\bar{\mathbf{x}})}{g(\bar{\mathbf{x}}) - g(\mathbf{x}_D)} \tag{2.52}$$

The reason for this interpolation, rather than just setting the design point as the new center point, is to ensure that it is taken sufficiently close to the actual limit state. Sampling is now repeated to form a new response surface, which is used as the basis for reliability analysis by any suitable method. An example of the exact limit state, along with the response surface and the corresponding sampling points is shown in figure 2.4.

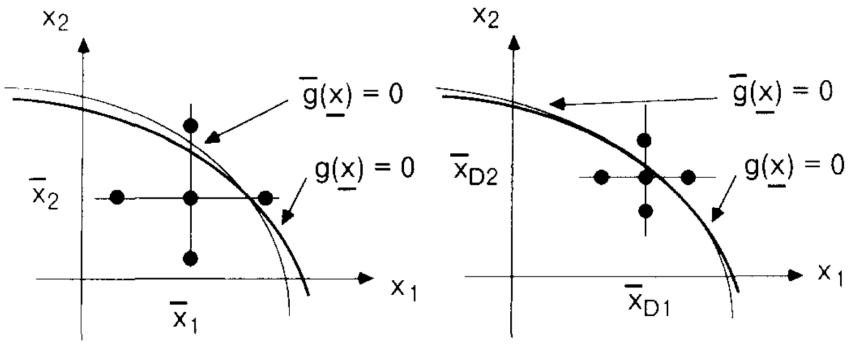

Figure 2.4: Response surface approach of Bucher-Bourgund, figure from [4]. Left side shows the limit state for sample set centered about the means, right hand side indicates the final result.

The resulting number of sampling points required for the reliability analysis becomes $4n + 3$. If the description of the safety margin using expression 2.51 is deemed inaccurate, it can be expanded by including cross terms:

$$\bar{g}(\mathbf{x}) = a + \sum_{i=1}^{n} b_i x_i + \sum_{i=1}^{n} \sum_{j \neq i} c_{ij} x_i x_j + \sum_{i=1}^{n} d_i x_i^2 \tag{2.53}$$

Expanding the polynomial as above has the consequence of more sampling. The polynomial description above would require $\frac{1}{2}n(n-1)$ additional sampling points as compared to 2.51. If necessary, also the second order cross terms could be included to attain a full quadratic polynomial.

Response surfaces found according to the method described in this section gives relatively small samples sets and still sufficient accuracy in the region of the design point, especially if the pure quadratic polynomial description (eq. 2.51) is deemed accurate. An obvious drawback of uniquely determined polynomials is that eg. ANOVA (Analysis of Variance) of the regression coefficients cannot be performed. It should also be noted that the accuracy of the response surface will be problem-dependent.

The method as described in the original article relies on the factors controlling the sampling point distance from the center point, f_i, that are somewhat arbitrary. Their values must be considered for each individual problem, which might lead to further uncertainty in the results. According to Rajashekhar and Ellingwood [28], experience shows that setting $f_i = 2$ for the first iteration and $f_i = 1$ for the second gives sufficient accuracy for most problems. This leads to a large coverage for the first sampling set, and a second set with more narrow spread about the design point. Thus, the important region (in the vicinity of the design point) will be described more accurately.

2.6.2. Improved Response Surface by Vector Projection

Kim and Na [15] argues that the procedure of section 2.6.1 might not guarantee convergence towards the correct design point and that the exact safety margin might have any shape, so that a second order approximation might not represent the curvature correctly. Instead, a perturbation technique based on vector projection of the limit state is suggested, which can be used as an expansion of the FORM-algorithm for cases when nonlinearity is suspected to influence the results. The basic idea is to use a strictly linear response surface, and shift the sampling points at each iteration so that the distance between approximate and analytical design point decreases for each step.

The method will now be briefly described. A first sampling set is taken at points $\mu_i \pm f_i\sigma_i$. From this set, a linear response surface is found according to:

$$\bar{g}(\mathbf{x}) = a + \sum_{i=1}^{n} b_i x_i \tag{2.54}$$

The design point is evaluated and defines the center point for the next sample set. The algorithm is started by finding the new sampling set based on projected unit vectors for each basic variable, δ_i. These are defined as:

$$\delta_j^i = \frac{h_j^i}{\sqrt{\sum_{k=1}^{n} \left(h_k^i\right)^2}} \tag{2.55}$$

where $\mathbf{h}_i$ are found from:

$$\mathbf{h}^i = \mathbf{u}^i - \mathbf{\Delta g}' \left(\mathbf{\Delta g}'^T \mathbf{u}^i \right) \tag{2.56}$$

Vectors $\mathbf{u}^i$ are defined as:

$$\mathbf{u}^i = \begin{bmatrix} e_1 & e_2 & \dots & e_n \end{bmatrix}^T \begin{cases} e_k = 1 & \text{if } k = i \\ e_k = 0 & \text{if } k \neq i \end{cases} \tag{2.57}$$

$\mathbf{\Delta \bar{g}}$ is the vector of partial derivatives at the design point:

$$\mathbf{\Delta \bar{g}} = \begin{bmatrix} \frac{d\bar{g}}{dx_1} & \frac{d\bar{g}}{dx_2} & \dots & \frac{d\bar{g}}{dx_n} \end{bmatrix} \mathbf{x}_D \tag{2.58}$$

The new, perturbed sampling set is then found from:

$$\mathbf{x}_S^i = \mathbf{x}_D \pm f_i \sigma_i \sqrt{n-1} \boldsymbol{\epsilon}^{i^T} \delta^i \tag{2.59}$$

The vector $\boldsymbol{\epsilon}^i$ contains the perturbation weights:

$$\boldsymbol{\epsilon}^i = \begin{cases} 1 & \text{if } k = i \\ 0.9 & \text{if } k \neq i \end{cases} \tag{2.60}$$

The process described above can now be repeated until acceptable convergence is achieved.

The only term that remains to be discussed are the sample spread, controlled by the factor f_i. These should be chosen with consideration of the curvature. Kim and Na suggests that the safety index is evaluated for $f = 1.0$ and $f = 1.5$. The following relation is then evaluated:

$$\Delta = \frac{|\beta_{1.0} - \beta_{1.5}|}{n - 1} \tag{2.61}$$

Where Δ is the nonlinearity index, which indicates the level of curvature on the analytical limit state. A final analysis (if necessary) is then performed by choosing f_i according to:

$$f = \begin{cases} 1.0 & \text{if } \Delta \leq 0.03 \\ 1.2 & \text{if } 0.03 < \Delta < 0.06 \\ f_{opt} & \text{else} \end{cases} \tag{2.62}$$

f_{opt} is found from the following figure:

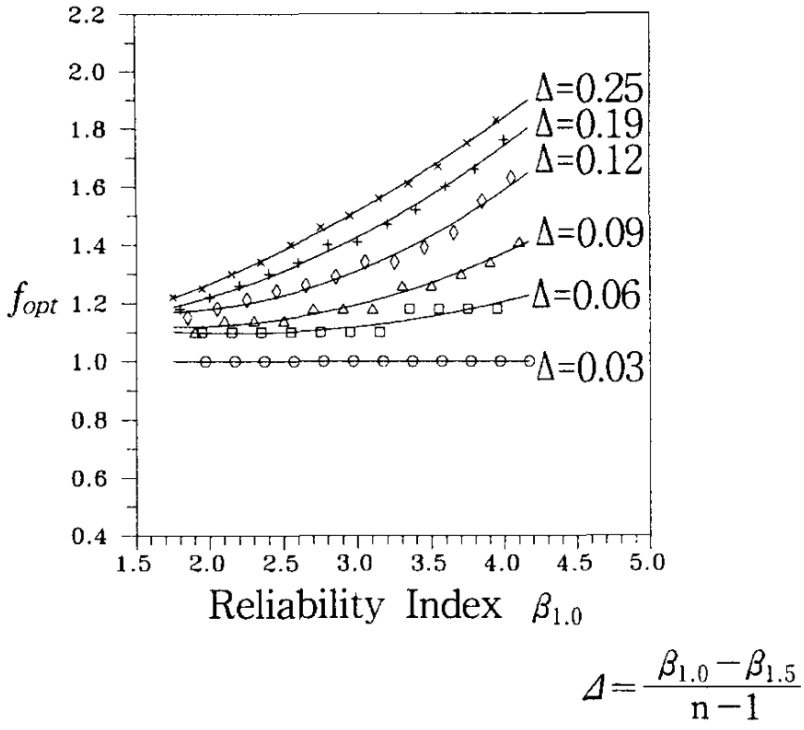

Figure 2.5: Spread factors for the vector projection algorithm, figure from Kim and Na [15]

If the original sampling points were chosen as $\mu_i \pm f_i\sigma_i$ it can be shown that equation 2.59 perturbs the sampling points towards/away from the origin in standardized coordinates.

2.7. Time-Dependent Reliability

All theory presented previously is based on so-called time-invariant reliability, implying that the probabilistic descriptions of structural resistance and applied loads are constant over time. However, these properties might be subject to changes over the service life. Structural resistance can be affected by fatigue deterioration (the occurence of cracks), corrosion or other effects. Loading can vary both discretely (e.g sudden changes in loading conditions for ships and offshore structures) or continuously as with waves and wind. The general expression of time dependent failure and corresponding safety margin can thus be written as:

$$p_f(t) = P\left[R(t) \leq S(t)\right] \tag{2.63a}$$

$$G(t) = R(t) - S(t) \tag{2.63b}$$

In terms of stochastic processes, the problem can be described by the safe domain D and the vector of time-dependent random variables, $\mathbf{X}(t)$:

$$p_f(t) = 1 - P[N(t) = 0 | \mathbf{X}(t = 0) \in D] P\left[\mathbf{X}(0) \in D\right] \tag{2.64}$$

where $N(t)$ defines the number of outcrossings of the vector $\mathbf{X}$ from D into the failure domain.

An assumption used previously in this thesis is that failure probabilities in structural reliability problems are generally small. When failures are rare, the outcrossings from the safe domain D are expected to be few and separated in time. The failure events can then be assumed as mutually independent and approximated by the Poisson distribution. It can also be noted that the only interesting outcrossing is the one that occurs first in time, a fact that becomes very beneficial. By the Poisson distribution, the probability of zero outcrossing in the time interval $[0, t]$ is:

$$P\left[N(t) = 0\right] = \frac{(vT)^0}{0} e^{-vt} \tag{2.65}$$

where $p_f(0, t_L)$ is the probability of failure at initial loading and v is the failure rate. It should be noted that this assumption becomes gradually less accurate with time if resistance deterioration is included, since failure events will become more and more common as $t \to \infty$.

Since the term $P\left[\mathbf{X}(0) \in D\right]$ in 2.64 is equivalent to $1 - p_f(0)$, the time variant failure probability, with first-loading failure included, becomes:

$$p_f(t) = 1 - \left[1 - p_f(0)\right] e^{-vt} \tag{2.66}$$

An upper bound for the failure probability can now be established by noting that $vt > 1 - e^{-vt}$ so that:

$$p_f(t) \leq p_f(0) + \left[1 - p_f(0)\right] vt \tag{2.67}$$

In order to apply formulas 2.66 and 2.67, the outcrossing rate, v, remains to be determined.

If $\mathbf{X}(t)$ is a stationary vector process, the outcrossing rate from a domain D can be found from:

$$v = \int_D E(\dot{X}_n | \mathbf{X} = \mathbf{x})^+ f_{\mathbf{X}}(\mathbf{x}) d\mathbf{x} \tag{2.68}$$

The above integral can be extended to cases where D varies with time as for structural deterioration. However, it is not easily evaluated. By this reason, it is commonly transformed into a time-invariant problem so that numerical solutions as described by section 2.5 can be applied.

As mentioned, failures are usually rare. It follows that commonly occuring load magnitudes cannot trigger an outcrossing. The first step in such a transformation is thus to substitute each load process by a random variable from a suitable extreme-value distribution.

2.7.1. Hazard rates

Time-dependent reliability, especially for aging structures, is commonly evaluated from the *hazard function*. First, a function that describes the cumulative distribution of structural life T, the unconditional failure rate, [17] is defined:

$$F_T(t) = P\left[T < t\right] \tag{2.69}$$

The usefulness of the hazard rate lies in the ability to predict the failure probability in a given service interval in time, e.g the probability of failure in the j^{th} service year given that the structure has already survived $j - 1$ years. On probability notation for a time interval dt:

$$P\left[(T \leq t + dt) \,|\, (T > t)\right] \tag{2.70}$$

Since $P\left[T > t\right] = 1 - P\left[T \leq t\right]$, Bayes' rule can be applied to 2.70 so that:

$$\begin{aligned} P\left[(T \leq t + dt) \,|\, (T > t)\right] &= \frac{P\left[(T \leq t + dt) \cap (T > t)\right]}{P\left[T > t\right]} \\ &= \frac{P\left[t \leq T \leq t + dt\right]}{1 - P\left[T \leq t\right]} \end{aligned} \tag{2.71}$$

The hazard rate function $h_T(t)$ can now be defined as the conditional failure rate as:

$$h_T(t) = \frac{f_T(t)}{1 - F_T(t)} \tag{2.72}$$

2.8. System reliability

In the previous sections, component reliability has been discussed. Component reliability relates the probability of failure to a particular failure mode described by the safety margin g. A structural system, in the present context, is defined as a structure (or a part of one) where failure can occur in m different ways described by the safety margins g_1, g_2, g_3, $\ldots$ g_m . The system fails when one or more of these safety margins are less than zero depending on how the system is defined.

It should be noted that these abbreviations are in conflict with the more physical interpretation, e.g a beam could be a structural component in the practical sense whereas here, a beam with multiple possible failure modes is considered a structural system. To separate the terms and avoid confusion, each failure possibility will in this section be denoted a *structural element*.

When loads and/or structural resistance parameters are considered as stochastic entities, different failure modes can be critical depending on the realizations of the contributing variables. Also, correlation between the corresponding safety margins might exist. Thus, the system reliability problem can not be reduced to finding the most probable failure mode and the corresponding probabilities. Instead, tools that incorporate all limit states and their mutual relations must be employed.

2.8.1. Fundamental Systems

For system reliability, the failure of one element is not necessarily the same as system failure. A definition of system failure is thus needed. First, the behaviour of each element in terms of failure properties are required. *Perfectly brittle* elements lose all load carrying capacity upon failure. *Perfectly ductile* elements maintain their capacity after failure , although deformations increase. More complex element types are commonly used but shall not be described here.

Series systems

For series systems, also known as *weakest-link* systems, system failure occurs when one or more elements fail so that failure in one element causes failure in the whole structure. For a system of n independent elements with M_i, $i = 1, 2, 3, \ldots n$ being the safety margin of the i^{th} element, the failure probability can be written as:

$$\begin{aligned} p_f &= 1 - P\left[(M_1 > 0) \cap (M_2 > 0) \cap (M_3 > 0) \cap \ \ldots \ \cap (M_n > 0)\right] \\ &= 1 - \prod_{i=1}^{n} P\left[M_i > 0\right] \\ &= 1 - \prod_{i=1}^{n} \left(1 - P\left[M_i \leq 0\right]\right) \end{aligned} \tag{2.73}$$

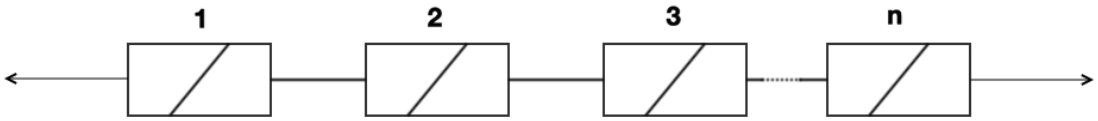

Figure 2.6: Series system of size n

Parallel systems

Redundant systems are described by a parallel model. Here, system failure requires the failure of all elements. In structural analysis, the parallel model can also be used as a subsystem to describe a failure mode, considering that one failure mode could require the simultaneous breakdown of many elements.

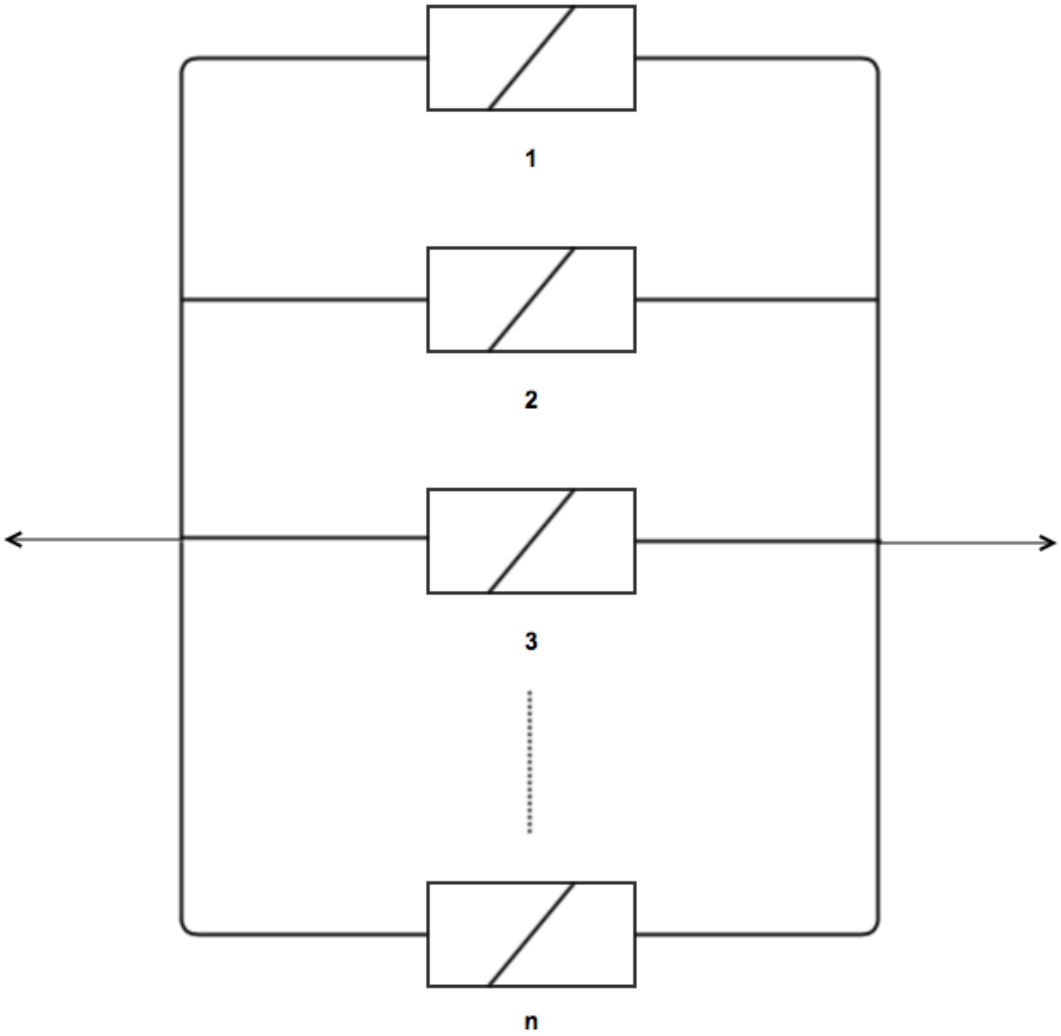

Figure 2.7: Parallel system of size n

2.9. Ditlevsen Bounds

Ditlevsen [9], suggested a reliability measure for structural systems based on so called *Narrow Reliability Bounds*, in the literature commonly abbreviated *Ditlevsen Bounds*. The theory is based on random variables in the standardized, uncorrelated, gaussian space.
A system is, as described in the introduction of this chapter, defined by a set of safety margins, g_j where $i = 1,\ 2,\ 3,\ \ldots\ m$. The corresponding failure domains are now denoted F_i and the safe domains S_i. By this, the domain of the participating random variables $\mathbf{x}$ is split into a safe part and a failure part. The failure domain and the safe domain of the entire system, respectively, is F and S.
For the evaluation of the Ditlevsen Bounds, two indicator functions are introduced:

$$I_{S_i} = \begin{cases} 1 & \text{if } \mathbf{x} \in S_j \\ 0 & \text{else} \end{cases} \tag{2.74a}$$

$$I_{F_i} = 1 - I_{S_j} \tag{2.74b}$$

The indicator function can thus take a value of zero or one, so that I_{S_j} is equal to one if the j^{th} safety margin is larger than zero. The opposite values are taken by the failure indicator F_j. The indicators for the entire system are now given the same properties and are denoted I_S and I_F. Since system failure has been defined as the event where one or more failure modes are activated, the system indicators can be found as:

$$I_S = I_{S_1} I_{S_2} I_{S_3} \ldots I_{S_m} \tag{2.75a}$$

$$I_F = I_{F_1} I_{F_2} I_{F_3} \ldots I_{F_m} \tag{2.75b}$$

This yields $I_F = 1$ and $I_S = 0$ in the event of any failure, and vice versa for the event of a random variate composition in the safe domain i.e the structure do not fail in any way.
Combining equations 2.74b and 2.75b gives, after some rearranging:

$$I_F = I_{F_1} + I_{S_1} I_{F_2} + I_{S_1} I_{S_2} I_{F_3} + \ \ldots I_{S_1} I_{S_2} I_{S_3} \ldots I_{S_{m-1}} I_{F_m} \tag{2.76}$$

According to fundamental probability theory, this equality holds also for the expected values of the indicator functions:

$$E[I_F] = E\left[I_{F_1}\right] + E\left[I_{S_1} I_{S_2} I_{F_3}\right] + \ \ldots\ + E\left[I_{S_1} I_{S_2} I_{S_3} \ldots I_{S_{m-1}} I_{F_m}\right] \tag{2.77}$$

With the properties of the indicator functions described by equation 2.74b, the following relations holds true for all $i \geq 2$ and $j < i$:

$$I_{S_1} I_{S_2} I_{S_3} \ldots I_{S_{i-1}} \leq I_{S_j} = 1 - I_{F_j} \tag{2.78a}$$

$$I_{S_1} I_{S_2} I_{S_3} \ldots I_{S_{i-1}} \geq 1 - \left(I_{F_1} + I_{F_2} + \ \ldots\ + I_{F_{i-1}}\right) \tag{2.78b}$$

As mentioned above, the indicator functions can be substituted for the corresponding expected values. Ditlevsen [9] now states that the probability of failure is equal to the expected value of the corresponding indicator function. From 2.78, when combined with 2.77, it can thus be shown that:

$$P(F) \geq P(F_1) + \sum_{i=2}^{m} \max \left\{ P(F_i) - \sum_{j=1}^{i-1} P\left(F_i \cap F_j\right),\ 0 \right\} \tag{2.79a}$$

$$P(F) \leq \sum_{i=1}^{m} P(F_i) - \sum_{i=2}^{m} \max_{j<i} P\left(F_i \cap F_j\right) \tag{2.79b}$$

Equations 2.79a and 2.79b, respectively, are now upper and lower bounds for the system failure probability. These bounds have been shown to give very narrow intervals for the failure probability when applied to highly reliable examples [9], which is often the case when structures are considered.

Chapter 3

Uncertainties in Marine Structural Analysis

Accurate reliability analysis of ships and offshore structures requires that the phenomena affecting the structural integrity throughout the lifetime is modelled correctly. For deterministic problems absolute values is sufficient but a probabilistic analysis requires more information, i.e. statistical data or hypotheses. The Joint Committee on Structural Safety [12], defines the following types of uncertainties to be considered in a reliability analysis model:

- **Intrinsic physical or mechanical uncertainty**
  -The aleatory uncertainty of the basic variables included in the model
- **Statistical uncertainty**
  -Epistemic uncertainty, arising when the statistical properties of basic variables is extrapolated from data sets.
- **Model uncertainty**
  -How well the calculation model describes the actual relation between load and response

This chapter will mainly describe the first of these three categories, i.e. ways of adressing the stochastic nature of typical load and resistance phenomena within marine/offshore structural engineering.

3.1. Limit states and failure categories

How failure is defined is the basis for the reliability analysis and a large factor in determining how accurate results will be. This definition is implemented through safety margin, as defined in section 2.2, and can be formulated according to which event one wishes to describe. To some extent, the limit state itself can be considered an uncertainty, since its definition is often only an approximation of the physical event one wishes to control. Most limit states can be prescribed to one of the following main categories [12], [8]:

- **Serviceability limit states**. Failure when the functional requirements are no longer fulfilled, e.g when:
  - Extent of deformations, vibrations, motions etc. disables the structure from fulfilling its intend purpose.
  - Local deformations/damages or fatigue cracking that requires repairs leading to a halt of operations.

- **Ultimate limit states**. Failure when the structure encounters loads in excess of its maximum load-carrying capability. In general irreversible and causes failure at the first limit state violation. Typical scenarios could be:
  - Loss of equilibrium for the whole structure, e.g overturning.
  - Exceedence of maximum load-carrying capacity for one or more members that are critical for the structural integrity.

- **Accidental Limit States**. Failure due to accidental events, e.g
  - Collisions
  - Fire/explosions
  - Operational errors

- **Fatigue limit states**. Failure due to repeated loading.

3.2. Material

Material properties of structural steel will be subject to some degree of variability that should be considered. It is distinguished between three different levels; macro, meso and micro-scale variability. At macro-scale, the variability is accounted for between different structures or components but properties are assumed constant within each subdomain. At meso-scale, variations in smaller areas are considered. A degree of correlation between a property at one point compared to another exist, which is high when these points are close and small when far apart. Micro-scale variations are typically material impurities, inhomogenities, pores and other deviations that fluctuate within ranges of centimeters down to particle size [12].

For the purpose of this thesis, it will suffice with a description of how to model the global (macro-scale) variations of the fundamental material properties. Suggested variabilities of these are shown in table 3.1. The corresponding correlation matrix is shown in 3.2.

Table 3.1: Variability for material parameters under static loading, as suggested by JCSS [12].

Property:	s_f	s_u	E	ν	ϵ_u
C.O.V	0.07	0.04	0.03	0.03	0.06

Table 3.2: Correlation matrix for macro-scale material propetry variability according to JCSS [12].

	s_y	s_u	E	ν	ϵ_u
s_y	1.00	0.75	0.00	0	-0.45
s_u		1.00	0.00	0	-0.60
E			1.00	0	0
ν		sym		1.00	0
ϵ_u					1.00

3.3. Geometry and Dimensions

3.3.1. Shape imperfections

When a structure is built, there is some degree of deviation from design to actual product. This difference can be critical and should be accounted for somehow. It is distinguished between three categories of geometrical eccentricities in structures:

- **Average eccentricity** - Translation between design and actual location of a member.
- **Out of straightness** - The curvature of a member which is designed to be straight.
- **Out of plumbness** - Angular displacements.

For steel and concrete columns, the normal distribution with mean zero is suggested by JCSS for all eccentricities. Recommended standard deviations are $0.001L$ for average eccentricity and out of straightness (measured at the point of maximum deflection), while a standard deviation of 0.0015 radians is employed for out of plumbness. For comparison, DNV tolerance requirements [7] are $0.0015L$ for out of straightness of bars, frames, stiffener web and stiffener flanges. For pillars and vertical columns, allowed initial relative translation is 0.001L.

In DNV guidelines [6] for stiffened panels, imperfections are handled implicitly by the dimensionless imperfection parameter μ, found as:

$$\mu = \left(0.34 + 0.08\frac{z_p}{i_e}\right)(\bar{\lambda} - 0.2) \tag{3.1}$$

for check at plate side, and:

$$\mu = \left(0.34 + 0.08\frac{z_t}{i_e}\right)(\bar{\lambda} - 0.2) \tag{3.2}$$

for check at stiffener side. z_t and z_p are distances from the neutral axis (for the cross-section with effective plate width) to the middle of the plate and the outermost fibre of the stiffener, correspondingly. $\bar{\lambda}$ is the reduced slenderness defined as the square root of the ratio between yield stress and Euler buckling stress:

$$\bar{\lambda} = \sqrt{\frac{s_f}{s_E}} \tag{3.3}$$

The buckling length for calculation of the Euler buckling stress is corrected for lateral pressure as follows:

$$L_k = L\left(1 - 0.5\left|\frac{p_{lat}}{p_{lat,f}}\right|\right) \tag{3.4}$$

Here, $p_{lat,f}$ is the lateral pressure required to cause yield in outer fibre at support, adjusted by a material safety factor. i_e is effective radius of gyration, given by:

$$i_e = \sqrt{\frac{I_e}{A_e}} \tag{3.5}$$

where I_e and A_e represents the moment of inertia and cross-section area for the equivalent beam. The effective width is found from:

$$\frac{b_e}{b} = C_{xs}C_{ys} \tag{3.6}$$

where b is the actual width between stiffeners. C_{xs} and C_{ys} is the reduction factor for stresses in the longitudinal and transverse directions. These are found from a comprehensive set of equations given in [6] but will not be described in detail here. The normalization of the imperfection coefficient is of the form [16]:

$$\mu = \frac{w_i A_e}{W_e} \tag{3.7}$$

where W_e is the bending resistance for effective cross-section and w_i the imperfection magnitude.

3.3.2. Dimensional uncertainty

There is no guarantee that the dimensions of a member are exactly the same as expected. There will be some extent of variation, throughout a member and between different members. The JCSS suggests a standard deviation of 3.2 % for cross-section areas and less or equal to 1 mm for height, thickness and width. These numbers are based on preliminary results from a study of beams from IPE 80 to IPE 200 [12]. The Gaussian distribution is suggested.

3.4. Environmental loads

3.4.1. Wave-induced loads

Ocean waves is a typical example of a stochastic process. Surface elevation at any time instant for a given location is thus a random quantity. By considering the vast number of factors that affect the upraising of the sea surface at a particular time instance, it follows from the central limit theorem that the gaussian distribution could be a fair assumption for this phenomenon. At least, it is widely utilized and considered a reasonably accurate model [21].

Factors such as wind, current, tide and temperature are all highly varying and affect wave characteristics. As a consequence, the statistical properties of the waves are not constant but varies over time in short time perspectives but also over the day and throughout the seasons of a year. The implication is that the surface elevation is a non-stationary process. To be able to statistically model the wave characteristics, however, the process is divided into sequences of typically 3 hours. This interval is denoted a *sea state*, and the wave process within each sea state is assumed to be stationary.

The assumptions of surface elevation as a stationary, gaussian process has been discussed. A third assumption is necessary, that the process is narrow banded. Narrow banded implies that each sea-state contains only a small interval of wave frequencies, and that there will be one, and only one, positive maxima between each crossing of the zero-level. If $v_x^+(x)$ denotes the expected number of upcrossings of any level x, then the cumulative distribution of wave peak height can be found as in equation 3.8

$$F_{X_p} = 1 - P\left[X_p > a\right] = 1 - \frac{v_x^+(a)}{v_x^+(0)} \tag{3.8}$$

For a zero-mean gaussian process, the probability density of 3.8 can be found as:

$$f_{X_p}(a) = \frac{a}{\sigma_X^2} \exp\left\{-\frac{a^2}{2\sigma_X^2}\right\} \quad a \geq 0 \tag{3.9}$$

This pdf belongs to the Rayleigh-distribution. From these results, it follows that the CDF of maximum wave height within a given time interval, $F_{M(T)}(a)$ is Gumbel-distributed [21] when a is large.

$$F_{M(T)}(a) = \exp\left\{-\exp\left(-\frac{a - \sigma_X\sqrt{2\ln\left(v_X^+(0)\,T\right)}}{\sigma_X / \left(\sqrt{2\ln\left(v_X^+(0)\,T\right)}\right)}\right)\right\} \tag{3.10}$$

The above discussion is, as stated, based on the assumption of the wave process as piecewise stationary and belong to the short-term description of the

wave field, i.e the stochastic nature of waves within such a short interval. For reliability analysis, statistics of waves and wave loads over longer time horizons might be necessary.

Long-term descriptions are often based on samples from relevant areas over large time intervals. The samples are then used to fit a distibution model. Depending on what the model should describe, different data can be extracted from the set and used for the fitting. Either all data is used, alternatively some extreme values can be extracted. Another common approach is the Peaks Over Threshold, "POT",-method where only peaks exceeding a predetermined level are used for the statistical inference. The trade-off to be considered when choosing between the aforementioned procedures is that a utilization of all data would give a larger sample for the inference, but could give a significant lack-of-fit in the tail regions. Using extreme values or POT would model extreme events better but the limited amount of data points introduces epistemic uncertainty.
A common distribution for empirical purposes, especially for extreme values of environmental phenomena, is the Weibull-model. The cumulative 2-parameter Weibull distribution is given as:

$$F_X(x) = 1 - \exp\left\{-\left(\frac{x}{\theta}\right)^{\xi}\right\} \tag{3.11}$$

where θ and ζ denote location and shape parameters, correspondingly, and $\Gamma()$ is the Gamma-function. The mean and standard deviation of a Weibull distribution are found from:

$$\mu = \theta\Gamma\left(1 + \frac{1}{\xi}\right) \tag{3.12}$$

$$\sigma = \theta\left\{\Gamma\left(1 + \frac{2}{\xi}\right) - \Gamma^2\left(1 + \frac{1}{\xi}\right)\right\}^{1/2} \tag{3.13}$$

Other distributions commonly employed for extreme, long-term wave heights are Gumbel, 3-parameter Weibull and, in cases of POT-data, the Generalized Pareto distribution [12].

3.5. Corrosion

When evaluating structural deterioration, corrosion becomes a crucial part of the analysis. Especially so when the structure, as is the case for ships and offshore structures, is exposed to highly corrosive environments. Traditionally, corrosion is described by a material loss at constant rate throughout the service life. This can be questioned. Effects such as quality of anti-corrosion measures (e.g painting, anodic protection), exposure to weather, surface treatments, material properties, hydro-chemical environment, etc. implies that a probabilistic corrosion model would be preferable. Furthermore, it should be noted that short-term and long term corrosion are predominately caused by anaerobic and aerobic chemical phenomena, respectively. Thus, measurements and models of short term effects cannot be extrapolated to the long-term case [18]. As might be suspected, accurate modelling of corrosion phenomena becomes a complex task. In this paper, the aim is not to describe details but to give a brief explanation of how corrosion can be introduced to the reliability analysis.

Generally, it is distinguished between two main types of corrosion. General and pitting corrosion. General corrosion is described as a material loss acting over the entire exposed surface so that the cross-sectional dimensions are decreased over time. Pitting corrosion, on the other hand, gives local material loss in the shape of pits which arises at multiple locations on the surface. An illustration is shown in figure 3.1.

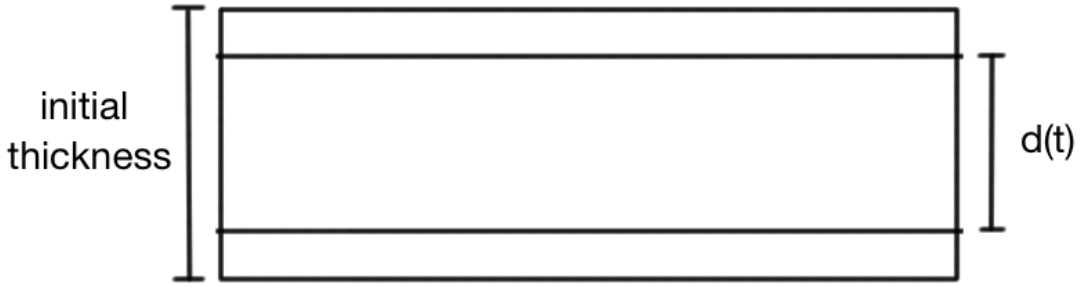

(a) General corrosion/Material loss

(b) Pitting

Figure 3.1: Corrosion

Studies have shown that the governing parameter for corrosion of submerged structures is the water temperature, T. Based on this, models for general and pitting corrosion have been suggested by Melchers [18]. These will be presented in the following sections.

3.5.1. General Corrosion

The material loss (decrease of cross-section dimensions) due to general corrosion is shown in figure 3.2. The parameters shown are described in table 3.3.

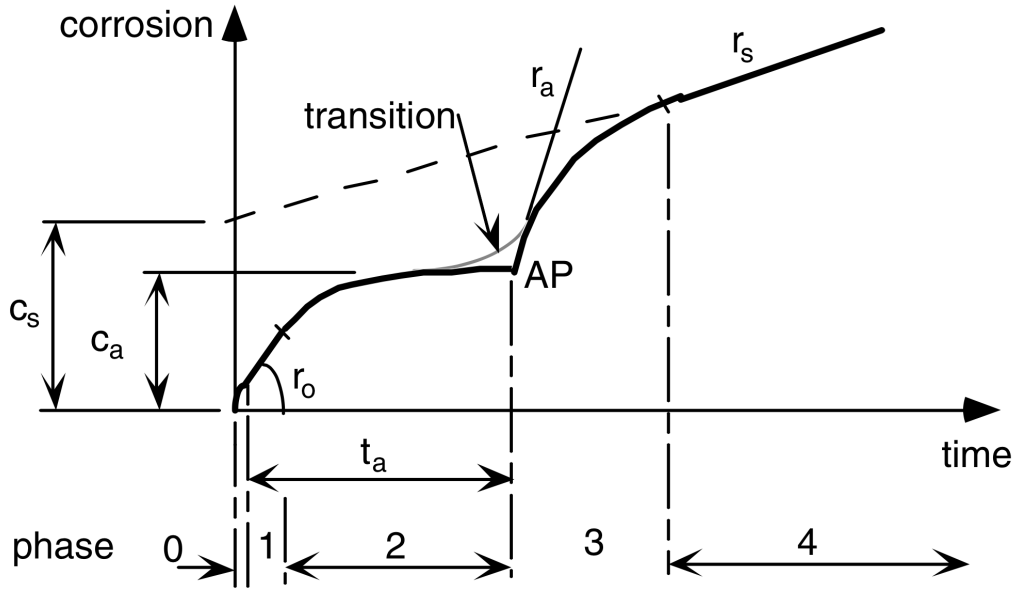

Figure 3.2: Melchers model for general corrosion of a submerged structure over time, from Melchers [18].

Table 3.3: Description of Melchers model for general (material loss) corrosion

Phase	**Description**	**Governing parameters**	**Correlation**
0	Short term initial corrosion	-	-
1	Linear corrosion governed by oxygen diffusion	$r_0 = 0.076e^{-0.054T}$	$R = 0.963$
2	Non-linear corrosion, oxygen diffusion through corrosion product layer	$t_a = 6.61e{-}0.088T$	$R = 0.99$
3	Anaerobic bacterial corrosion	$r_a = 0.066e^{0.061T}$	$R = 0.97$
4	Near linear long-term anaerobic bacterial corrosion	$c_s = 0.075 + 5678T^{-4}$	-
		$r_s = 0.045e^{0.017T}$	$R = 0.71$

3.5.2. Pitting Corrosion

Pitting depth as a function of time is shown in figure 3.3, and the parameters shown are given in table 3.4.

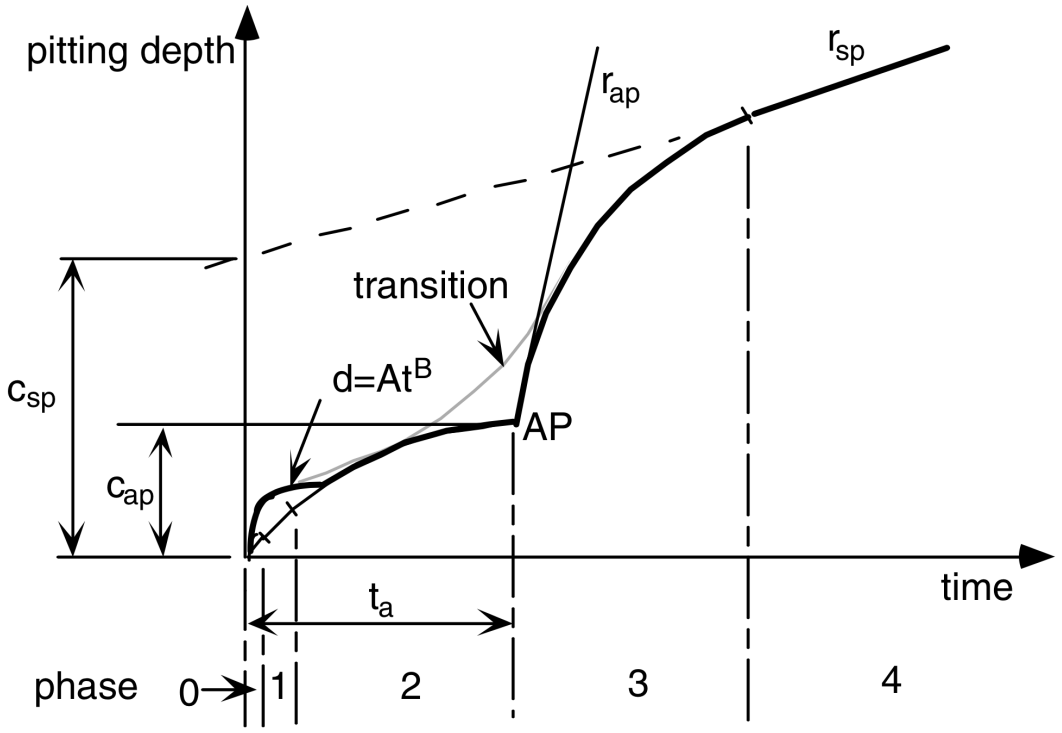

Figure 3.3: Melchers model for pitting corrosion of a submerged structure over time, from Melchers [18].

Table 3.4: Description of Melchers model for pitting corrosion

Phase	**Description**	**Governing parameters**
0	Short term initial pit growth	-
1 - 2	Aerobic pit growth	$t_a = 6.61e^{-0.088T}$
		$c_{ap} = 0.99e^{-0.052T}$
3	Rapid anaerobic pit growth	$r_{ap} = 0.596e^{0.0526T}$
4	Steady-state anaerobic pit growth	$c_{sp} = 0.641e^{0.0613T}$
		$r_{sp} = 0.353e^{-0.0436T}$

3.5.3. Applications to Reliability Analysis

An appropriate procedure would be to compare corrosion models described in the previous sections versus available data corresponding to the specific need. From this, parameters in tables 3.3 and 3.4 are treated as random variables from a suitable distribution. The example in [18] employs gaussian distributions for this purpose.

For exact treatment of corrosion phenomena, time-variant reliability is required. The loss in strength due to corrosion could then be incorporated into the model for time-dependent resistance, $R(t)$ in eq. 2.63. An estimate could be found, however, by time-invariant reliability analysis at discrete time points. This is not exact since the probability of failure at one point in time is conditional with respect to an earlier point. However, it is a valid estimate [18].

3.6. Fatigue

Any marine structure will be subject to dynamic or repeated loading. Thus, fatigue failure and crack propagations becomes important to consider. In the following, a brief outline of the general equations and their applications to reliability analysis will be presented.

Fatigue life is defined as the expected time until failure for a given structure under repeated loading. The impact of repeated loading is highly dependent on the occurrence of local stress concentrations, which in turn could arise by many reasons (e.g welding, geometry, applied loads). The response, in terms of fatigue, to such oscillating stresses depend on several material parameters (e.g modulus, impurities, yield stress, fracture toughness) that are to some extent uncertain. A full picture becomes complex with many uncertainties, which makes probabilistic analysis suitable. Typical class requirements for offshore structures prescribes fatigue lives of three or ten years, depending on whether the member is available for inspection or not [1]. Furthermore, probabilistic modelling of repeated loading can be based on damage accumulation or crack propagation (fracture mechanics).

3.6.1. Damage-accumulation models

The principle of damage accumulation is based on the well-known Palmgren-Miner Rule:

$$D = \sum_{i=1}^{n} \frac{N_i}{N_{f,i}} \tag{3.14}$$

where N_i is the number of cycles at a given stress amplitude and $N_{f,i}$ the number of cycles to failure at this stress amplitude. D is the cumulative damage for all n stress amplitudes. Failure is usually defined as $D \geq 1$, but might typically range from 0.9-1.5 [17]. The number of cycles to failure for a stress amplitude s_a with zero mean stress is commonly assumed to be on the following form:

$$N_f = K s_a^{-m} \tag{3.15}$$

Here, K and m are constants for a given material, typically found from experiments and assigned a conservative value. In a probabilistic analysis, these would rather be considered as random variables about the actual mean values. Equation 3.15 gives a linear relationship between number of cycles to failure and stress amplitude in log-log coordinates. Lately it has been found that this relation can be refined by using a bi-linear relation (two sets of constants), to better account for the material response at low stress amplitudes [30].

If the relation given by 3.15 is assumed, it could be combined with the Palmgren-Miner rule to formulate a safety margin for fatigue failure as:

$$G = D_{crit} - X_0 \sum_{i=1}^{n} K^{-1} s_{a,i}^m \tag{3.16}$$

where X_0 is a factor suggested by Melchers [17] to account for model uncertainties. Furthermore, eq. 3.16 requires that all cycles are handled individually. This becomes problematic since n would typically be treated as a random variable. The procedure could be simplified by sorting the stress amplitudes into l intervals, with the random variable N_i representing the number of cycles within each. The safety margin would then be:

$$G = D_{crit} - X_0 \sum_{i=1}^{l} N_i K^{-1} s_a, i^m \tag{3.17}$$

3.6.2. Crack-Growth models

The fatigue problem can also be adressed using Fracture Mechanics. Fracture Mechanics employs a crack growth criterion as opposed to the Palmgren-Miner rule, so that cracks are assumed to grow under repeated loading until a critical crack length, a_F, is reached. Under a given loading, a crack of this length will lead to fracture and thus failure of the component. Crack growth rate at any number of cycles N is commonly described by the Paris' law:

$$\frac{da}{dN} = C\,(\Delta K)^m \tag{3.18}$$

where a is the crack length and ΔK stress intensity range. C and m are constants. Stress intensity range is generally found from the stress range $\Delta S = S_{max} - S_{min}$ as:

$$\Delta K = F * \Delta S \sqrt{\pi a} \tag{3.19}$$

where F is a coefficient depending on the geometry and the ratio of crack size and cross-section dimension in the crack direction. As for the S-N curve, Paris' law can be transformed to a linear relation by using logarithmic coordinates. The constants C and m in e. 3.18 can then be found as the intersection and slope of this line. A graphical representation of the basic fracture mechanics phenomena is shown in fig. 3.4.

Based on the Paris' law, Wirsching et.al [31] suggest a probabilistic model for the number of cycles required for a crack to grow from length a_0 to length a as given in eq. 3.20-3.21. The basic parameters involved are shown in figure 3.4.

$$N = \frac{1}{CB^m S_e^m} \int_{a_0}^{a} \frac{dx}{G\left(x\right) Y^m\left(x\right) \left(\pi x\right)^{m/2}} \tag{3.20}$$

where:

$$G(a) = \frac{\bar{S_0^m}(a)}{S_e^m} \tag{3.21a}$$

$$\bar{S_0^m} = \int_{S_0(a)}^{\infty} s^m f_s(s) ds \tag{3.21b}$$

$$S_0(a) = \frac{\Delta K_{th}}{Y(a)\sqrt{\pi a}} \tag{3.21c}$$

Here, $\bar{S_0^m}$ is equivalent to $E\left[S^m\right]$. S_e^m is found from eq. 3.21b but with lower integral bound taken as zero.

When using a crack growth approach uncertainties are introduced. The method cannot accurately describe crack initiation time , i.e. the part of fatigue life before cracks develop, or initial crack sizes/aspect ratios. These parameters are affected by many contributing factors that are difficult to model. As remedy, SN-curves and damage-accumulation data is used to calibrate crack growth models. However, it is also argued that for fatigue problems of welded components, initiation time is small so that it can be neglected which would then be a slightly conservative approach.

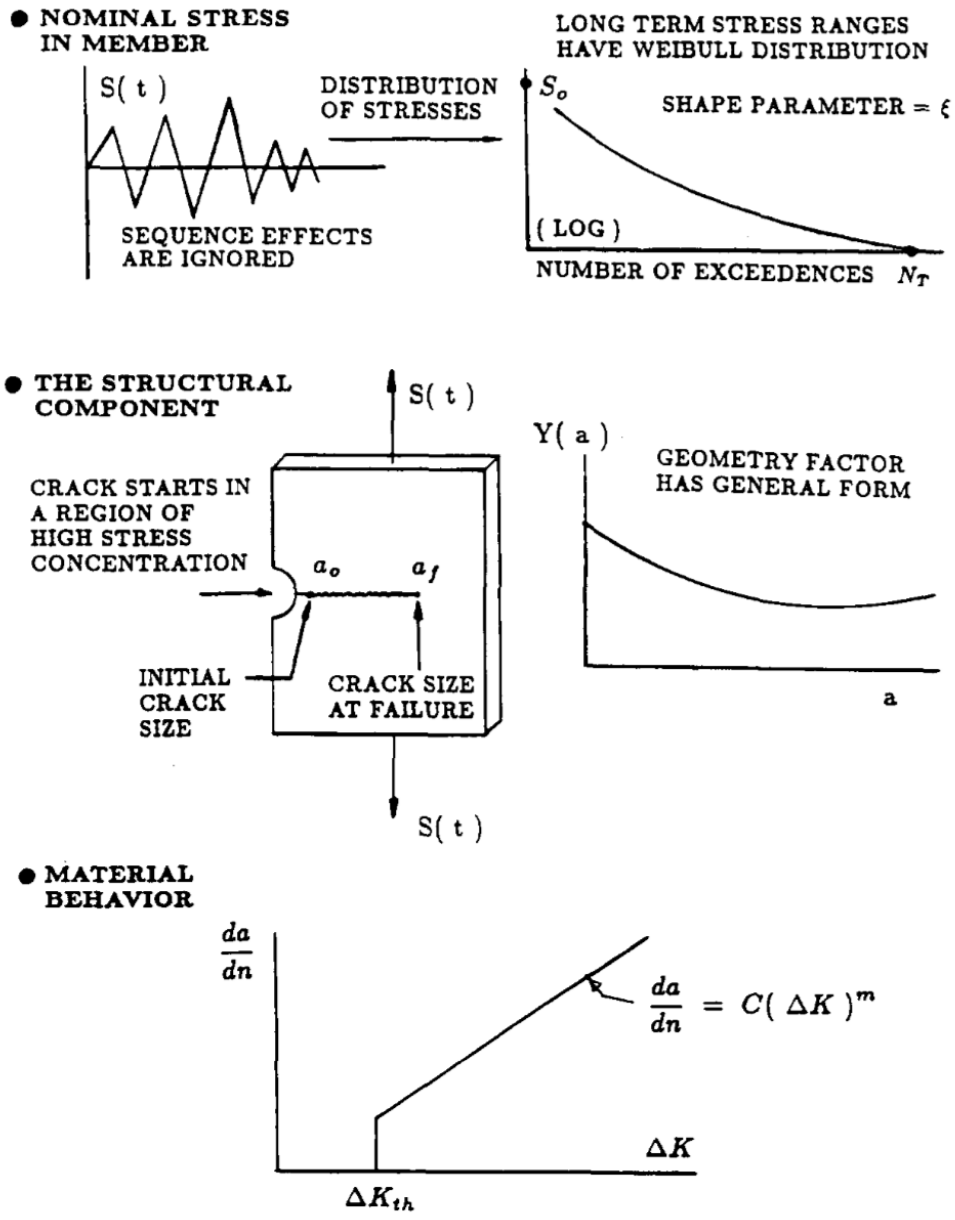

Figure 3.4: Schematic representation of basic fracture mechanics (from Wirsching et. al [31])

3.6.3. Effects of inspection and repairs

Ayala-Uraga and Moan [2] argues that effects of inspection and repair can only be modelled in an accurate way by the Fracture Mechanics approach. The reason is that damage accumulation according to Palmgren-Miner rule does not consider development of cracks and their characteristics.

When inspecting for cracks, it cannot be guaranteed that all cracks above a given size are detected. Also, inherent measuring uncertainties can cause the lower limit for detectable crack sizes to vary. By these reasons, a *Probability of Detection, POD*-curve is of often employed. The POD-curve is equivalent to a distribution function for detectable crack sizes during inspection, so that a probabilistic approach even for the inspection procedure is possible.

Chapter 4

Benchmark Study of Stiffened Panel

The example chosen for the calculations is a stiffened panel, which is perhaps the most common component in a wide range of marine structures. In ships, such panels form the basis for the hull and deck. Pontoons in semi-submersibles, walls of subsea structures are other examples. Reliability computations are preceeded by a benchmark study of the plate, in order to form a basic understanding of the problem and a starting point for further analysis.

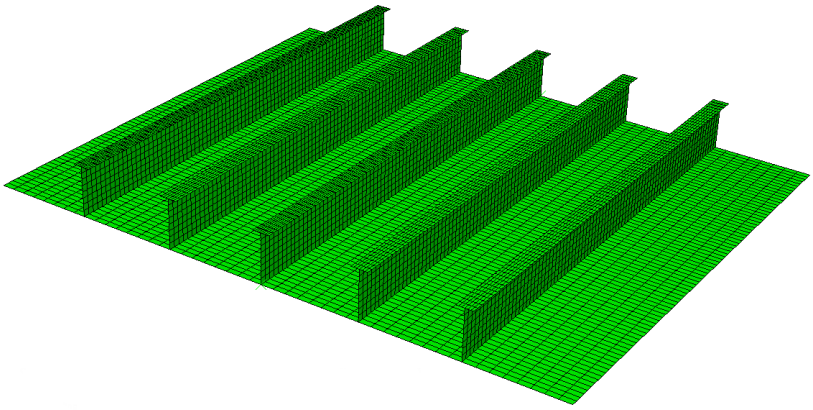

Figure 4.1: Stiffened panel.

4.1. Stiffened plate failure - definitions

The theory of plate mechanics is widely described in the literature, with respect to a vast variety of phenomena. This chapter aims to give a brief description of the most relevant theory considering the calculations performed in this thesis.

For ships, stiffened panels typically form the deck, bottom and sides. Thus, the stiffened panels are located on the extreme coordinates seen from the neutral axis, which will make them vulnerable to global bending stresses. Also, wave induced pressures, ice loads or impacts can cause high local lateral forces that the plating should withstand. It follows that stiffened panel failure, either plastic collapse, buckling or fatigue fracture, can be seen as the governing reason for catastrophic structural failure.

Stiffened panel collapse is complex and requires consideration of multiple failure modes. According to Ultimate Limit State-design (ULS), Paik and Thayamballi [25] presents the following classification for panels under axial compression:

- **Mode I:** overall collapse of plating and stiffeners as a unit, often elastic buckling. Common mode when stiffeners are weak relative to plating.
- **Mode II:** collapse due to biaxial compressive loads, causing yielding in the plate at the plate-stiffener intersections close to the plate edges.
- **Mode III:** beam-column type collapse, can be expected when the stiffeners are neither strong nor weak.
- **Mode IV:** local buckling of stiffener web, i.e the deformations in the plate are transferred to the stiffeners so that they lose load-carrying capability.
- **Mode V:** stiffener tripping, also known as flexural-torsional buckling. Similar to Mode III but the stiffener flange follows the deformations.
- **Mode VI:** gross yielding, requires a very stocky cross-section or tensile stresses.

It is common that modes interact or occur simultaneously, especially when there are other loads in addition to axial compression. To be able to analyze the ultimate strength, however, modes are often treated separately. The strength of the panel in the mode with the smallest resistance is then taken as the ultimate strength [11].

Formulations for analytical/semi analytical evaluation of these failure modes exist, but differ from one another depending on which loads are applied to the panel. To describe all possible load combinations is comprehensive, thus a restriction is made to axial (parallel to stiffener axis) compression and lateral pressure.

4.2. Model description

4.2.1. FEM-Model

ABAQUS finite element software has been used to model the panel. The element type is standard abaqus shell elements (S4R). The mesh, as indicated in figure 4.1, is relatively fine. The reason for this choice is that a number of analysis types will be performed, some of which will be highly non-linear, thus a relatively fine mesh hopefully reduces the risk of convergence problems. The element size on stiffener web and flanges is reduced with respect to the plate, in order to capture buckling and tripping of stiffeners in a sensible way.

Axial force and boundary conditions on transverse edges are handled by a rigid body constraint, which enables the load and boundary conditions to be applied to only one point per side. The physical interpretation is that all nodes on the edge under consideration are fixed relative to one another, so that in total a rigid body is formed. Thus, the edge cannot deform, only translate and rotate. This rigid body is then pinned to a reference point, so that loads and boundary conditions acting on this point acts on the whole edge, which is now a rigid body. This reference point is set so that the acting point of the load and boundary condition is through the neutral axis of the plate.
The material model is elastic-perfectly plastic with a yield stress of $f_y = 315$ MPa, elastic modulus of $E = 206$ GPa and Poisson ratio $\nu = 0.3$. The plate thickness is $t_p = 20$ mm, web thickness $t_w = 10$ mm and flange thickness is $t_{fl} = 16$ mm. The height of the web is $h_w = 420$mm and flange width $h_{fl} = 140$ mm. Length of the panel in longitudinal (parallel to stiffener axis) is $L = 4000$ mm. The distance between stiffeners is $s = 840$ mm. In the FEM-model, five stiffeners and a plate flange of $0.5s$ at each side is included.

4.2.2. DNV-RP-C201

Benchmarking, and subsequent reliability analysis, is also performed based on the DNV recommended practice for buckling strength of plated structures [6].

The main modeling difference as compared to the previously described FEM-model, is the boundary conditions. The equations used are taken from the case of continous stiffeners which implies that the stiffeners are held by rotational resistance from the girders. Also, imperfections are implicitly included, as discussed in section 3.3.

4.2.3. Boundary Conditions

Two cases of boundary conditions are tested for in the benchmark study. For both cases, the longitudinal edges (parallel to stiffeners) are simply supported and kept straight. Transverse edges are either fixed or simply supported. Which one is more relevant can be discussed. The model in question should be seen as one span out of many throughout a ship structure or similar. If the lateral pressure on all adjacent spans are equal, it could be argued that fixed short edges are more accurate due to symmetry in deflections (no rotation at transverse supports). However, if the lateral pressure is varying over adjacent spans, symmetry in the deflections could be lost so that a fixed boundary condition is questionable. A third alternative would be to model the boundary condition in rotation as a spring with stiffness corresponding to the rotational stiffness of adjacent girders.

4.2.4. Imperfections

The global imperfection shape utilized in the FE-model is taken as a sinusoidal half-wave, so that the initial lateral deflection is given by:

$$z(x) = z_0 + w \sin\left(\frac{\pi x}{L}\right) \tag{4.1}$$

where z_0 is the vertical coordinate for a perfect panel.

To be exact, such a displacement would also cause some translation of a given point in longitudinal direction. However, these displacements are small compared to the vertical translation (due to the limited height of the panel) and are hence neglected. The amplitude, w, is taken as scaled values of a standard deviation $\sigma_w = L/1000$, which is equivalent to 4 mm in this case.

Effects of angular error on the stiffeners is tested in the non-linear analysis. This procedure will be presented along with the results in section 4.3.3.

In the DNV-code, imperfections are handled implicitly as described under section 3.3.

4.3. Panel Capacity

4.3.1. DNV-Buckling Strength of Plated Structures

For a stiffened panel subject to axial stress and lateral pressure from the plate side, the DNV recommended practices states four different interaction equations. These are semi-empirical formulations, where each equation checks one corresponding critical location in the panel. If all are fulfilled, it is considered adequately designed to resist:

- Plate yielding in bending due to lateral load
- Buckling of slender plates
- Panel buckling
- Stiffener buckling
- Local buckling of stiffener webs, flanges and brackets.

The interaction equations correspond to the following locations in the panel:

- **Equation 1:** Stiffener side at transverse supports.
- **Equation 2:** Plate side at transverse supports.
- **Equation 3:** Stiffener side at midspan.
- **Equation 4:** Plate side at midspan.

Each of these has to be fulfilled, i.e be smaller or equal to unity, in order for the panel to pass the requirement. As a first step, the fulfillment of these are checked for a range of lateral pressures, axial stresses, plate thicknesses and yield stresses when all other parameters are kept fixed at the base-state levels. The boundary conditions used for the evaluations correspond to continous stiffeners. The results are shown in figure 4.2.

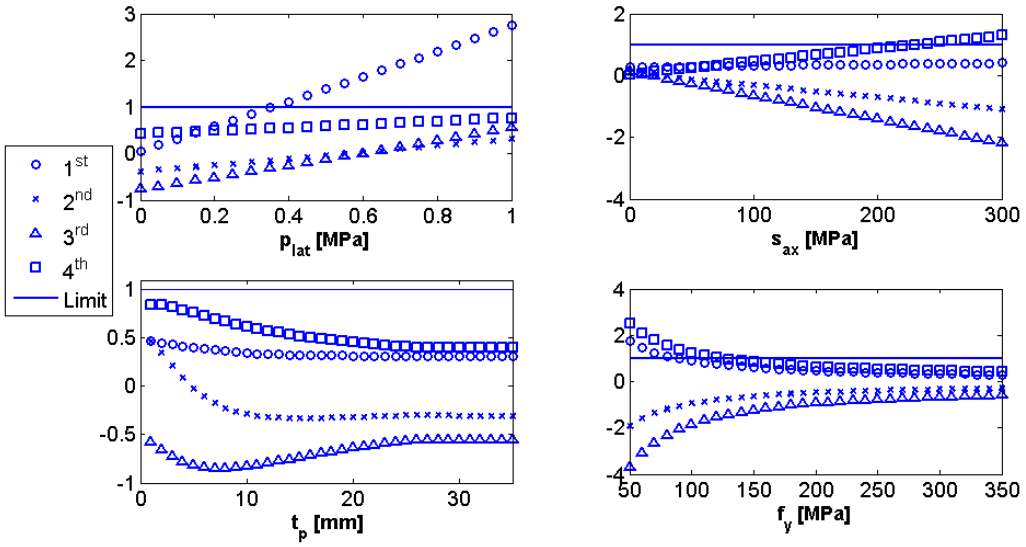

Figure 4.2: Parameter study on the effect of different physical variables on the DNV-RP-C201 requirements.

From the above figure, only the first and fourth requirement are violated. Non-fulfillment of requirement 4 is found at high axial stresses ($>$ 220 MPa) and low values of yield stress ($<$ 130 MPa). Equation 1 is not fulfilled for lateral pressures larger than approximately 0.35 MPa, as well as for low values of yield stress ($<$ 90 MPa). Limit state corresponding to the fourth requirement with respect lo lateral pressure and axial stress is shown in figure 4.3

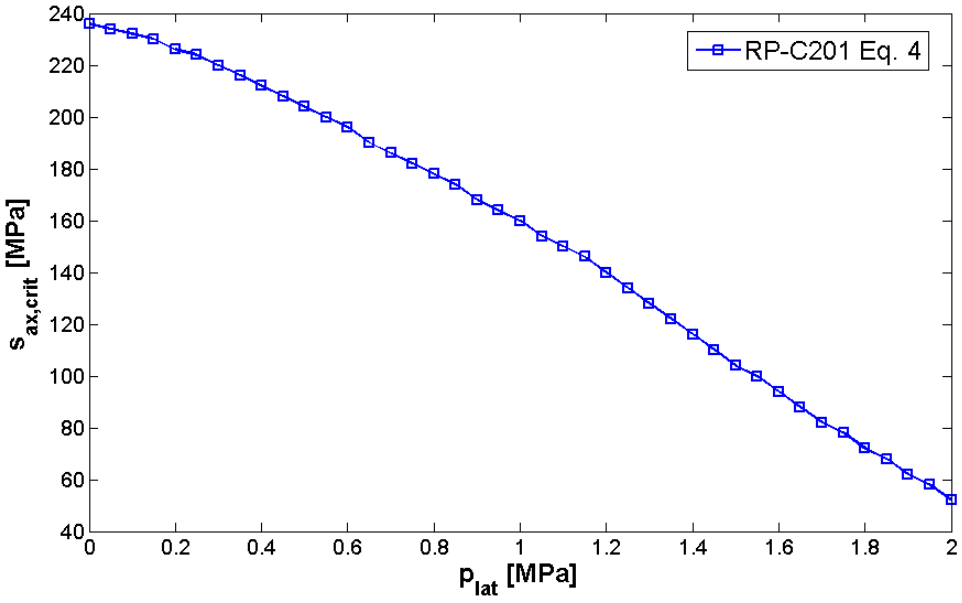

Figure 4.3: Limit state for lateral pressure and axial force interaction according to DNV buckling code for check at midspan plate side

4.3.2. Linear buckling analysis

A linear buckling analysis is performed in ABAQUS for lateral pressure magnitudes of 0, 0.1, 0.2 and 0.3 MPa for both the perfect panel and the panel when subject to a global imperfection shape. Imperfection shape is taken as a sinusoidal half-wave, with amplitude equal to L/1000. The critical linear buckling loads for both geometry cases are shown in tables 4.1 and 4.1.

Table 4.1: Linear buckling loads for different lateral pressures without imperfection

B.C	Cr. load [MPa] p=0.0MPa	Cr. load [MPa] p=0.1MPa	Cr. load [MPa] p=0.2MPa	Cr. load [MPa] p=0.3MPa
S.S	259.1	252.9	253.5	257.3
Fixed	313.7	318.1	331.5	345.5

Table 4.2: Linear buckling loads for different lateral pressures with global imperfection equal to one half sine-wave with amplitude L/1000

B.C	Cr. load [MPa] p=0.0MPa	Cr. load [MPa] p=0.1MPa	Cr. load [MPa] p=0.2MPa	Cr. load [MPa] p=0.3MPa
S.S	257.5	252.1	253.2	257.6
Fixed	313.7	321.7	332.4	346.7

For the perfect panel when simply supported, there is a drop in critical load when lateral pressure is applied. However, increasing lateral load further increases capacity. When transverse boundaries are fixed, there is no drop in capacity when pressure is applied. Instead capacity is increasing with lateral pressure.

The effect of adding imperfection is small for both boundary conditions, and effect of lateral pressure is similar to the perfect panel.

Critical buckling mode shapes for the panel with a lateral pressure of 0.1 MPa are different depending on boundary conditions. However, inclusion of shape error does not change the buckling modes. Critical buckling patterns are shown in figures 4.4 and 4.5 for simply supported and fixed transverse edges, respectively.

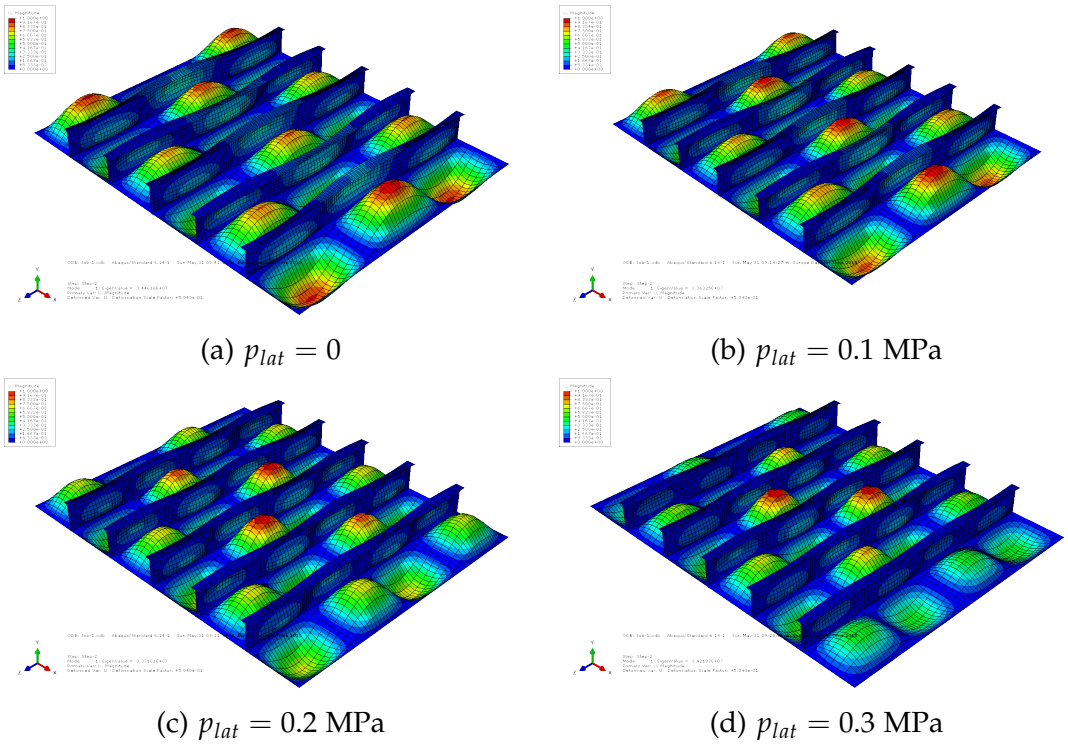

(a) $p_{lat} = 0$ (b) $p_{lat} = 0.1$ MPa

(c) $p_{lat} = 0.2$ MPa (d) $p_{lat} = 0.3$ MPa

Figure 4.4: 1^{st} linear buckling modes for different pressure levels, without initial imperfections. The panel is simply supported.

For simply supported boundary conditions, it is seen that the buckling pattern is equal for $p_{lat} = 0$ and $p_{lat} = 0.1$ MPa. The two subsequent changes in lateral pressure changes the buckling pattern compared to the previous pressure level. This could explain the unexpected increase in buckling load with increased pressure from table 4.1. The reason for the increase in capacity can be that lateral pressure forces a change in buckling shape to a less critical one. When the mode shape does not change, an increase in pressure lowers the capacity, as seen when p_{lat} goes from 0 to 0.1 MPa.

With fixed transverse edges, buckling pattern is equal for $p_{lat} = 0$ and $p_{lat} = 0.1$. A shift in shape is seen when pressure is increased to 0.2 MPa, but does not change again with increase to 0.3 MPa. Still, capacity increases with pressure for all levels. It is thus concluded, for fixed transverse edges, that lateral pressure counteracts the linear buckling so that axial capacity increases with pressure even though the buckling shape is constant. This could be explained by the fact that plate deformation between stiffeners without axial force would be different from the shapes in figure 4.5.

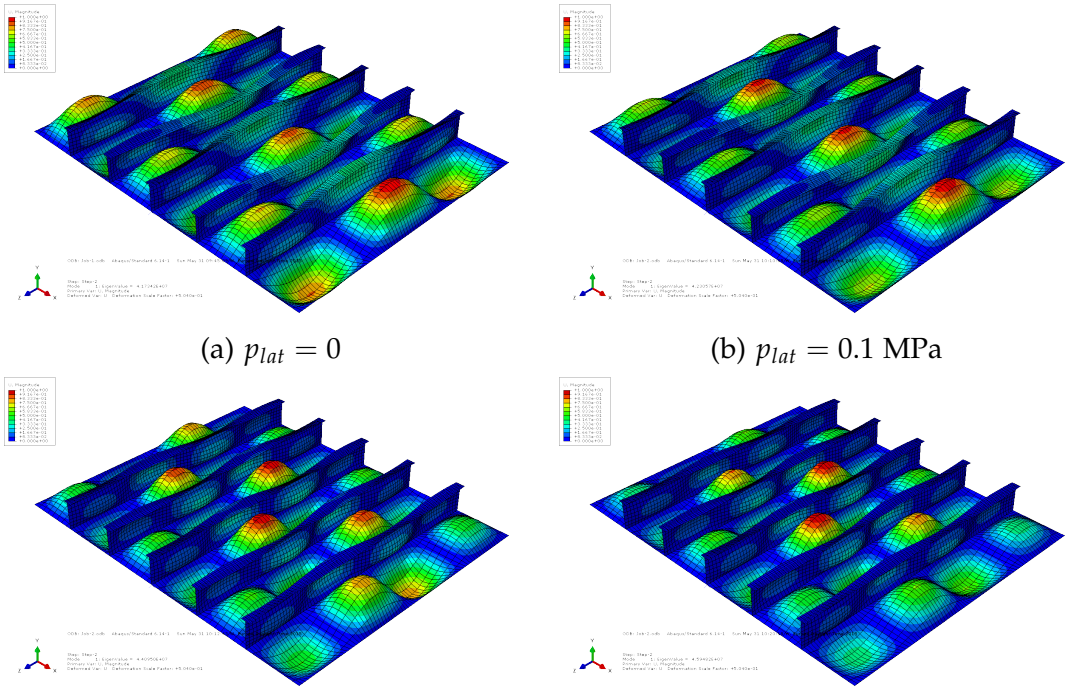

(a) $p_{lat} = 0$ (b) $p_{lat} = 0.1$ MPa

(c) $p_{lat} = 0.2$ MPa (d) $p_{lat} = 0.3$ MPa

Figure 4.5: 1^{st} linear buckling modes for different lateral pressure levels, without initial imperfections. Transverse edges are fixed.

4.3.3. Nonlinear buckling analysis

The panel is now checked for axial capacity for both simply-supported and fixed short-edges by ninlinear analysis. Capacity is tested for lateral pressures of 0.1, 0.3 and 0.5 MPa in order to determine the effect of varying pressure. Figure 4.6 shows the ultimate states for both boundary conditions at a pressure level of 0.1 MPa. While the simply supported case renders a fairly uniform deflection shape, fixed short edges gives considerable sideway deflection of the stiffeners, which also reaches the yield stress to a large extent. This utilization of the stiffeners raises the capacity compared to simply supported short edges, as shown in table 4.3.

Table 4.3: Capacity with respect to axial load and end shortening for different lateral pressure levels and simply supported (S.S)/Fixed boundary condition on short transverse edges.

B. C. \ Lat. Pressure	p_{lat}=0.1 MPa	p_{lat}=0.2 MPa	p_{lat}=0.2 MPa
s_{ax}, S. S [MPa]	240.7	210.3	104.3
s_{ax}, Fixed [MPa]	-307.7	279.2	241.3
ΔL, S. S [mm]	-6.2	-5.9	-6.0
ΔL, Fixed [mm]	-6.1	-5.9	-5.9

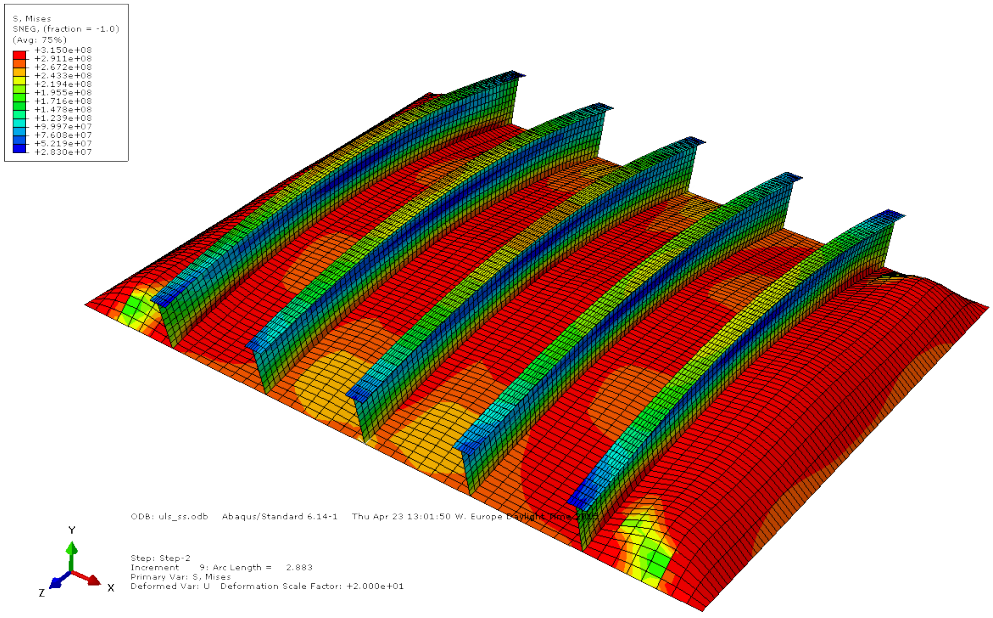

(a) Simply supported

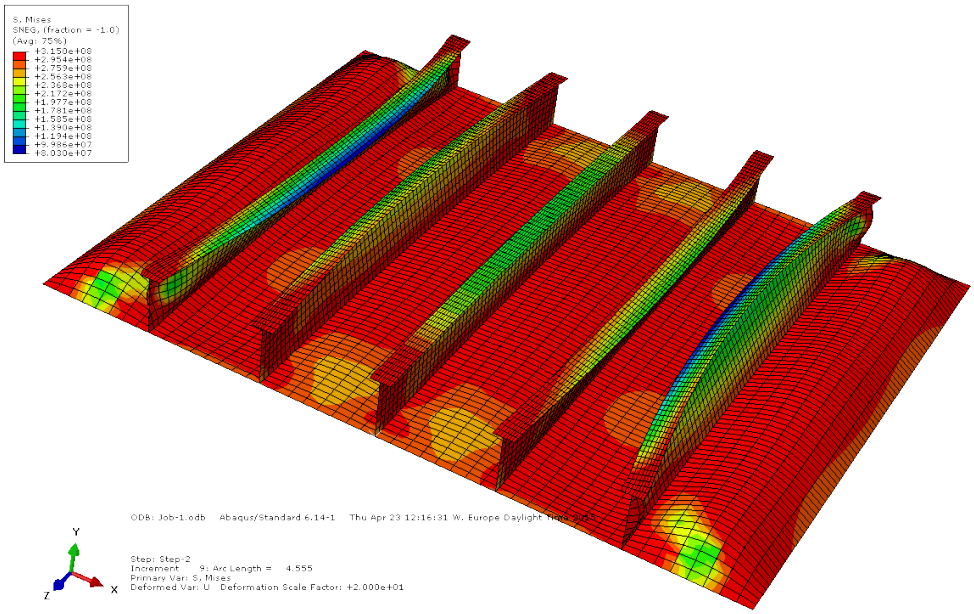

(b) Fixed

Figure 4.6: Ultimate limit states for simply supported and fixed short edges with $p_{lat} = 0.1$ MPa. Deformations are scaled by a factor of 20.

The end-shortening versus axial load relation for three different pressure levels (0.1, 0.2 and 0.3 MPa) is shown in figure 4.7.

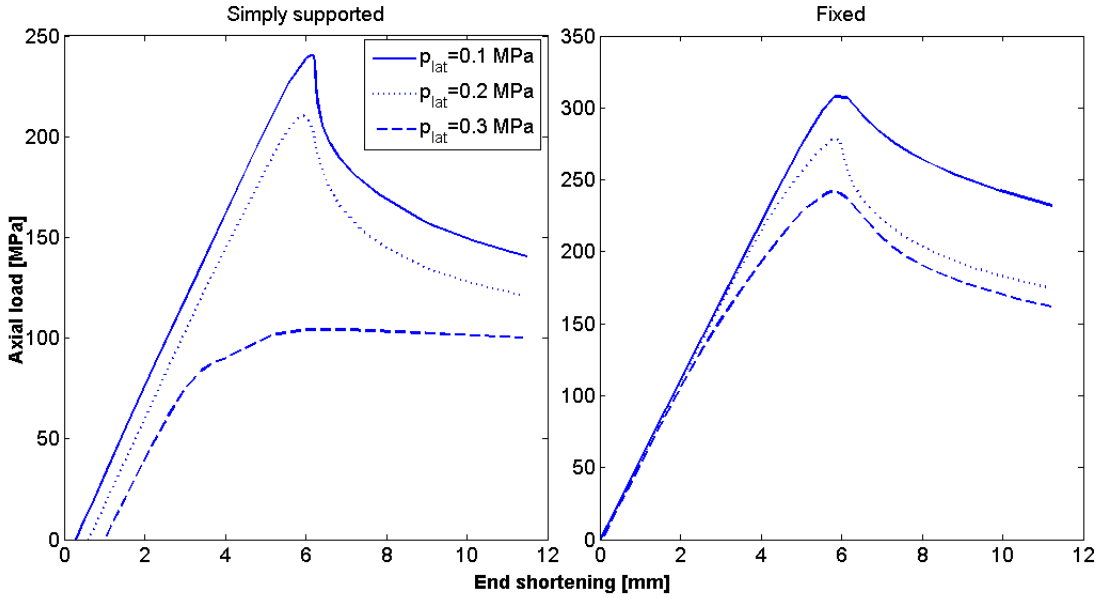

Figure 4.7: Relation between applied axial load and end shortening for different lateral pressures.

The panel in a failed state, taken at a load carrying capacity decrease of 50 % as compared to ultimate capacity, is shown in figure 4.8. As for the ultimate limit state, the fixed case shows more stiffener utilization. Longitudinals are heavily deformed both in web and flange close to transverse boundaries. It can also be noted that stresses are shifted, from yield level over practically the entire plate surface in the ultimate capacity state, towards a concentrated stress picture close to the midspan as failure progresses.

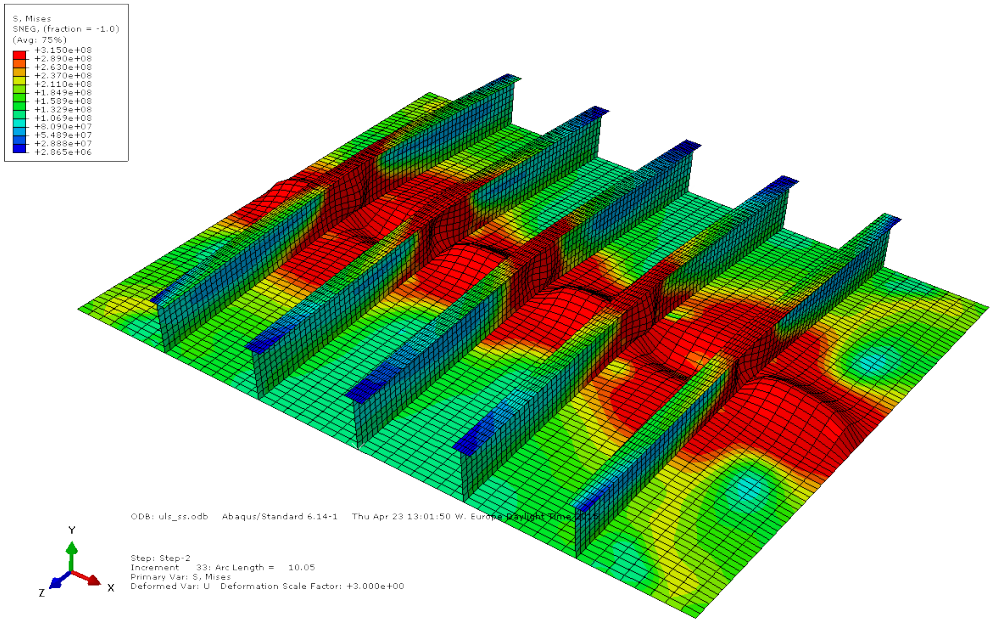

(a) Simply supported

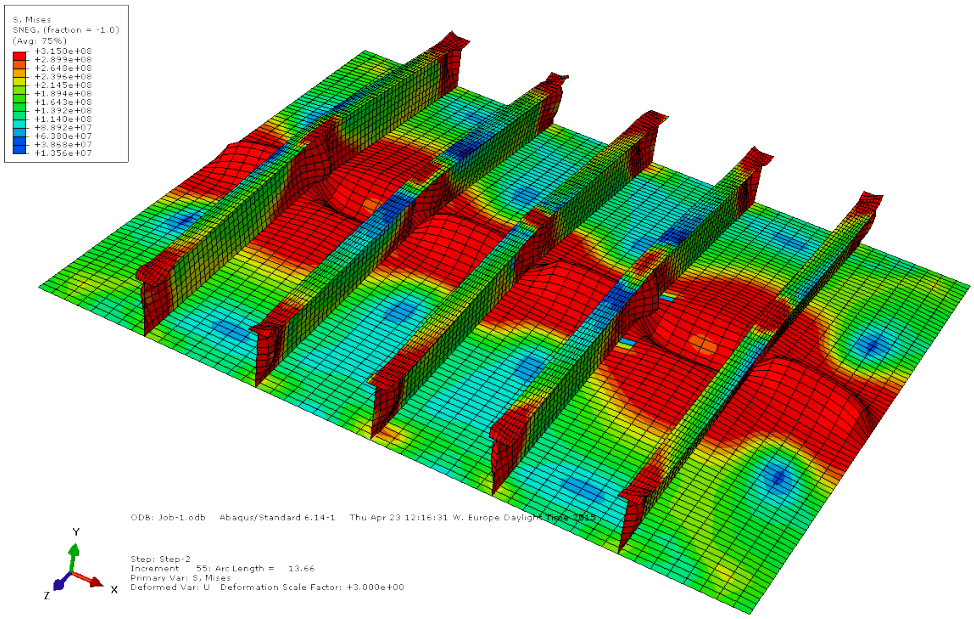

(b) Fixed

Figure 4.8: Panel (simply supported and fixed, respectively) in failed state, at a load carrying capacity loss of 50 % compared to ultimate capacity. Deformations are scaled by a factor of 3.

Effects of initial imperfections are now considered using the FE-model. Linear buckling mode shapes, that would generally be a suitable choice as imperfection shapes are not considered, since these do not correspond to the global failure mode as shown by figure 4.8. Instead, attention was focused on tilting of stiffeners and a global sinusoidal initial shape error as described under section 4.2.4.

For the upcoming reliability analysis, it is of interest to keep the number of basic variables at a minimum. Hence, tilt angles used here are of one magnitude for all stiffeners. Three different imperfection regimes was tested.

The first one was found by considering the failure mode of figure 4.8b, i.e tilting stiffeners on each side of the central stiffener towards each another and keeping the central stiffener straight. This gave practically no difference in load-carrying capability for pressure levels of 0.1, 0.2 and 0.3 MPa at tilt angles of 0.01 or 0.02 radians.

The next scenario that is tested tilts the stiffeners every other way i.e.
$\theta_k = [\theta \ -\theta \ \theta \ -\theta \ \theta]$ for the k^{th} stiffener where k=1 and k=5 are the stiffeners closest to the longitudinal edges. Similar to the first scenario, no significant difference in strength was noted.

The third imperfection shape tested is the tilting of all stiffeners the same way. This also has a negligable effect on axial capacity for the tested pressures when angles are small to moderate.

To summarize the effects of stiffener tilting, it is very small on the axial capacity for all tested regimes. The effect is mainly seen for tilt angles above 0.03 radians ($\approx 1.72^{\circ}$), but even then capacity reduction is fairly small (5 % capacity decrease for tilt angles of 0.04 radians when all stiffeners are tilted the same way).

A global imperfection shape is now considered. The effect on the load/end shortening-relation is shown in figures 4.9 and 4.10 for positive and negative values of w, respectively. The magnitudes of w for the tests are taken as scaled values of standard deviation of such shape errors according to JCSS recommendations, described in section 3.3.

It is noted that the axial capacity decreases with increasing imperfection magnitude when transverse edges are simply supported. When transverse edges are fixed, the effect is seen mostly in the post-buckling behaviour. For this boundary condition, it is also seen that the difference when increasing imperfection magnitude from $1\sigma_w$ to $3\sigma_w$ is small.

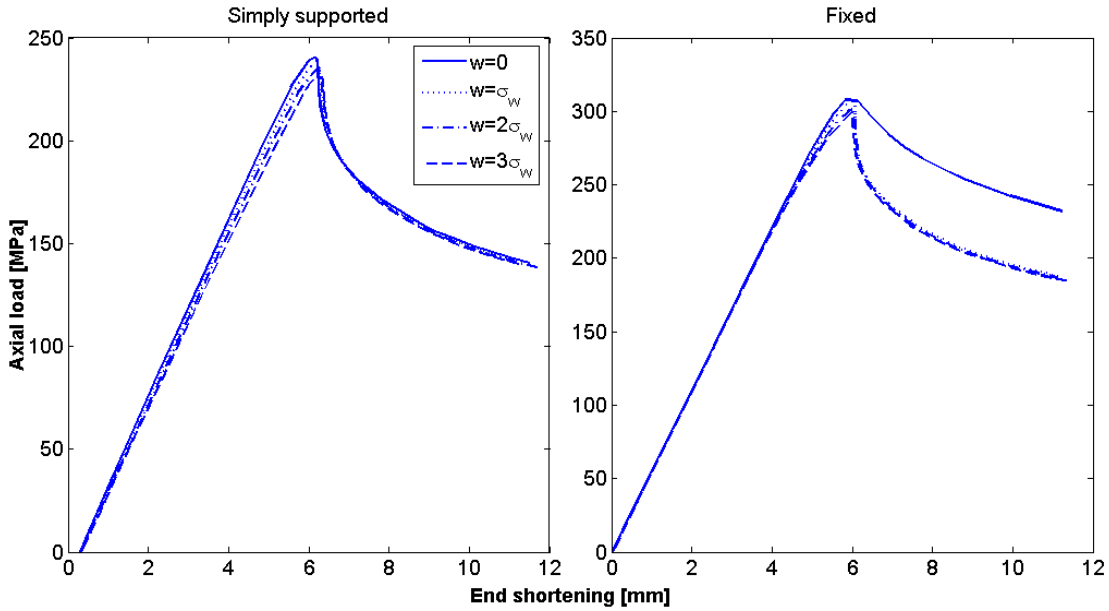

Figure 4.9: Relation between applied axial load and end shortening for global imperfections of positive magnitudes, at a lateral pressure level of $0.1MPa$. σ_w denotes the JCSS recommended standard deviation for such shape errors.

For negative imperfection magnitudes, i.e. opposite to pressure direction, axial capacity is somewhat raised and post-buckling capacity is larger for simply supported boundary conditions. For fixed short edges, ultimate capacity is close to identical for all levels of imperfections, but post-buckling capacity is smaller.

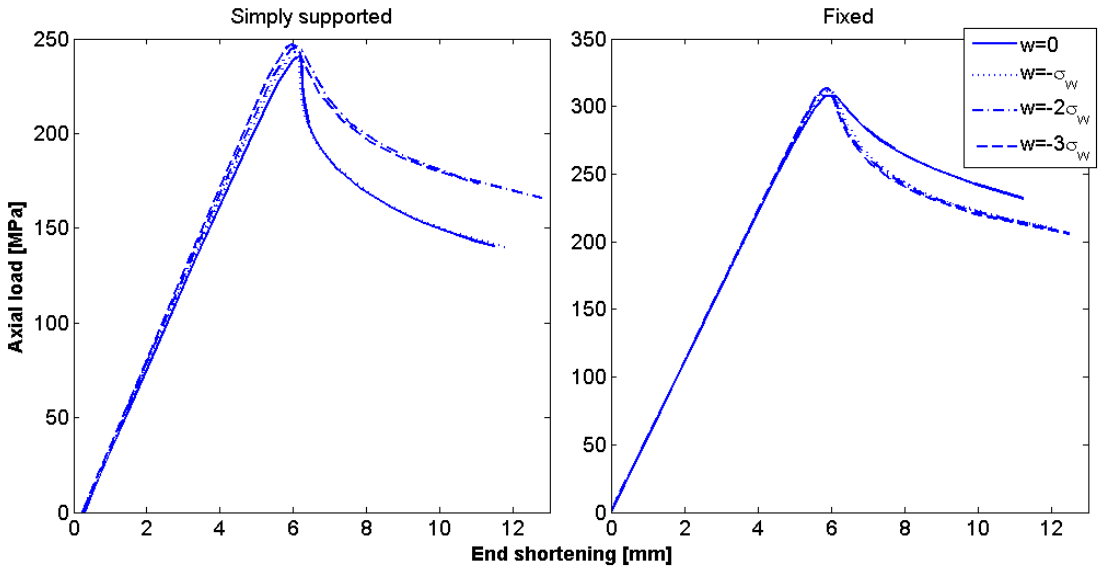

Figure 4.10: Relation between applied axial load and end shortening for global imperfections in the shape of a half sine-wave and lateral pressure $0.1MPa$. σ_w corresponds to an amplitude of L/1000.

4.3.4. Linear vs Non-Linear Results

Results from linear analysis shows large discrepancies compared to non-linear analysis. While non-linear analysis shows a decrease in axial capacity with increasing lateral pressure, linear buckling loads are generally larger when lateral pressure is increased.

If results from the non-linear analysis are considered, the bifurcation point is preceeded by considerable yield in the plate, especially when lateral pressure is high. This is typical for stocky cross-sections, and implies that geometrical instability will be present only after yielding has occured. Effects of yielding material are not captured by a linear analysis. A possible explanation to the confusing results would thus be that yield is required to force the panel into a global deflection shape. When material effects are neglected, overall panel buckling is prevented and the critical mode becomes as in figure 4.4.

To investigate the validity of the above discussion, a non-linear analysis with increased yield stress is performed . The load-end shortening relation for simply supported transverse edges and twice the original yield stress is shown in figure 4.11. Lateral pressure is taken at 0.1 and 0.3 MPa. When compared to figure 4.7, it is noticed that the capacity drop when increasing the pressure is reduced significantly.

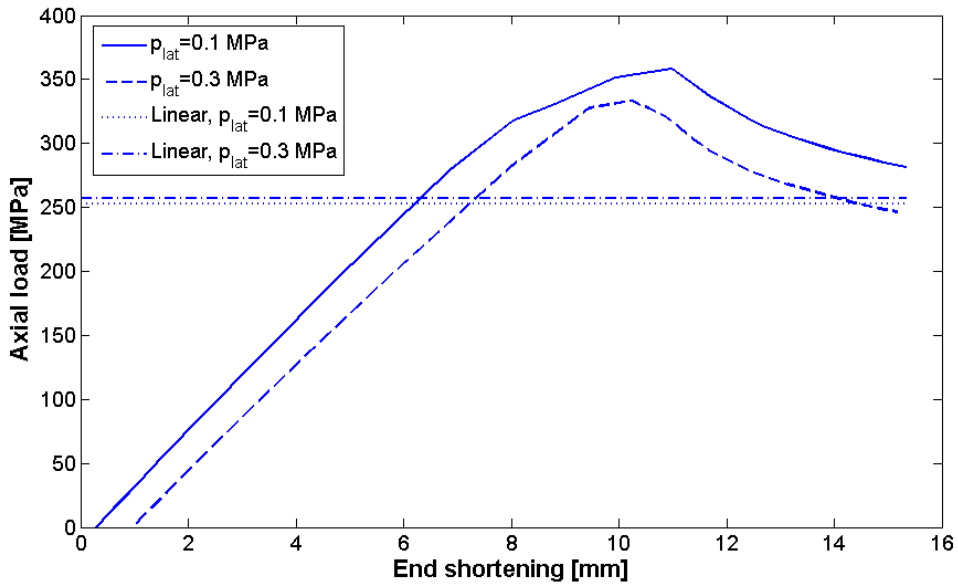

Figure 4.11: Relation between applied axial load and end shortening for lateral pressure levels of 0.1 and 0.3 MPa when the yield stress is doubled, i.e $s_f = 630$ MPa instead of 315 MPa. Transverse edges are simply supported.

Deflection shape at the point of maximum utilization for panel with extreme yield stress material and 0.1 MPa lateral pressure is shown in figure 4.12. The fundamental shape is equal for 0.3 MPa. It is clear from this figure that raised yield stress, and hence smaller material effects, introduces local plate buckling in the failure mode.

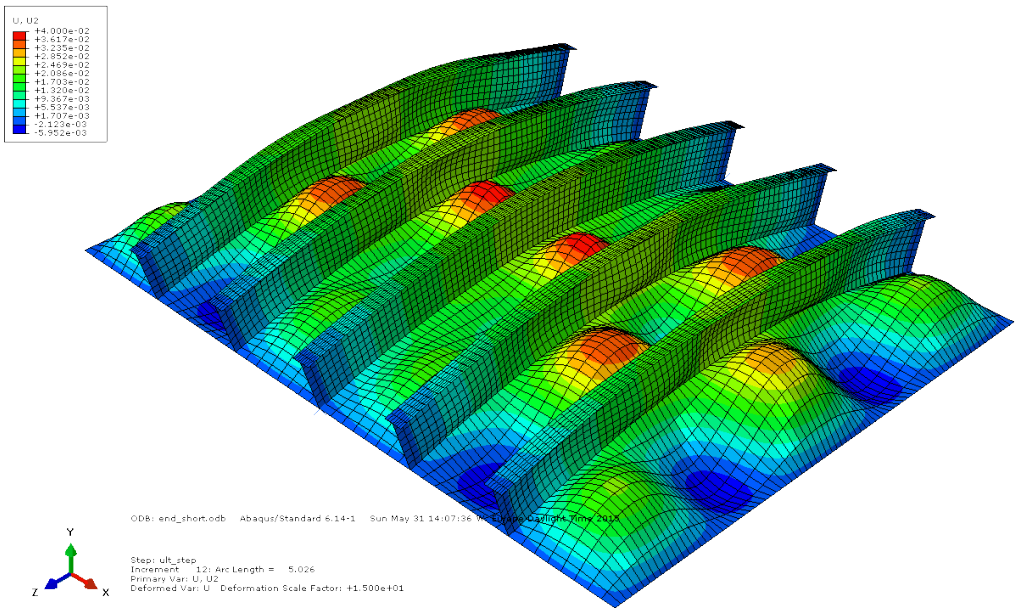

Figure 4.12: Panel with extreme yield stress in the state of maximum utilization. Color scalings shows the distribution of lateral deflection magnitudes. Lateral pressure is 0.1 MPa and deformations are scaled by a factor of 20.

Chapter 5

Reliability Analysis of Stiffened Panel

This chapter presents a number of reliability computations for the stiffened panel as presented in chapter 4. Emphasis is given to evaluation of reliability by means of implicit limit states, which represents problems of practical applicability. Comparison of response surface approaches and methods of determining failure probabilities from them will be performed.

5.1. Description of methods

5.1.1. Sampling source

Sampling will be performed using ABAQUS finite element code, and the model presented in chapter 4. A third limit state and the corresponding safety margin is tested for using the DNV guidelines for buckling of stiffened panels.

For the finite element model, boundary conditions has been set to simply supported, where all edges are kept straight. This choice is made based on DNV recommendations, stating that the boundary conditions should be accurate or conservative [8]. Fixed short edges, as shown in chapter 4, yields non-conservative results and the accuracy could be argued (following the discussion of section 4.2.3). The boundary conditions employed in the DNV-sampling represents continous stiffeners, i.e. receiving rotational support from adjacent girders.

5.1.2. Basic Variables

The selection of which parameters to take as variables, and which ones should be deterministic has been made by considering the variability of the respective parameter in relation to the sensitivity of structural capacity for this parameter. An increase in the number of basic variables raises the computational effort substantially. Thus, a trade-off has been attempted so that the number of basic variables are large enough to demonstrate the differences between methods, but small enough to enable multiple analysis for comparative reasons. For this case, the number of basic variables was chosen equal to 5.

Effect of distribution choice for the basic variables will be checked by first using a simplified approach, where the gaussian distribution is employed for all variables. Subsequently, a more realistic choice of distributions are used. Use of gaussian, especially independent gaussian, variables simplifies the analysis, it is thus interesting to see which consequences this shortcut gives. Means and coefficients of variation for all variables are given in table 5.1, where C.O.V denotes the coefficient of variation given by $\sigma = C.O.V * \mu$

Table 5.1: Data for basic variables

Parameters:	t_p	s_{ax} [MPa]	p_{lat}	w	s_f
μ_i	20 mm	100 MPa	0.1 MPa	0 mm	315 MPa
σ_i	0.4mm	20 MPa	0.01 MPa	4 mm	22.05
C.O.V	0.02	0.2	0.1	-	0.07

For the second analysis, the Weibull distribution is chosen for the loads. The material parameters and plate thickness are taken from the recommended distributions of JCSS [12]. Thus, the plate thickness and shape error are normally distributed and the yield strength is log-normal. All variables are assumed mutually independent for both distribution regimes.

5.1.3. Bucher-Buorgund Response surface

An uncertainty regarding this method is the effect of sampling spread factors, f_i. Therefore, the arbitrary choice of $f_i = 3$ for both steps is evaluated, as well as the suggested regime of Rajashekhar and Ellingwood [28] with $f_i^{(1)} = 2$ and $f_i^{(1)} = 1$ for the two response surface iterations, respectively. The polynomial description of equation 2.51 is employed, i.e. a pure quadratic response surface.

5.1.4. Response Surface by Vector Projection

As suggested by the founders of the method, described in section 2.6.2, the analysis will be performed with both $f_i = 1.0$ and $f_i = 1.5$. From these results, the nonlinearity index, Δ, of the limit state will be evaluated. If necessary, a third analysis is performed with corrected f_i according to figure 2.5.

5.1.5. Monte Carlo

Two simulation methods are used on the response surfaces obtained by the Bucher-Buorgund method, Crude Monte Carlo (direct sampling) and Importance Sampling. The Importance Sampling center point is taken at the approximate design point found from FORM, and the sampling functions are taken as the multivariate gaussian as discussed in section 2.5.2, with variances corresponding to either the actual ones (for plate thickness and shape error, and for all variables when gaussian distributions are employed) or the approximations at the design point as found during the transformations in the FORM-analysis.

Simulations are performed in a sequence of totally 100 steps in order to see the simulation history and thus the convergence rate. For Crude Monte Carlo and Importance sampling, each set contains 10^6 and 10^3 samples respectively, giving total sample sizes of 10^8 and 10^5.

5.1.6. Assumptions and simplifications

The plate thickness does not affect the axial stress. In the true scenario, a constant axial load distributed over the cross-section would yield a higher distributed load when the dimensionality increases. Here, the axial load is found from a point load distributed over the cross-section with mean plate thickness. Thus, the axial load does not change with the plate thickness during the sampling.

When evaluating the probability of failure from the DNV buckling code, the limit state is chosen from the fourth interaction equation, corresponding to check of plate side at midspan. The reason for not including all four is to avoid a systems formulation. Furthermore, it was found in section 4.3.1 that the fourth equation was dominant over the others in terms of being prone to reach the allowed limit. Also, the imperfections in these guidelines, as discussed in section 3.3, are handled implicitly. Hence, the dimensionality is decreased by one variable for this safety margin.

5.2. Plate Yield in Midspan

Failure is defined as the von-Mises stress exceeding yield level in the plate at midspan. The safety margin is normalized with respect to mean yield stress and becomes:

$$g = \frac{1}{\mu_{s_f}} \left(\gamma_m s_f - s_{vM,max} \right) \tag{5.1}$$

where γ_m is a model uncertainty factor, which has been set to 0.8.

Gaussian variables

The design points and sensitivity factors when all variables are gaussian is shown in table 5.2.

Table 5.2: Design point from evaluation of von-Mises stress, plate side at midspan, with gaussian variables at two different spread factor regimes.

	t_p [mm]	$s_{ax}[MPa]$	$p_{lat}[MPa]$	w	s_f [MPa]
$x^{\star}_{i,33}$	19.711	137.53	0.1075	2.5779	284.55
$x^{\star}_{i,21}$	19.746	139.94	0.1068	2.3429	285.27
$\alpha_{i,33}$	-0.2738	0.7129	0.2860	0.2448	-0.5246
$\alpha_{i,21}$	-0.2399	0.7542	0.2559	0.2212	-0.5092

The corresponding probabilities of failure are given in table 5.3, including errors of FORM and Importance Sampling when compared to Crude Monte Carlo.

Table 5.3: Failure probabilities from quadratic response surface evaluation with gaussian variables along with errors compared to Crude Monte Carlo.

	$p_{f,HL}$	$p_{f,CMC}$	$p_{f,IS}$	e_{HL} [%]	e_{IS} [%]
$f_i^{(1)} = f_i^{(2)} = 3$	$4.24 * 10^{-3}$	$4.15 * 10^{-3}$	$4.17 * 10^{-3}$	2.2	0.5
$f_i^{(1)} = 2, f_i^{(2)} = 1$	$4.05 * 10^{-3}$	$4.32 * 10^{-3}$	$4.32 * 10^{-3}$	-6.3	0

Non-gaussian

For the more realistic models, the design point with sensitivity factors on the quadratic response surface is found as in table 5.4.

Table 5.4: Design point from evaluation of von-Mises stress, plate side at midspan, with non-gaussian variables at two different spread factor regimes.

	t_p [mm]	$s_{ax}[MPa]$	$p_{lat}[MPa]$	w	s_f [MPa]
$x^{\star}_{33}$	19.627	133.12	0.1080	3.2792	281.67
$x^{\star}_{21}$	19.666	135.22	0.1075	3.0130	281.81
$\alpha_{i,33}$	-0.3298	0.6421	0.2758	0.2898	-0.5648
$\alpha_{i,21}$	-0.2924	0.6856	0.2530	0.2640	-0.5575

Failure probabilities were found from FORM (Hasofer-Lind safety index), crude Monte Carlo-sampling and importance sampling were found as given in table 5.5.

Table 5.5: Failure probabilities from quadratic response surface evaluation with non-gaussian variables along with errors compared to Crude Monte Carlo.

	$p_{f,HL}$	$p_{f,CMC}$	$p_{f,IS}$	e_{HL} [%]	e_{IS} [%]
$f_i^{(1)} = f_i^{(2)} = 3$	$2.33 * 10^{-3}$	$1.88 * 10^{-3}$	$1.88 * 10^{-3}$	24	0
$f_i^{(1)} = 2, f_i^{(2)} = 1$	$2.16 * 10^{-3}$	$1.89 * 10^{-3}$	$1.90 * 10^{-3}$	14	0.5

5.2.1. Vector Projection

Gaussian distributions

Results for gaussian basic variables and the two proposed sampling weights:

- $\beta_{1.0} = 2.6205.$ for sampling weights $f_i = 1.0$
- $\beta_{1.5} = 2.7127.$ for sampling weights $f_i = 1.5$

From this, the nonlinearity index is 0.0230. Since this is smaller than 0.03, there is no need to update the sampling and the results from $f_i = 1.0$ are taken as final. The probability of failure is $p_f = \Phi(-\beta_{1.0}) = 4.39 * 10^{-3}$. Design point and sensitivity factors are given in table 5.6

Table 5.6: Design point and sensitivity factors for plate stress at midspan and gaussian basic variables with vector projection response surface.

	t_p [mm]	$s_{ax}[MPa]$	$p_{lat}[MPa]$	w	s_f [MPa]
$x_i^\star$	19.75	139.62	0.1067	2.2914	285.66
α_i	-0.2394	0.7559	0.2564	0.2186	-0.5077

Non-gaussian distributions

With variables from non-gaussian distribution types, the analysis required 4 iterations for both sampling factors. The resulting safety indices are:

- $\beta_{1.0} = 2.8184$
- $\beta_{1.5} = 2.9338$

From this, the nonlinearity index becomes 0.0287, which is smaller than 0.03. Hence, the final safety index is $\beta_{1.0}$, corresponding to a failure probability of $2.41 * 10^{-3}$. Final design point and sensitivity factors are found in table 5.7.

Table 5.7: Design point and sensitivity factors for plate yield at midspan and non-gaussian basic variables using the vector projection method.

	t_p [mm]	$s_{ax}[MPa]$	$p_{lat}[MPa]$	w	s_f [MPa]
$x_i^\star$	19.671	134.91	0.1075	2.9530	282.24
α_i	-0.2920	0.6868	0.2541	0.2619	-0.5567

Figure 5.1 shows the convergence rate, where the safety index found from each iteration is normalized with the final result.

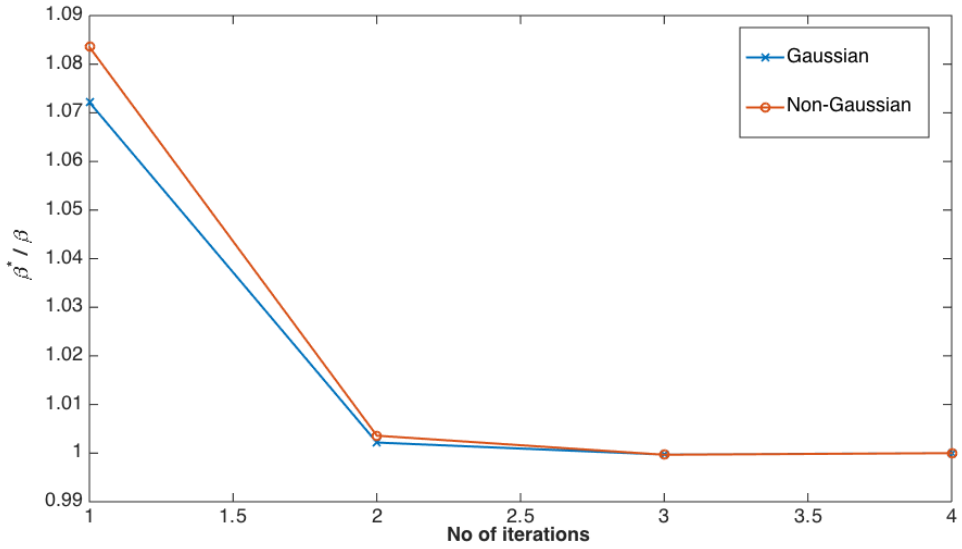

Figure 5.1: Convergence plot of the vector-projection algorithm, with the safety index at each iteration normalized with the final result.

5.3. Axial capacity

Reliability with respect to exceedence of axial capacity is now evaluated. Sampling is performed through ABAQUS by evaluating the ultimate axial capacity, s_{ult}, with respect to the other variables. This capacity is then compared to the sampled axial load and normalized with respect to mean load according to:

$$g_{uc} = \frac{1}{\mu_{s_{ax}}} \left(\gamma_m s_{ult} - s_{ax} \right) \tag{5.2}$$

As before, γ_m is a model uncertainty factor set to 0.8.

5.3.1. Bucher-Buorgund Response Surface

Gaussian distributions

The design points and corresponding sensitivity factors obtained for both sampling regimes and gaussian distributions for all variables is shown in table 5.8.

Table 5.8: Design point and sensitivity factors from evaluation of axial capacity with gaussian variables at two different spread factor regimes.

	t_p [mm]	$s_{ax}[MPa]$	$p_{lat}[MPa]$	w	s_f [MPa]
$x^{\star}_{33}$	19.722	162.90	0.1035	1.3750	271.04
$x^{\star}_{21}$	19.708	162.83	0.1033	1.3285	271.30
$\alpha_{i,33}$	-0.1818	0.8235	0.0905	0.0900	-0.5221
$\alpha_{i,21}$	-0.1913	0.8235	0.0877	0.0871	-0.5195

Probabilities of failure from different calculation techniques are shown in table 5.9.

Table 5.9: failure probabilities from quadratic response surface evaluation with gaussian variables along with errors compared to Crude Monte Carlo.

	$p_{f,HL}$	$p_{f,CMC}$	$p_{f,IS}$	e_{HL} [%]	e_{IS} [%]
$f_i^{(1)} = f_i^{(2)} = 3$	$6.70 * 10^{-5}$	$7.08 * 10^{-5}$	$6.91 * 10^{-5}$	-5.4	-2.4
$f_i^{(1)} = 2, f_i^{(2)} = 1$	$6.82 * 10^{-5}$	$6.01 * 10^{-5}$	$6.04 * 10^{-5}$	13	0.5

Non-gaussian distributions

When the actual distribution types are employed, the resulting design point is found as in table 5.10

Table 5.10: Design point from evaluation of ultimate capacity with non-gaussian variables at two different spread factor regimes.

	t_p [mm]	$s_{ax}[MPa]$	$p_{lat}[MPa]$	w	s_f [MPa]
$x^{\star}_{33}$	19.551	153.26	0.1058	2.2570	259.28
$x^{\star}_{21}$	19.540	153.27	0.1061	2.3674	259.74
$\alpha_{i,33}$	-0.2482	0.7286	0.1129	0.1249	-0.6158
$\alpha_{i,21}$	-0.2543	0.7287	0.1221	0.1310	-0.6101

Failure probabilities were found from FORM (Hasofer-Lind safety index), crude Monte Carlo-sampling and Importance Sampling for both sampling regimes as given in table 5.11.

Table 5.11: Failure probabilities from quadratic response surface and non-gaussian variables. Results according to Hasofer-Lind Safety index ($p_{f,HL}$), crude Monte Carlo ($p_{f,CMC}$) and Importance Sampling ($p_{f,IS}$)

	$p_{f,HL}$	$p_{f,CMC}$	$p_{f,IS}$	e_{HL} [%]	e_{IS} [%]
$f_i^{(1)} = f_i^{(2)} = 3$	$3.11 * 10^{-6}$	$2.69 * 10^{-6}$	$2.62 * 10^{-6}$	16	-2.6
$f_i^{(1)} = 2, f_i^{(2)} = 1$	$3.11 * 10^{-6}$	$2.42 * 10^{-6}$	$2.77 * 10^{-6}$	29	14

5.3.2. Vector Projection

Gaussian variables

For gaussian basic variables, 6 and 5 iterations for $f_i = 1.0$ and $f_i = 1.5$ respectively were required to reach the convergence criteria. The obtained safety indices for the two sampling weights are:

- $\beta_{1.0} = 3.812$
- $\beta_{1.5} = 3.792$

The nonlinearity index becomes 0.005. The results with sampling weights $f = 1.0$ are thus kept as final and is presented in table 5.12. No more sampling is necessary so that the total number of sampling points is $(6 + 5) * 10 = 110$. The probability of failure is $6.89 * 10^{-5}$.

Table 5.12: Design point and sensitivity factors for vector projection response surface method with gaussian basic variables.

	t_p [mm]	$s_{ax}[MPa]$	$p_{lat}[MPa]$	w	s_f [MPa]
$x^\star$	19.72	162.59	0.1034	1.3403	270.8
α_i	-0.1834	0.8209	0.0891	0.0879	-0.5261

Non-Gaussian variables

With the more realistic distribution set, the safety indices for $f_i = 1.0$ and $f_i = 1.5$ were found as follows.

- $\beta_{1.0} = 4.502$
- $\beta_{1.5} = 4.486$

The nonlinearity index becomes is 0.0042, so the results using $f_i = 1$ are taken as final. Probability of failure is then $3.36 * 10^{-6}$. For $f_i = 1.0$, 17 iterations were required to reach the convergence limit. For $f_i = 1.5$, the required number of iterations was 7. Design point data and sensitivity factors are given in table 5.13.

Table 5.13: Design point and sensitivity factors for vector projection response surface method with gaussian basic variables.

	t_p [mm]	$s_{ax}[MPa]$	$p_{lat}[MPa]$	w	s_f [MPa]
$x^\star$	19.564	152.95	0.1059	2.2673	259.1
α_i	-0.2418	0.7258	0.1167	0.1259	-0.6207

The convergence rate in terms of ratio between temporary result and the final safety index is shown in figure 5.2.

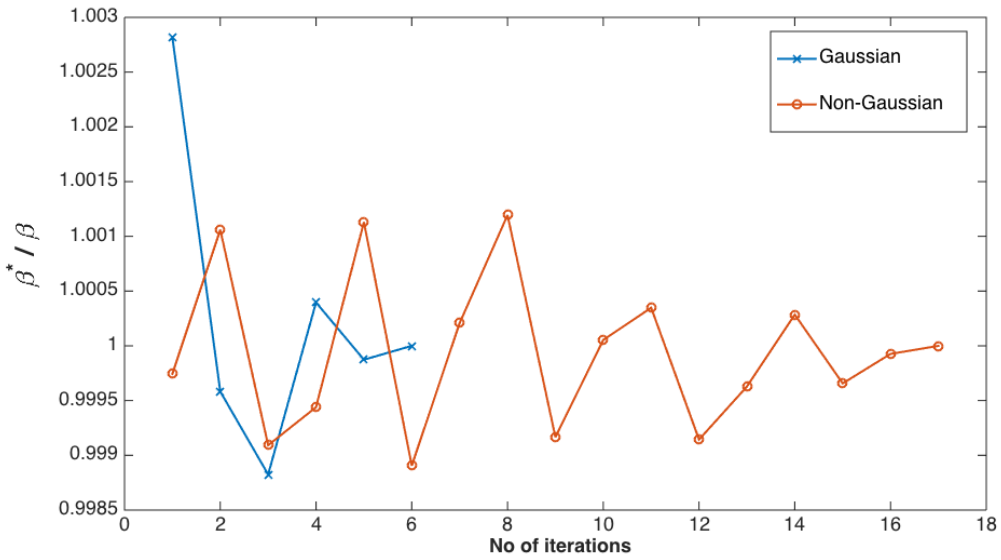

Figure 5.2: Convergence plot of the vector-projection algorithm, with the safety index at each iteration normalized with the final result

5.4. DNV-RP-C201-Plate side at midspan

The limit state is now chosen from the fourth interaction equation of DNV-RP-C201 which controls plate side along the midspan. Again, a model uncertainty factor γ_m is chosen equal to 0.8. Since acceptable values of the interaction equation is less or equal to 1, the safety margin becomes:

$$g = \gamma_m - f_{DNV,4} \tag{5.3}$$

where $f_{DNV,4}$ denotes the value of the fourth interaction equation of DNV-RP-C201, corresponding to a check for plate side at midspan.

5.4.1. Bucher-Bourgund response surface

Gaussian distibutions

The resulting design point and sensitivity factors for both sampling approaches are given in table 5.14

Table 5.14: Design point from evaluation of DNV recommended practice for plate side check at midspan with gaussian variables at two different spread factor regimes.

	t_p [mm]	$s_{ax}[MPa]$	$p_{lat}[MPa]$	s_f [MPa]
$x^{\star}_{33}$	19.897	164.46	0.1009	275.48
$x^{\star}_{21}$	19.896	165.37	0.1009	276.83
$\alpha_{i,33}$	-0.0694	0.8716	0.0245	-0.4847
$\alpha_{i,21}$	-0.0701	0.8813	0.0247	-0.4667

Corresponding results for the failure probabilities are given in table 5.15.

Table 5.15: Failure probabilities from bucher-bourgund response surface evaluation with gaussian variables with error of FORM and IS compared to Crude MC.

	$p_{f,HL}$	$p_{f,CMC}$	$p_{f,IS}$	e_{HL} [%]	e_{IS} [%]
$f_i^{(1)} = f_i^{(2)} = 3$	$1.09 * 10^{-4}$	$1.19 * 10^{-4}$	$1.21 * 10^{-4}$	-8.4	-1.7
$f_i^{(1)} = 2, f_i^{(2)} = 1$	$1.04 * 10^{-4}$	$1.16 * 10^{-4}$	$1.16 * 10^{-4}$	-10	0

Non-Gaussian distributions

When the more realistic distribution models are used, design points and sensitivity factors are shown in table 5.16.

Table 5.16: Design point from evaluation of DNV recommended practice with non-gaussian variables at two different spread factor regimes.

	t_p [mm]	$s_{ax}[MPa]$	$p_{lat}[MPa]$	s_f [MPa]
$x^{\star}_{33}$	19.818	156.83	0.1027	259.23
$x^{\star}_{21}$	19.813	157.64	0.1027	260.48
$\alpha_{i,33}$	-0.0994	0.7854	0.0347	-0.6100
$\alpha_{i,21}$	-0.1019	0.7980	0.0355	-0.5930

Proabability of failure according to the different methods and sampling procedure are shown in table 5.17.

Table 5.17: Failure probabilities from quadratic response surface with non-gaussian variables with errors from FORM and IS compared to Crude MC.

	$p_{f,HL}$	$p_{f,CMC}$	$p_{f,IS}$	e_{HL} [%]	e_{IS} [%]
$f_i^{(1)} = f_i^{(2)} = 3$	$2.48 * 10^{-6}$	$2.56 * 10^{-6}$	$2.34 * 10^{-6}$	-3.1	-8.5
$f_i^{(1)} = 2, f_i^{(2)} = 1$	$2.32 * 10^{-6}$	$2.05 * 10^{-6}$	$2.20 * 10^{-6}$	13	7.3

5.4.2. Vector Projection

Gaussian distributions

The analysis required 4 iterations to reach the convergence criteria of 0.001 with respect to β for both sampling weights. Results for gaussian basic variables and the two proposed sampling weights:

- $\beta_{1.0} = 3.6923.$ for sampling weights $f_i = 1.0$
- $\beta_{1.5} = 3.6595.$ for sampling weights $f_i = 1.5$

The corresponding nonlinearity index becomes 0.011 which implies that the results with $f_i = 1.0$ are final and $p_f = \Phi(-\beta_{1.0}) = 1.11 * 10^{-4}$. Design point and sensitivity factors are given in table 5.18

Table 5.18: Design point and sensitivity factors for DNV-check at plate side midspan with gaussian basic variables.

	t_p [mm]	$s_{ax}[MPa]$	$p_{lat}[MPa]$	s_f [MPa]
$x_i^\star$	19.897	165.82	0.1009	278.57
α_i	-0.0686	0.8913	0.0252	-0.4474

Non-gaussian distributions

Safety indices for $f_i = 1.0$ and $f_i = 1.5$ are now found as:

- $\beta_{1.0} = 4.5439$
- $\beta_{1.5} = 4.4888$

As before, a convergence limit was set at 0.001. The nonlinearity index becomes 0.0184, which is less than 0.03. Thus, the safety index becomes $\beta = \beta_{1.0} = 4.5439$ which correspond to a probability of failure of $2.76 * 10^{-6}$. The design point and sensitivity factors are given in table 5.19.

Table 5.19: Design point for plate stress at midspan and gaussian basic variables.

	t_p [mm]	$s_{ax}[MPa]$	$p_{lat}[MPa]$	s_f [MPa]
$x_i^\star$	19.817	157.71	0.1027	261.73
α_i	-0.1005	0.8056	0.0359	-0.5827

Convergence rate in terms of ratio between temporary and final safety index is shown in figure 5.3.

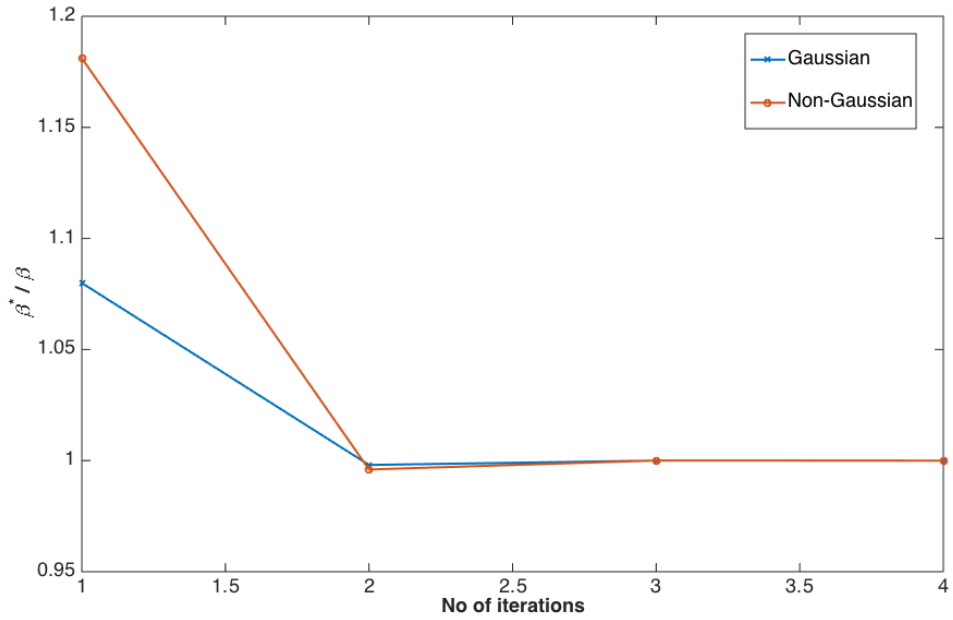

Figure 5.3: Convergence plot of the vector-projection algorithm, with the safety index at each iteration normalized with final result.

5.5. Convergence Study and Comparison of Results

The accuracy of Monte Carlo simulations is relative and depending on whether or not convergence has been achieved. It is therefore interesting to see how the simulation results change as the number of samples increases, since this is an indication on the level of convergence.

Figures 5.4 shows the percent-wise deviation from the final result over the simulation from the response surface analysis with gaussian probability distributions for Crude Monte Carlo and Importance Sampling.

When the other distribution types are employed, simulation histories for Crude Monte Carlo and Importance Sampling in terms of percent-wise deviation are shown in figure 5.5.

It can be seen how the von-Mises limit state has a fast convergence pattern while the capacity and DNV-requirements are more fluctuating.

Taking the Crude Monte Carlo results from the quadratic approach with $f_i^{(1)} = 2$ and $f_i^{(2)} = 1$ as reference, the mean absolute errors for all limit states are calculated. Results when compared to the other probability of failure methods and the Vector Projection approach for non-gaussian variables are found as:

- Bucher-Buorgund, FORM: 18.7%
- Bucher-Buorgund, Importance Sampling: 7.3%
- Vector Projection: 33.7%

Even though the above numbers suggest a significant difference between the two methods, it should be noticed that there might be other reasons for this error. First, the possibility that Monte Carlo simulations are not sufficiently converged must be considered. Furthermore, the transformations to standard gaussian space are more influent on the results of the Vector Projection method than for Crude Monte Carlo. For the gaussian distribution regime, corresponding mean absolute error between Vector Projection and Bucher-Buorgund with Crude Monte Carlo is 6.9%.

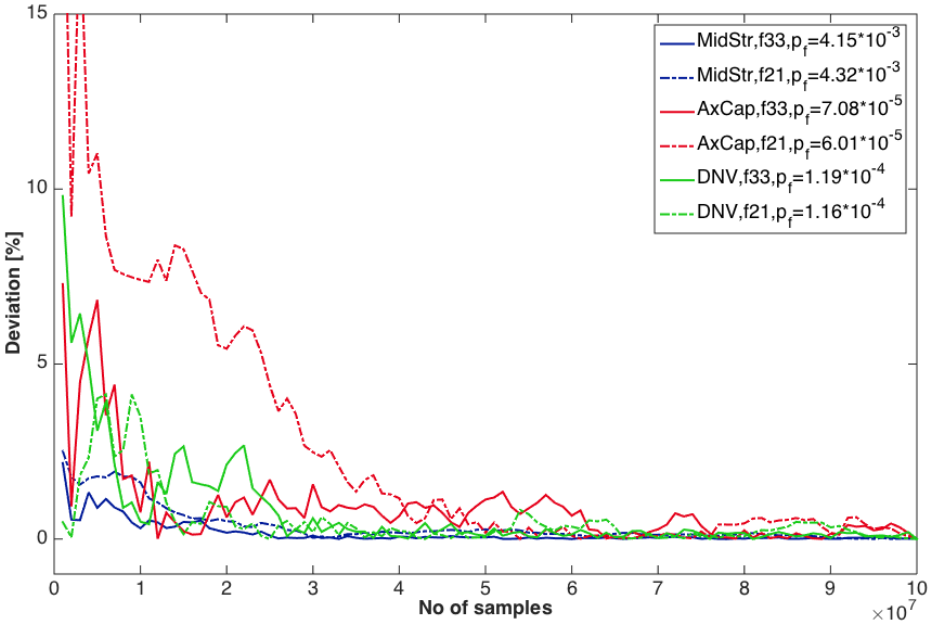

(a) Crude Monte Carlo

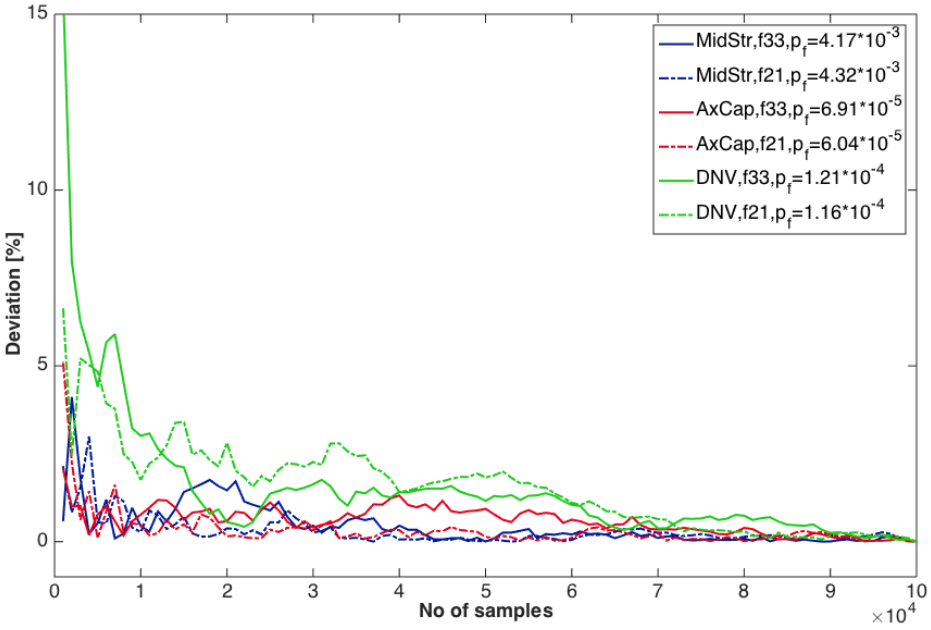

(b) Importance Sampling

Figure 5.4: Plot of the simulation histories from the quadratic limit states with gaussian distributions, where deviation is measured in terms of percent-wise difference from the final result.

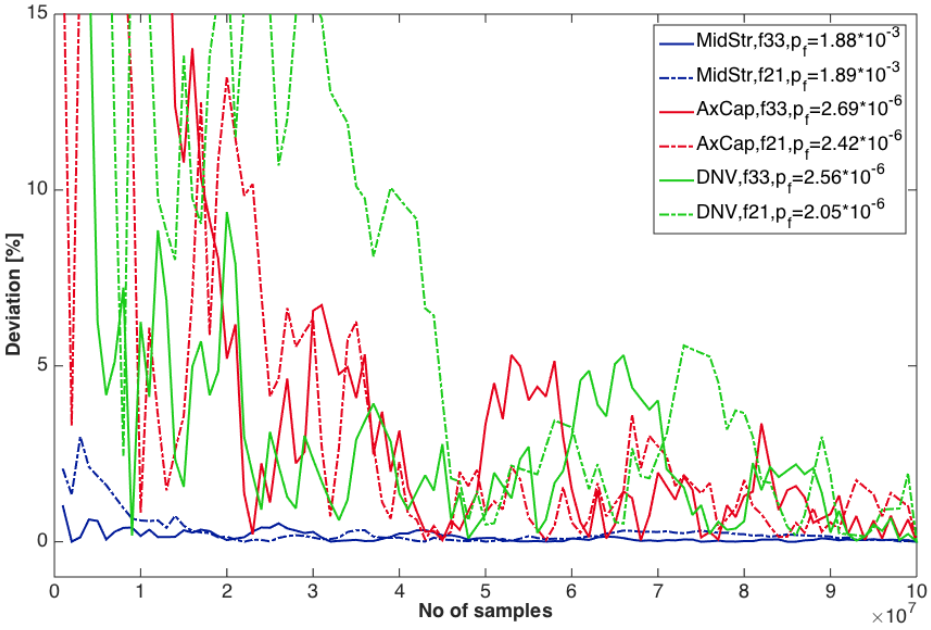

(a) Crude Monte Carlo

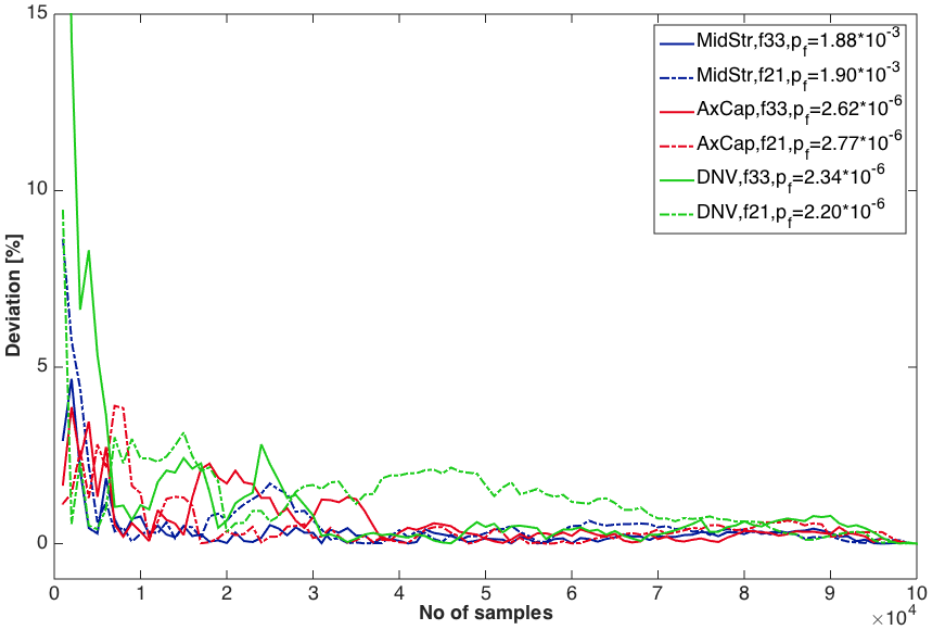

(b) Importance Sampling

Figure 5.5: Plot of the simulation histories from the quadratic limit states with non-gaussian distributions, where deviation is measured in terms of percent-wise difference from the final result.

Chapter 6

Discussion

6.1. General

It is recognized that both mechanical and probabilistic models applied here are subject to numerous simplifications. The reliability results should thus not be interpreted as directly applicable to design without further consideration. Furthermore, probabilities of failure based on buckling code and FEM-model should not be compared directly since different boundary conditions are used.

However, the example cases shows the work flow of a general reliability analysis and how both FEM-softwares and classification requirements can be introduced as a sampling source in a sensible manner.

When comparing results from both response surface methods, it is seen that there are some differences. This difference is generally smaller for gaussian distributions than for the non-gaussian case. The reason for this might be that the gaussian cases has a higher failure probability so that the level of convergence for the simulations are higher. It could also be that the transformations, which are approximate, causes this increased discrepancy. Following this discussion, and the fact that both methods are approximate, it can not be determined whether these differences are intrinsic in the methods or caused by underlying calculations.

6.2. Basic variables

The choice of basic variables is important, since it affects both the computational burden and the accuracy of the analysis. In the example case studied in this thesis, the loads are perhaps the most obvious since they are generally highly varying, and since a change in loading has direct impact on the safety margin. An example of this effect is shown in figure 4.7, where the pressure increase leads to a dramatic change in axial capacity. Furthermore, the plate thickness is taken as a variable, along with yield stress and a global shape error. Yield stress is taken as one common variable for both the plate, and all the stiffeners. This is an obvious simplification, since steel of different thicknesses would probably origin from separate batches and because this property could vary even within batches.

It is assumed that both longitudinal supports have the same imperfections and that the panel follows this form. A more correct description might be to use one variable for each side and some degree of correlation between the two. It was found that tilt imperfections on the stiffeners had little or no effect on the panel resistance. It cannot be excluded that other possible, but perhaps more complex in a modelling sense, imperfections would give higher probabilities of failure.

Distribution types has a profound impact on the results and is the most important factor among those studied in the examples. This is interesting since means and variances are equal for both gaussian approximations and the more physical models.

6.3. Limit States

In the examples, results from three different safety margin formulations are presented. The first is modelled with respect to yield stress in the plate along the midspan, which was seen to be a critical location from the benchmark study using both FE-model and the DNV framework. An alternative way of sampling the von-Mises stress limit is to find a measure of displacement (e.g end-shortening, lateral deflection) where yielding is seen to occur for most load/resistance combinations and employ this as the limit. This way, a realistic material model can still be employed in the FE-analysis without risking failed samples. On the other hand, this leads to inherent modelling errors if the chosen deflection measure varies with load and resistance parameters.

An alternative safety margin formulation for axial capacity, as for the von-Mises stress limit, would be to choose a geometrical quantity such as end-shortening as the limit parameter. This would include non-linear terms for axial load in the response surface. From the above mentioned figures, it is seen that axial capacity for all pressures and imperfections are reached at end-shortenings in the region of 6 mm which would then have been a suitable limit for the safety margin. However, a complication arises when realising that it is impossible to retrieve a result with an axial load above the capacity.

6.4. Bucher-Buorgund Response Surface

It is seen that the effect of sampling spread factors is generally noticeable but of the same order. This would support the thesis of low curvature in limit states of the type evaluated here. There might be a reason to consider the choice of sampling regime in light of which probability of failure method to be performed and which distributions that are at hand for the basic variables. The Hasofer-Lind safety index is based on finding one single point. Thus, this technique would be more and more accurate only depending on how close the distance is from this point at the response surface to the analytical design point. Hence, the Hasofer-Lind safety index could arguably yield more accurate results with more narrow sampling about this point. However, too narrow sampling could endanger the whole analysis, since this could imply that a false design point is found when the analytical limit state is of higher order.

Simulation techniques do not search one single point, but scatters safety margin samples based on the distributions of basic variables. The outcomes will be focused in the region of the failure domain with most probability density, i.e. in the vicinity of the design point. Thus, these techniques will increase in accuracy with the polynomial description in the region of the design point and not only of the design point itself. This is a significant difference, and perhaps the reason to why Bucher and Bourgund suggest simulation techniques rather than FORM-analysis in conjunction with their response surface approach.

In terms of computational effort, this response surface approach is questionable in conjunction with a FEM-tool since the data found in the first iteration is discarded. Thus, valuable information that required a fair amount of effort to obtain is lost. If the FEM-model is comprehensive and the number of variables is large, samples of great computational cost is only used for establishing a center point for the next iteration but is not used as a contribution to regression of the final response surface.

A beneficial property compared to the Vector Projection approach is that the number of safety margin samples is predetermined. If it is deemed that FORM is unsuitable in conjunction with this response surface, Monte Carlo methods are required. It can then be argued that the Bucher-Buorgund approach would be a beneficial choice when safety margin sampling is demanding but failure probabilities are moderate.

6.5. Response Surface by Vector Projection

The Vector Projection algorithm shows a steady convergence, and the criteria is generally reached after 4 repetitions with both distibution types for the DNV limit state as well as for the linear von-Mises analysis. The exception is the ultimate capacity check where more iterations are needed, particularly when the realistic distribution regime is employed.

A drawback of the vector projection method when each sample point requires a significant computational effort (e.g, a large FEM-model), is that the number of required FE-runs is unknown. From the examples calculated in this thesis, it is found that anything between 4 and 17 iterations i s required. This corresponds to sampling in the range of 40-170 FE-runs for 5 basic variables. Considering that many practival problems might have a significantly larger number of variables, and that the FE-calculations might be more comprehensive, this would be a major uncertainty regarding cost and effort of an analysis. The positive side of using a method that converges such as the vector projection method, is that underlying modelling errors can be picked up during the analysis by lack of convergence as opposed to the method of Bucher-Buorgund where the response surface is assumed sufficiently accurate after the second iteration. Hence, it might be valid to question the results of the ultimate capacity limit state. Especially so when considering that temporary safety indices, as shown in figure 5.2, are found as smaller than the final result. This should not be possible according to the definition of equation 2.10. However, small deviations to the negative side during convergence, as in figure 5.3, could be explained by the inherent inaccuracy of FORM when applied to curved limit states.

A beneficial property of the vector projection method is that the procedure is well defined by the article authors, so that inaccuracy following from e.g arbitrary sampling regimes is minimized. A drawback is the linear safety margin approximation, which makes comparative analysis using e.g simulations inaccurate for curved limit states. Also, as for the quadratic response surface method, the sampling results are only used to position the response surface for the following iteration, and is not used for regression of the new approximation.

Since this response surface utilizes only FORM, but requires an unknown number of safety margin samples, it can be argued that it is a suitable choice for low probabilities of failure in conjunction with computationally light FE-models or formulations such as the DNV-guidelines as applied in the examples.

6.6. Reliability Methods

The response surface method as suggested by Bucher-Buorgund and employed in the examples with a quadratic limit state approximation utilizes FORM to locate the first design point. This location sets the center point for the final sampling. Thus, the limit state itself is depending on FORM, so that Monte Carlo simulations performed are not independent from the FORM-methodology. The only thing that can be concluded from the Crude Monte Carlo-simulations are thus the ability of FORM to locate an accurate design point given the polynomial description at hand. This dependence is even stronger for the Importance Sampling, which is centered at the design point found from FORM. It is therefore important to realize that the analytical limit state could be of higher order. If so, this implies that there might be a global design point which is unidentified, so that the response surface describes the region about a local minimum on the limit state rather than the analytical design point. This error is then inherited by the simulation algorithms.

Although the above discussion of its weakness, FORM as applied in these examples is highly efficient and requires virtually no computation time once the analysis is set up. The results are somewhat inaccurate compared to the simulations. On the other hand, the ability to obtain approximate results in a matter of short time is valuable in terms of comparison and validation of other methods.

A true Monte-Carlo simulation would be to sample the FE-model directly. This might be possible for high probabilities of failure, and possibly more computationally economic FE-models than those created for this thesis. For sample sources such as the DNV-requirements, direct Monte Carlo is generally beneficial since each sample is computed swiftly.

From the convergence plots of section 5.5, the benefits of Importance Sampling compared to Crude Monte Carlo can be noted in terms of convergence rate, especially for the lower failure probabilities. However, it should be considered that each sample is associated with increased effort compared to Crude Monte Carlo so that a direct comparison based on only required sample size is somewhat misleading in terms of simulation time.

6.7. Further work

Further analysis with more accurate modeling of basic variables and limit states is a suitable starting point for further analysis. In particular, the effect of boundary conditions in the FEM-model and a larger set of basic variables could be investigated further. Regarding the basic variables, the model could include more geometric and material uncertainties including also the stiffeners. Correlation among these variables as well as for loads are also neglected here but would be included in a more accurate analysis.

It was intended to address the applicability of reliability analysis to life time extensions and inspection planning, but these themes were left out as the other tasks were more comprehensive than anticipated. The related subjects of corrosion and fatigue are adressed in theory but not applied in the examples.

Another interesting perspective is the reliability level in DNV guidelines versus FEM-models. The examples here, as discussed previously, does not enable such a comparison due to differences in boundary conditions, imperfections and possibly other factors as well. An adjustment of these in the FEM-model so that the panel is modelled on the same basis as the rules, along with a system formulation including all interaction equations would make a direct comparison of the reliability possible.

References

[1] Efren Ayala-Uraga. *Reliability-based Assessment of Deteriorating Ship-shaped Offshore Structures*. PhD thesis, NTNU, 2009.

[2] Efren Ayala-Uraga and Torgeir Moan. Fatigue reliability-based assessment of welded joints applying consistent fracture mechanics formulations. *International Journal of Fatigue*, 29:444–456, 2007.

[3] W.C Broding, F.W Diederich, and P.S Parker. Structural optimization and design based on a reliability design criterion. *Journal of Spacecraft and Rockets*, 1(1):56–61, 1964.

[4] C.G Bucher and U. Bourgund. A fast and efficient response surface approach for structural reliability problems. *Structural Safety*, pages 57–66, 1990.

[5] Christian Bucher. *Computational Analysis of Randomness in Structural Mechanics*, volume 3. CRC Press, Taylor Francis Group, London, UK, 2009.

[6] Det Norske Veritas. *Recommended Practice DNV-RP-C201 Buckling Strength of Plated Structures*, October 2010.

[7] Det Norske Veritas. *Offshore Standard DNV-OS-C401 - Fabrication and Testing of Offshore Structures*, April 2013.

[8] Det Norske Veritas. *Recommended Practice DNV-RP-C208 Determination of Structural Capacity by Non-Linear FE-methods*, June 2013.

[9] Ove Ditlevsen. Narrow reliability bounds for structural systems. *Journal of Structural Mechanics*, 7(4):453–472, 1979.

[10] Charles Elegbede. Structural reliability assessment based on particles swarm optimisation. *Structural Safety*, 27:171–186, 2005.

[11] Owen F. Hughes and Jeom Kee Paik. *Ship Structural Analysis and Design*. The Society of Naval Architects and Marine Engineers, 2010.

[12] Jont Committee on Structural Safety. *Probabilistic Model Code*, 2000.

[13] Halil Karadeniz. *Stochastic Analysis of Offshore Steel Structures - An Analytical Appraisal*. Springer-Verlag London, 2013.

[14] Armen Der Khiureghian and Pei-Ling Liu. Structural reliability under incomplete probability information. *Journal of Engineering Mechanics*, 112(1), 1986.

[15] Sang-Hyo Kim and Seong-Won Na. Response surface method using vector projected sampling points. *Structural Safety*, 19(1):3–19, 1997.

[16] Bernt J. Leira, K.Syvertsen, J.Amdahl, and C.M Larsen. *Compendium in TMR 4170 Marine Structures Basic Course, NTNU*. 2011.

[17] Robert E. Melchers. *Structural Reliability Analysis and Prediction*. John Wiley and Sons, 2 edition, 1999.

[18] Robert E. Melchers. The effect of corrosion on the structural reliability of steel offshore structures. *Corrosion Science*, 47:2391–2410, 2005.

[19] A. Naess, B.J. Leira, and O.Batsevych. System reliabilty analysis by enhanced monte carlo simulation. *Structural Safety*, 31(5):349–355, 2009.

[20] A. Naess, B.J. Leira, and O.Batsevych. Reliability analysis of large structural systems. *Probabilistic Engineering Mechanics*, 28:164–168, 2012.

[21] Arvid Naess and Torgeir Moan. *Stochastic Dynamics of Marine Structures*. Cambridge University Press, 2013.

[22] Jinsuo Nie and Bruce R. Ellingwood. Directional methods for structural reliability analysis. *Structural Safety*, 22:233–249, 2000.

[23] International Maritime Organization. Formal safety assessment. http://www.imo.org/OurWork/Safety/SafetyTopics/Pages/FormalSafetyAssessment.aspx, 2015.

[24] International Maritime Organization. Goal-based standards. http://www.imo.org/OurWork/Safety/SafetyTopics/Pages/Goal-BasedStandards.aspx, 2015.

[25] Jeom Kee Paik and Anil Kumar Thayamballi. *Ultimate Limit State Design of Steel-Plated Structures*. John Wiley and Sons, 2003.

[26] Apostopolos Papanikolaou, Carlos Guedes Soares, Andrzej Jasionowski, Jørgen Jensen, Dag McGeorge, Esa Pöyliö, Pierre C Sames, Rolf Skjong, Jeppe Skovbakke Juhl, and Dracos Vassalos. *Risk-Based Ship Design*. Springer Verlag Berlin Heidelberg, 2009.

[27] Rüdiger Rackwitz and Bernd Fiessler. Structural reliability under combined random load sequences. *Computers & Structures*, 9:489–494, 1978.

[28] Malur R. Rajasjekhar and Bruce R. Ellingwood. A new look at the response surface approach for structural reliability. *Structural Safety*, 12:205–220, 1993.

[29] Palle Thoft-Christensen and Michael J. Baker. *Structural Reliability Theory And It's Applications*. Springer Verlag Berlin Heidelberg New York, 1982.

[30] Paul H. Wirsching and Y.-N. Chen. Considerations of probability-based fatigue design for marine structures. *Marine Structures*, (1):23–45, 1988.

[31] Paul H. Wirsching, Tony Y. Young, John F. Geyer, and Bernhard Stahl. Fatigue reliability and maintainability of marine structures. *Marine Structures*, (3):265–284, 1990.

Appendix A

Probability Distributions

Normal Distribution

$$f_X(x) = \frac{1}{\sqrt{2\pi}\sigma_x} \exp\left\{-\frac{1}{2}\left(\frac{x-\mu_x}{\sigma_x}\right)^2\right\}$$

Log-Normal distribution

$$f_X(x) = \frac{1}{x\sqrt{2\pi}\sigma_x} \exp\left\{-\frac{1}{2}\left(\frac{\ln x-\mu_x}{\sigma_x}\right)^2\right\}$$

Weibull distribution

$$f_X(x) = \frac{\xi}{\theta}\left(\frac{x}{\theta}\right)^{\xi-1} \exp\left[-\left(\frac{x}{\theta}\right)^{\xi}\right]$$

Appendix B

Program Structures

B.1. Sampling from FE-Model

The reliability analysis based on FE-sampling from abaqus has a flow shown in figure B.1. The Matlab scripts control the sampling and performs all the reliability calculations. The general idea is that this main script generates a sample which, through two subfunctions is printed to a text file and initiates ABAQUS. The ABAQUS-script reads the variables, generates a model, meshes and performs the FE-analysis. At the end of the script, a postprocessor is called, that access the output database file (.odb) generated from the FE-analysis and prints the results needed for the current safety margin. The MATLAB-subroutine controllign the sampling reads these results, stores them and proceeds with the next sampling point. When all samples in the current iteration are evaluated, the safety margin is passed to the main script which proceeds with the response surface method.

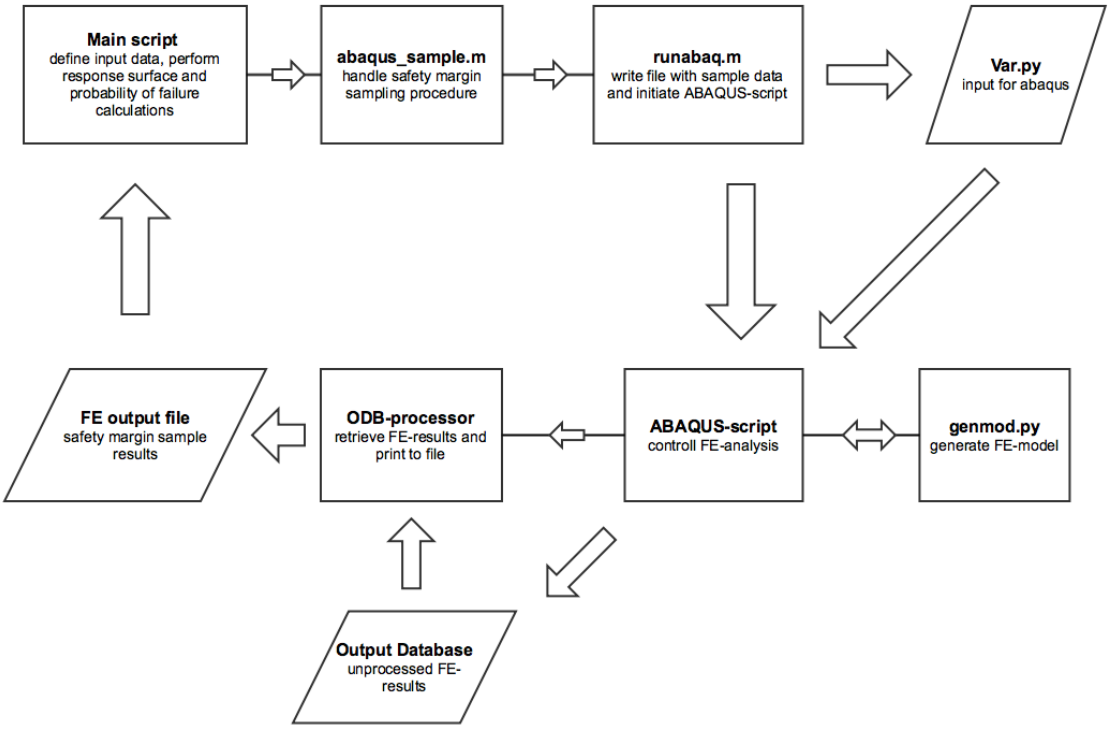

Figure B.1: General program flow for safety margin sampling through ABAQUS.

B.2. Sampling from DNV Guidelines

The principle here is similar to the general idea of programmes sampling from ABAQUS. The difference is that all data is treated inside MATLAB so that no external files is necessary. The DNV guidelines are thus programmed as a separate function package that can be called without passing of external files.